# A probabilistic approach to sheet pile driveability predictions by vibro hammers

J.M. Sinke

Technische Universiteit Delft

TU Delft

# A probabilistic approach to sheet pile driveability predictions by vibro hammers

by


## J.M. Sinke


to obtain the degree of Master of Science

at the Delft University of Technology,

to be defended publicly on Tuesday April 21, 2020 at 10:00 AM.

| | | |
|---|---|---|
| Student number: | 4464060 | |
| Project duration: | November 30, 2018 – April 21, 2020 | |
| Thesis committee: | Dr. ir. J.G. de Gijt, | TU Delft, supervisor |
| | Prof. dr. ir. R.J.D.M. Steenbergen, | TNO |
| | Dr. ir. A.P. van den Eijnden, | TU Delft, Geo-engineering |
| | Dr. ir. M.A.N. Hendriks, | TU Delft, Applied Mechanics |
| | Ir. J.P. van der Linde, | Hakkers BV |
| | Ir. R.F. van Dorp, | Allnamics BV |
| | Ing. M. Meeuwsen MSEng RC, | BV Ingenieursbureau M.U.C. |



TU Delft

# Preface

The writing of this thesis concludes a period of nearly 7 years. This period started in Wageningen and ends in Delft. During this time I had the privilege to explore many topics. These topics vary widely; from decision-making of smallholder farmers on crops to the strength of cold-formed steel beams. Despite this variety, these topics had in common that there was always a link with water, the most essential element on this planet. The 7-year-period is concluded by the writing of this Master's thesis.

During the writing of this Master's thesis I was assisted by a gifted committee of seven people. I would like to thank every committee member for his assistance along the way. Rob van Dorp was always prepared to give some good advice on pile driving practice and Allnamics' software. Mark Meeuwsen provided critical views on practical application from his perspective as a professional civil engineer. Peter van der Linde helped me during the daily struggle of writing the report and organizing ideas. Max Hendriks provided a critical, but constructive opinion on the topic near completion of the thesis. Raphaël Steenbergen was always enthusiastic about the topic and was prepared to offer instructive thoughts on formulation of ideas. Bram van den Eijnden offered assistance by his thorough knowledge on the application of probability theory on geotechnics. Jarit de Gijt provided innovative ideas and kept me motivated along the way with his lively attitude. Next to that, Jarit made it possible to create this respectable committee with his large network.

Special thanks go to Allnamics, which provided software to predict driveability. Also all assistance I required to get acquintained with the software was provided without any difficulty. Hakkers B.V. provided me a work spot throughout the process of writing this thesis. In an atmosphere with hard-working and passionate colleagues I was able to stay motivated throughout this process.

Last but not least, I would like to thank my family for providing a real home throughout all the years. A special thanks goes to Marlinde, who gave me all the support and never lost confidence in me during the lengthy process of writing this thesis.

*J.M. Sinke*
*Werkendam, April 2020*

# Abstract

During the design phase of a foundation installation aspects are easily overlooked. When this aspect is overlooked a foundation element risks not reaching its design depth or getting damaged during the installation process. As a result significant delays and/or costs could occur. A driveability study gives insight in the installation aspects of a foundation element. Driveability is the ability of a foundation element to be driven to a designated depth with a reasonable speed and without exceeding acceptable material stress. A driving speed under 1 mm/s or pile damage leads to refusal.

In this report will be researched how the probability of refusal of a sheet pile installed by vibro-driving can be predicted by means of a driving speed-depth-curve ($v_p$-z-curve). Having insight in probability of refusal improves risk assessment and decision-making on driving projects. The focus is on sheet pile installation by vibro hammers as these projects are generally executed in large numbers and under similar conditions. Therefore, these project types are very suitable for application of probability theory. Allwave-PDP is used as a basis to create a probabilistic prediction method. Allwave-PDP is a commercial software program which uses the wave equation to predict pile driveability.

Parameters of the pile driving system (pile, hammer and soil) modelled in Allwave-PDP are turned into stochastic parameters in the probabilistic method. The driveability prediction is repeated a number of times with a set of stochastic parameters in a Monte Carlo simulation to predict probability of refusal. After field observations and measurements is concluded that pile and hammer parameters are best modeled by deterministic parameters. Variability of soil parameters is caused by spatial and transformation variability.

Transformation variability is caused by an error in the transformation relation, which relates a field measurement to a soil model parameter. This variability is quantified by experimental data from previous reports. To take into account the transformation uncertainty a systematic error is randomly sampled for each geological layer (a layer with homogeneous soil properties). Spatial variability is caused by soil heterogeneity. Hence, uncertainty of actual soil properties at installation location occurs, as only a limited number of CPT's (Cone Penetration Test) is made. Spatial variability is incorporated by adding a random field to a trend line of the one-dimensional soil model parameters.

The probabilistic method is validated with well-reported case studies in Woudsend, Den Oever and Rotterdam. Predicted results show agreement with measured results; predicted and measured refusal percentages have a similar order of magnitude.

The model is a proof of concept that shows the potential of applying probability theory to driveability prediction methods. A proof of concept of the modelling (transformation and spatial variability) and the method (extension of Allwave-PDP) is given. Not any existing model is known to incorporate probability theory in driveability prediction methods. A probabilistic driveability prediction method improves risk assessment of the driving process. The result of the method, probability of refusal, could assist decision-makers on selection of hammer type and/or deployment of remedial measures (e.g. fluidization or pre-drilling). Presumably, application of this method will be first to a field where consequences of failure are large, e.g. offshore engineering. Ultimately, it can become a tool which provides additional information to support decision-making in high risk projects. The probabilistic method can simply be extended to other pile types or impact hammers. Therefore, this method is promising to predict different pile driving system configurations. The method should be considered as complementary to deterministic driveability prediction methods.

The probabilistic method is not without limitations. Due to use of just one CPT to represent soil conditions, remaining CPT's of the soil investigation are left unused. Variation between the CPT's offers additional information on the spatial variability of the soil. This information should be taken into account in future work. In future research safety factors used in deterministic prediction methods must be revised with the probabilistic method. The relation between safety factors and probability of refusal serves to distinguish conditions where deviating factors of safety are needed.

# Contents

# 1 Introduction

## 1.1. General

During the design phase of a foundation the installation aspects are easily overlooked. Typically, foundation design is based on ultimate axial and lateral capacity requirements only. Incorporating driveability in the design requires a driveability prediction. The driveability is the ability of a foundation element to be driven to a designated depth with a reasonable speed and without exceeding acceptable material stresses (Rooduijn and De Gijt, 2017).

Driveability can be predicted both for impact hammer and vibro hammer installation. In this thesis is only focused on installation with vibro hammers. In this brief introduction chapter a general overview on foundation installation is given.

## 1.2. Foundation engineering

In foundation design ensuring good driveability is important as a foundation element must reach its design depth. When this is not the case, there is a risk of lateral or axial instability of a structure. In figure 1.1a and 1.1b the failure mechanism of respectively a monopile and sheet pile are shown when installation depth is insufficient. When the foundation element in a project cannot reach its design depth or gets damaged during the installation process, overall installation duration could double or triple due to remedial work (Seaway Heavy Lifting, 2009). In general, small-displacement piles, like sheet piles and open-ended pipe piles, are used in hydraulic structures design. Small-displacement piles have a knife-effect during driving, contrary to displacement piles which push the soil aside during driving. In general, sheet piles are installed by vibro hammers or press-in equipment. Open-ended pipe piles are normally installed by vibro hammers or impact hammers.

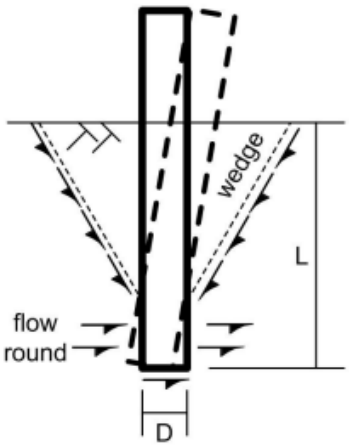


(a) Monopile (Schneider and Senders, 2010)

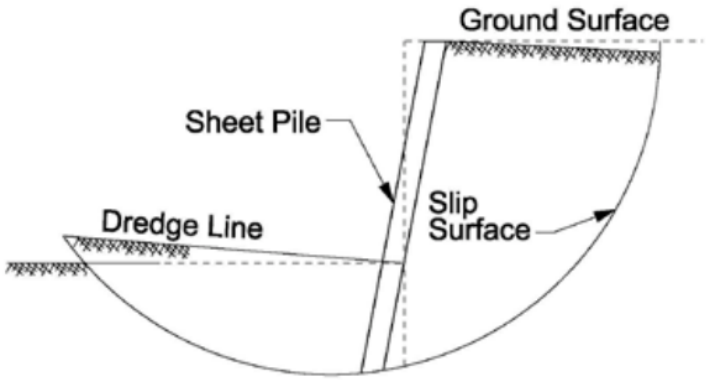


(b) Sheet pile (Wisconsin Department of Transportation, 2017)

Figure 1.1: Lateral failure mechanism

## 1.3. Pile driving system

Many factors are involved to make installation of a foundation a success. Except of having the equipment and skilled construction workers at the right time and place, it is important to select the adequate equipment. This means that all auxiliary equipment must be in place, like a safe working platform and sufficiently strong lifting devices. Above all a sufficiently strong hammer must be available. The required hammer for a successful installation depends on the pile and soil properties. These three elements (hammer, pile and soil) form the pile driving system (Rooduijn and De Gijt, 2017). The hammer generates the driving force to drive the pile in the soil. The soil generates most resistance to driving as it must be displaced during the driving process. The dimensions of the pile influence the resistance of the soil as the more soil is displaced, the more soil resistance is met. The pile mass adds extra driving resistance in the form of inertia. In figure **??** the three elements are clearly shown by respectively a sheet pile, vibro hammer and soil.

Figure 1.2: Pile driving system

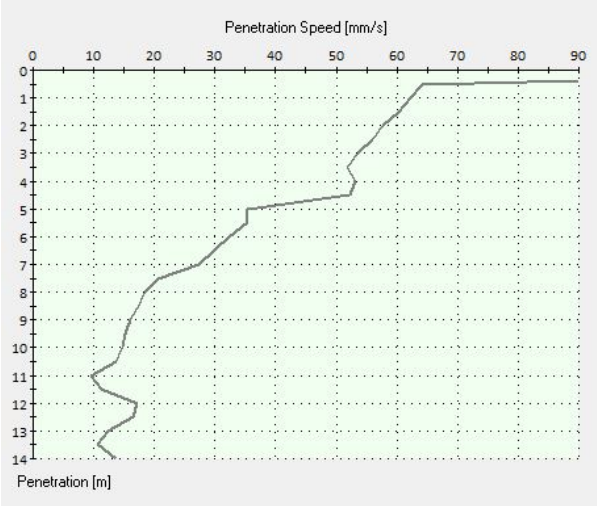


Figure 1.3: Example of $v_p$-z-curve

## 1.4. Driveability prediction method

Throughout the years various methods have been developed to predict driveability of foundations. This started with formulas for driving of displacement piles by impact hammers (Likins et al., 2012). Also for vibro hammers driveability formulas have been developed (CUR, 2012). Most formulas are empirical and cannot be theoretically explained. More sophisticated methods use a more complex algorithm to calculate the driveability. For example, TNOWAVE, Vibdrive, Karlsruhe or Vipere model. In these algorithms physical theory is introduced, e.g. soil fatigue and wave propagation. Resistance is introduced by springs, dampers and inertia. The result of these prediction methods can be modelled by a penetration speed as a function of the depth; a $v_p$-z-curve, see figure 1.3. The depth is measured at the pile toe level. Refusal is defined as when the penetration speed falls below a specified design value. Pile refusal could also occur because of pile damage. This is caused by exceedance of yield stresses.

# 2

# Research description

## 2.1. Problem analysis

By quantifying the risk of refusal, decision-making on (vibro-)hammer selection and remedial measures (fluidization or pre-drilling) can be improved. A stronger hammer results in a reduced risk of refusal, except when obstacles lead to refusal. However, a stronger hammer is more expensive and thus a trade-off must be made between risk and costs. This also applies to taking remedial measures; risk is reduced, but costs of the pile driving process go up. Current pile driveability prediction methods do not predict the probability of pile refusal. Reliability-based design theory must be applied to the foundation installation process. This theory is an advanced method to incorporate risks in the design. Reliability-based design calls for a willingness to accept that absolute safety is an unattainable goal and that probability theory can provide a formal framework for developing design criteria that would ensure that the probability of failure (used herein to refer to pile refusal) is acceptably small.

## 2.2. Scope

To make a reliability-based design for a driveability prediction, probability theory must be incorporated in the driveability prediction method. This implies that variability of the pile driving system's elements (pile, hammer and soil) must be taken into account in the prediction. Also failure in the form of pile refusal must be defined.

In this research the concept of a probabilistic prediction method will be applied to vibro-driving of sheet piles. Installation of sheet piles happens in larger numbers in a typical hydraulic engineering project than installation of open-ended pipe piles. This is advantageous when prediction and practice are compared. Namely, the law of large numbers states that a large number of repetitions leads to the expected value. This implies that during a sheet pile driving project the average observed driveability is less likely to be disturbed by a local phenomenon (obstacles in soil) than in case of a open-ended pipe pile installation. In general, sheet piles are driven by a vibro hammer. Therefore, only vibro driving is considered and impact driving is not.

### 2.2.1. Variability

Uncertainty is caused by variability of driving system properties. The variability of the soil (geotechnical properties) is complex and is separated into different components by figure 2.1. Random testing errors are neglected in this research. It is assumed that temporal variation does not have significant impact on the variability of driving system properties. The spatial variation is a component of significant importance. Namely, measurements are only made at discrete locations, whilst the soil is continuously varying in the spatial domain. The systematic error, consisting of a statistical error in the trend and a bias in the measurement procedure, is accounted for by transformation uncertainty. The transformation uncertainty takes into account both components of the systematic error. The pile and hammer variability cannot be split out into the components of figure 2.1 as these are point statistics.

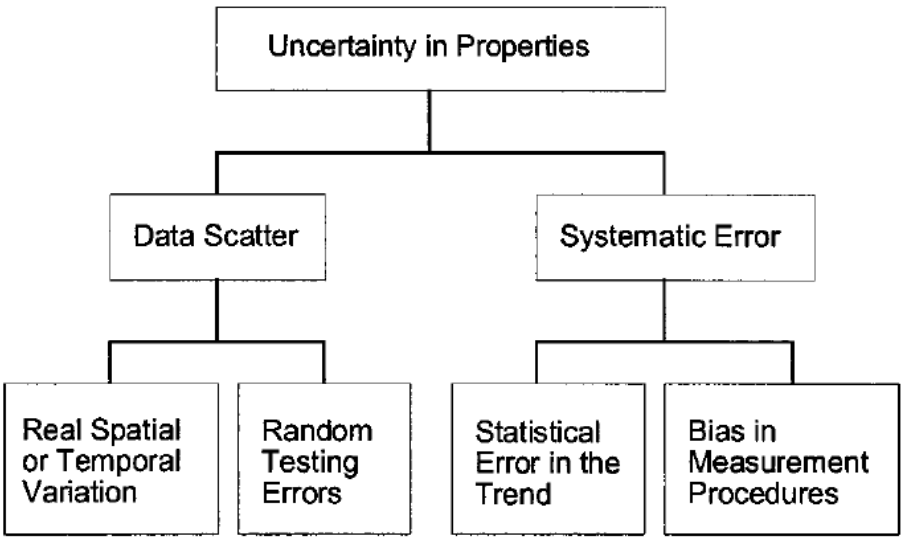


Figure 2.1: Separation of geotechnical uncertainty (Christian, 2004)

#### Hammer and pile variability

The statistical properties of pile and hammer can be expressed as point statistics. This means that spatial variability does not play a role as it does for soil properties. A hammer is manufactured under strict conditions. Default properties of the hammer are given by the manufacturer. Due to wear and tear hammer properties will change throughout its lifetime. Also during the driving process properties change as these are dependent on the resistance the hammer meets from the soil. Also default dimensions of sheet piles are given by the manufacturer. Piles are made with certain tolerances on its dimensions (Byfield and Nethercot, 1997). Therefore, the dimensions can vary in practice. The research will focus on to what extent hammer and pile properties vary.

#### Spatial variability

Soil properties vary with space; heterogeneity (Hicks, 2015). The soil investigation in a typical foundation installation project gives a limited representation of the soil. For example, in the Netherlands vertical soil profiles (CPT) are measured at every 25 m horizontal distance in a typical hydraulic engineering project. In between the vertical soil profiles no measurements are taken of the soil. This introduces uncertainty as soil properties vary as a result of soil heterogeneity. The spatial variability caused by the heterogeneity can be described by autocorrelation. Autocorrelation refers to correlation of values with its own surrounding values. In other words; soil properties influence each other when 'nearby'. (Phoon, 2016) (Lloret, 2012)

#### Transformation uncertainty

The transformation of field measurements to soil model parameters introduces uncertainty. The driving process is a system where dynamic and inertial resistance also play a role as respectively velocity and acceleration are involved. Furthermore, the loading is cyclic, which means that fatigue of the soil also influences driveability. Soil model parameters that describe these properties cannot be directly measured by most field measurements. Relations between measurements and soil model parameters have been established by laboratory experiments or matching of predictions with practice (postdictions). A relation is established by best-fitting the experimental results. The variation of experimental results is neglected by best-fitting the relation. In this research this variation is taken into account. To add to that, the database of experimental data is always a limited representation of the soil. This limited database adds more variation to the transformation relation.

### 2.2.2. Failure definition

The design penetration speed adopted in this research is 1 mm/s. This design value is used by experts on driveability predictions (van Dorp, 2019). Using design value of 1 mm/s is most intuitive; as long as the pile moves downwards, there is no refusal.

In other literature much higher design penetration speeds are found. In the Technical European Sheet Piling Association (TESPA) brochure it was stated that a value of approximately 8 mm/s for $v_p$ could be adopted as a

limiting value for vibro-driveability that would serve as a guide for limiting possible vibration-related nuissance factors. According to TESPA, vibratory driving below this recommended limit ($v_p \sim 8$ mm/s) requires careful monitoring to avoid excessive heat production in the interlocks. In another paper driveability is defined as hard when the penetration speed is lower than 22 mm/s (Rao, 1993). In this same paper, driveability is defined as easy when penetration speed is higher than 60 mm/s . The design penetration speed recommended by literature is much higher than used in this research. It is assumed that these recommended values are intended for the mean speeds of the driving process. The value of 1 mm/s indicates the limit below which refusal occurs at local penetration speed.

### 2.2.3. Prediction accuracy

The accepted probability of failure of execution (refusal) is much higher than that of failure of the founded structure itself. Namely, refusal has much smaller consequences than failure of a structure. This implies that less repetitions are required in a Monte Carlo simulation to reach sufficiently high accuracy, see figure 2.2 and formula 2.1. In figure 2.3 the 95% confidence interval is plotted as a function of number of simulations ($N$) for a refusal rate of 10%. The figure shows that the 95% confidence interval becomes smaller as the number of simulations increases. As the number of simulations increases, the effect on the 95% confidence interval becomes increasingly smaller. For 40 simulations the standard deviation, $\sigma_{P_f}$, is 0.047. In other words, there is a 5% probability that the experimental refusal rate is outside the interval 0.4% and 19.4%, whilst the expected refusal rate is 10%. A 10% refusal rate is used to define the number of repetitions as 40. Namely, as shown in figure 2.2 convergence of the 95% confidence interval decreases after 40 repetitions.

The number of simulations is limited as much as possible. Due to limited automation of the pile driveability prediction method the process is labour-intensive. After implementing these automation steps making 10 predictions takes approximately 1.5 hour. This is also limited by the computing power of the used computer.

The formulas below are used to determine the number of simulations (Jonkman et al., 2017):

$$\sigma_{P_f} = \sqrt{\frac{P_f(1-P_f)}{N}} \tag{2.1}$$

$$V_{P_f} = \frac{\sigma_{P_f}}{P_f} \tag{2.2}$$

where

| | | |
|---|---|---|
| $\sigma_{P_f}$ | = | Standard deviation of failure rate |
| $P_f$ | = | Probability of failure |
| $N$ | = | Number of repetitions |
| $V_{P_f}$ | = | Relative error |

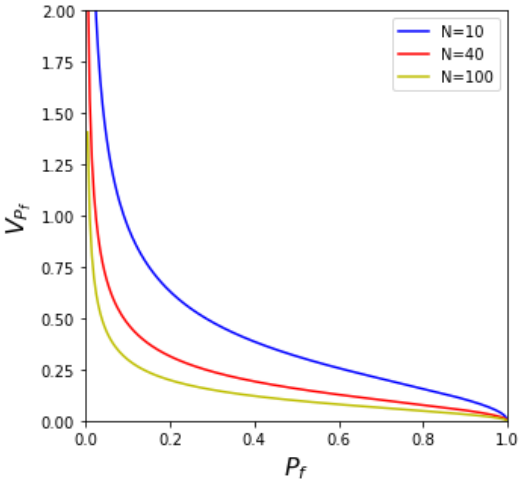


Figure 2.2: Variance of refusal rate as a function of refusal rate

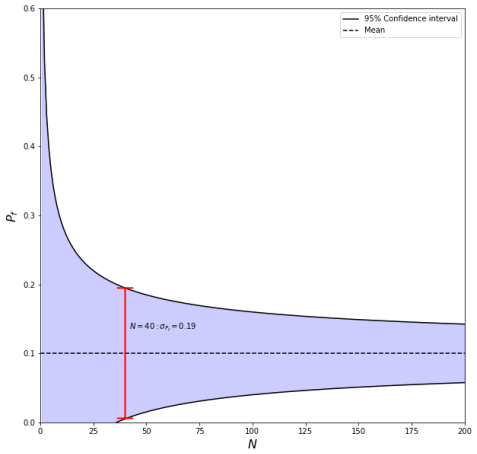


Figure 2.3: Refusal rate as a function of number of simulations

## 2.3. Problem definition

The application of driveability predictions as a decision-making tool for contractors is limited. To assess the risks of foundation installation a probability and consequences of refusal must be known. Driveability prediction methods are often a 'black box' for installation contractors. In case of application of a failure definition of 1 mm/s to a $v_p$-z-curve the outcome is either refusal or succesful installation. In practice, a more nuanced prediction is required. It must be predicted how large the probability of significant driveability problems is. With this information decision-making on taking preventive measures to improve driveability is improved, like using a stronger hammer or applying water jet fluidization. This leads to the formulation of the main problem:

> *To improve risk assessment and decision-making on driveability it is required to know the probability of refusal. Current driveability methods do not predict a probability of refusal.*

## 2.4. Objectives and research questions

### 2.4.1. Objective

The main goal of this research is to create a model to predict the probability of refusal. The focus is on driveability of sheet piles by vibro hammers.

### 2.4.2. Research question

> *How can the probability of failure of a driving process of sheet piles installed with a vibro hammer be predicted by means of a $v_p$-z-curve?*

## 2.5. Work approach

A concept is developed to incorporate probability in the pile driveability prediction method. This is done by replacing deterministic parameters of the pile driving system by stochastic parameters. Doing this for the soil parameters requires considering the transformation uncertainty and spatial variability. The former takes into account the uncertainty introduced by transformation of measurement results to soil model parameters. The latter takes into account the spatial character of the soil parameters. This leads to two subquestions:

1. What is the transformation uncertainty of soil model properties of the pile driveability prediction?
2. What method incorporates the spatial variability of soil model properties in the pile driveability prediction?

The point statistics, which are spatially independent and can be directly measured (without a transformation model), are found by the following subquestion:

1. What is the variability of hammer and pile properties?

The probabilistic driveability prediction method is consequently validated with results from practice. The prediction is made on the basis of conditions as found in practice. The following subquestion is formulated:

2. What is the validity of the probabilistic pile driveability prediction method?

## 2.6. Report overview

In chapter 2 and 3 a literature study is provided. In chapter 2 the process of vibro driving is described. In chapter 3 various methods to predict driveability are discussed. At the end of this chapter one method for driveability prediction is selected which is used to build a probabilistic model. In chapter 4 the probabilistic model is described and subquestions 1, 2 and 3 are answered. In chapter 5 the probabilistic model is validated with case study analyses. This chapter provides answers to subquestion 4. In chapter 6 this research is discussed and recommendations for future research are given. The last chapter contains the conclusion to this research. In short:

1. Introduction
2. Physics of vibro driving
3. Driveability prediction method
4. Probabilistic model
5. Validation

6. Discussion and recommendations
7. Conclusions

# 3

# Physics of vibratory pile driving

## 3.1. Introduction

In this chapter is explained what process takes place in the pile driving system during driving. The pile driving system consists of three elements; hammer, pile and soil. The hammer generates the forcing of the system. The resistance of the system consists of soil friction and damping and pile inertia. There will only be focused on vibro hammers. The process is described in physics terminology as much as possible. The conclusions of this chapter will be used to formulate conclusions to the next chapter. In the next chapter is determined which driveability prediction method resembles driving physics best.

## 3.2. Vibratory hammer

The hammer is responsible for the forcing of the driving system. A vibratory hammer gives a sinusoidal forcing to the system. In this section is explained how a vibratory hammer works mechanically. Also some background information on vibratory hammers is given.

### 3.2.1. History

The development and first large scale use of vibratory hammers was by the Russians in the late 40's (Barkan, 1957). The early vibratory hammers were driven by electric power. Similar vibrators to those of the Russians have been developed in Germany, France and Japan and at a later stage also in the United States. Hydraulically driven vibrators came into the market in the early 60's. (Jonker, 1987)

### 3.2.2. Application

In all cases where low-displacement piles such as sheet piles, H-beams and open-ended tubular piles have to be driven, the vibratory hammer has proven to be an excellent option. In the Netherlands about 80% of sheet piles is driven by vibratory hammers. The remainder is either pushed or driven by an impact hammer (Azzouzi, 2003). In correct ground conditions (sandy and soft clay soils) vibratory driving has several advantages: (Deep Foundations Institute, 2015)

- Installation times. Three to four times faster installation process when compared to impact hammering. The time required for pile driving itself is around three to four times faster. If the process of handling the pile is also taken into account, then the entire installation may be even quicker due to the easier pile handling. (Rausche, 2002)
- Low noise level. Vibro hammering introduces much lower accelerations in the surrounding soil or guiding structures and is considerably lighter in weight than an impact hammer (Jonker, 1987). This is particularly interesting in environments where the noise generated in the driving process is a major constraint such as in urban works or offshore piling. The noise problem during construction of offshore structures is particularly important because the acoustic emissions generated during the driving can have a negative impact on marine mammals. The reduction of noise levels compared to impact driving when using the vibratory hammer is approximately 15—20 dB and can be larger depending on the pile and soil conditions.

- Possibility of extraction and correction of misplacement error. Piles can be removed after their service life time.
- Practically no diameter limitation. Vibratory hammer have a very unique property that they can be joined together to form a bigger hammer, as demonstrated in the Hong Kong-Zhuhai-Macau and Riffgat projects. (de Neef et al., 2013)

A large disadvantage of vibratory hammer driving is the control and reliability of bearing capacity (Deep Foundations Institute, 2015). Currently, offshore open ended pipe piles must be impact driven for the last part. It is assumed that impact driving creates a plug in the pile to ensure sufficient bearing capacity.

### 3.2.3. Principle of operation

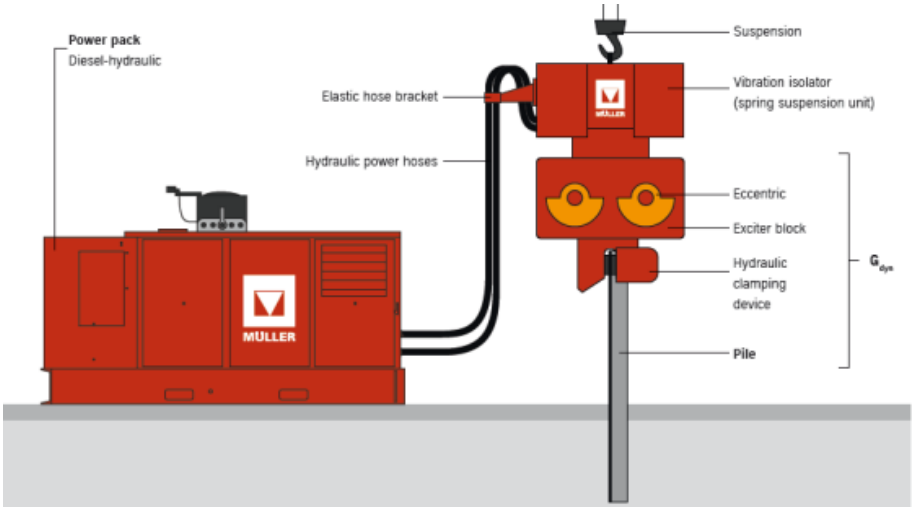


Figure 3.1: Configuration of vibratory hammer (Deep Foundations Institute, 2015)

The most common mechanical configuration, as shown in figure 3.1, used for a vibratory hammer consists of the following major components:

- an (even) number of eccentric masses;
- an oscillator (vibratory case) incorporating the eccentric weights and hydraulic motors;
- a spring-isolated suppressor (hammerhead);
- one or a set of hydraulic clamps;

The pairs (one or more) of counter-rotating eccentric masses generate centrifugal forces. The eccentrics itself are phased such that horizontal components of the centrifugal forces cancel and the vertical components add, see figure 3.2.

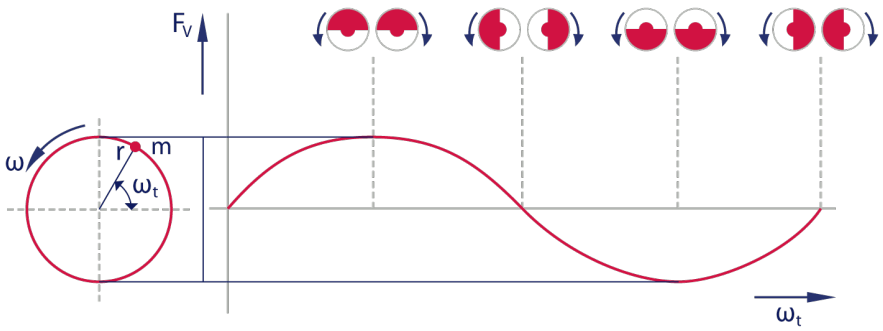


Figure 3.2: One rotation of two eccentric masses (PVE-Holland, 2019)

The hydraulic motors are driven by a hydraulic power pack. A hydraulic power pack is a self-contained unit that generates power by a diesel engine. The power is transmitted from one location to another by a fluid in order to run a machine. The operating frequency of the hammer can be regulated by the speed of the diesel engine of the power pack. The operating lines consist of a set of 5 hoses.

- pressure and return-line for the hydraulic motors
- drainhose for the hydraulic motors
- pressure and return-line for the pile clamps

### 3.2.4. Hammer specifications

Various property of the hammer influence the driving process. These properties are described below.

#### Eccentric moment

The eccentric moment is the eccentric mass multiplied by the distance between the point of gravity of the eccentric mass and rotation point (Rooduijn and De Gijt, 2017):

$$m_r = g_r \cdot d_r \tag{3.1}$$

where
$m_r$ = eccentric moment (kgm)
$g_r$ = eccentric mass (kg)
$d_r$ = distance between point of gravity of eccentric mass and rotation point (m)

The eccentric moment ($m_r$) can be increased by assembling several vibratory hammers together. (Deep Foundations Institute, 2015)

#### Frequency

The vibrational frequency is commonly used to classify the vibratory hammers: from 15 to 30 Hz is considered as normal or standard frequency, from 30 to 80 Hz is considered as high frequency, and from 80 to 150 Hz as super high frequencies. The division of frequency ranges is not clearly delineated and each author and manufacturer considers different ranges. In the Netherlands vibratory hammers with a frequency of 38.3 Hz (2300 rpm) are normally applied in hydraulic engineering projects. The selection of certain driving frequency depends on the proximity to vibration-sensitive areas. High and super-high frequency vibratory hammers are recommended when working close to these areas. From 5 m distance standard frequency hammers with variable eccentric moment can be used. These hammers contain technology to phase the eccentrics such that both horizontal and vertical components cancel out. From 25 m distance standard driving frequency hammers with fixed eccentric moment can be used (Deep Foundations Institute, 2015).

The driving force is a function of frequency and eccentric moment and is shown below: (CUR, 2012)

$$F_c = m_r(2\pi \cdot f)^2 \tag{3.2}$$

where
$F_c$ = centrifugal force (kN)
$m_r$ = eccentric moment (kgm)
$f$ = frequency (Hz)

In practice the frequency of the vibratory hammer will turn out to be 5 to 10 percent lower than the maximum frequency given by the manufacturer. Due to high soil resistance, an overflow valve reduces the hydraulic flow and reduces the frequency. This results in a significant reduction of centrifugal force (Rooduijn and De Gijt, 2017).

#### Weight

The weight of the hammer is divided in a static surcharge force ($F_s$) and a dynamic mass. The dynamic mass is defined as the sum of the masses that move in the same axial direction as the driven object. The static mass consists of the hammerhead, see figure 3.1. The static mass is hard to determine for free-hanging systems as a part of the static mass is absorbed by the crane's hook. As a fully rigid connection is made between pile, clamps

and vibratory case, these elements form the dynamic mass. Also weight of the soil moving with the pile adds up to the dynamic mass.

#### Amplitude

The amplitude is the displacement between the isolator and vibrating part. The amplitude value provided by the manufacturer will be smaller in operation, because the soil and pile weight increase the dynamic mass. As a rule of thumb can be stated that an amplitude of 5 mm is required to overcome toe resistance (CUR, 2012). The amplitude is a function of eccentric moment and total dynamic mass:

$$d = \frac{m_r}{m_{dyn}} \tag{3.3}$$

where
$m_r$ = eccentric moment (kgm)
$m_{dyn}$ = dynamic mass (kg)
$d$ = displacement amplitude (m)

## 3.3. Pile

The pile is subject to a sinusoidal forcing in case of vibro driving. This forcing is exercised on the top of the pile. The forcing must be transmitted to the whole pile. This results in a displacement of the pile. When this displacement is sufficiently large, the soil deforms plastically and the pile is driven deeper. The resistance to deformation depends on the dimensions of the pile. In this section behaviour of the pile as a result of the forcing is discussed. Next to that, interlock friction will be discussed. This friction is specific for sheet piles as it is caused by locks of the sheet piles.

### 3.3.1. Wave equation

Pile driving is not a simple problem of impact that may be solved directly by Newton's laws. The effect of an applied, localised disturbance in a medium soon transmits or 'spreads' to other parts of the medium, but cannot be transmitted from one point to a different point instantaneously. The disturbance is transmitted by waves. This propagation of waves is described by the wave theory. The wave equation is the most important formula in this field: (Metrikine and Vrouwenvelder, 2001)

$$\frac{\partial^2 u}{\partial x^2} = \frac{1}{c^2}\frac{\partial^2 u}{\partial t^2}, \quad c = \sqrt{\frac{\rho}{E}} \tag{3.4}$$

where
$u$ = displacement (m)
$c$ = wave velocity (m/s)
$\rho$ = mass density (kg/m$^3$)
$E$ = Young's modulus (MPa)

The wave theory can be used to describe stress waves in rods. In this respect, piles may be considered to be rods and the same applies to the parts of pile driving hammers. The simplest form of wave theory assumes that the material of a pile shows no internal damping and that during driving, the pile is not subject to skin friction. In case of the absence of body forces, the familiar wave equation can be used. (Voitus van Hamme et al., 1974)

### 3.3.2. Reflection of waves at boundaries

In this section the wave reflection from simple boundaries, i.e. from a fixed end and a free end, will be considered. The reflection process in these cases can be easily analysed by applying the method of the images. An incident pulse travelling to a an end of the rod is considered. The first case considers a free end, the displacement in the reflected pulse is opposite to that in the incident pulse. However, the stresses in the reflected incident pulse are of the same sign. This causes stress doubling during reflection from a fixed end. This phenomenon is called "stress multiplication", see figure 3.3. At the free end, the displacement in the reflected pulse is identical to that in the incident pulse. However, the stress in the reflected pulse is opposite to the stress in the incident pulse. So, in contrast to the case of a fixed end, reflection from a free end does not provide doubling of the stress, but of the displacement field, see figure 3.4. (Metrikine and Vrouwenvelder, 2001).

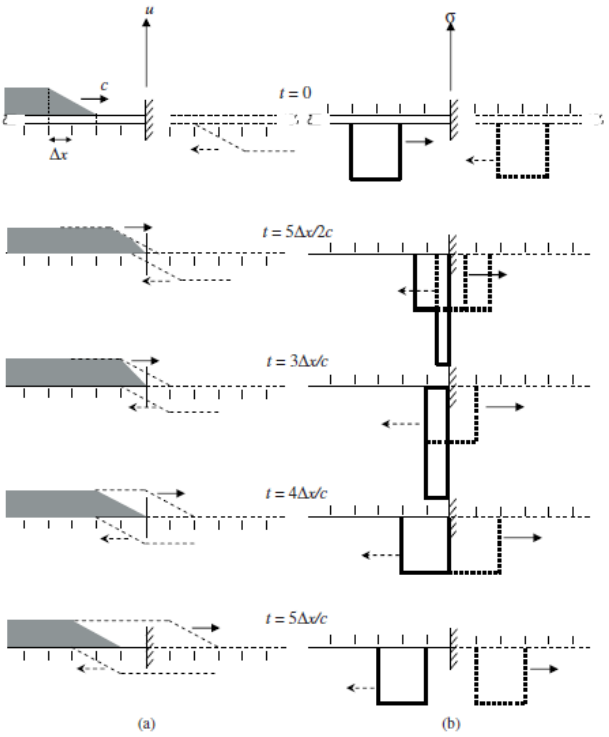


Figure 3.3: Reflection of (a) displacement pulse and (b) stress pulse from a fixed end (Metrikine and Vrouwenvelder, 2001)

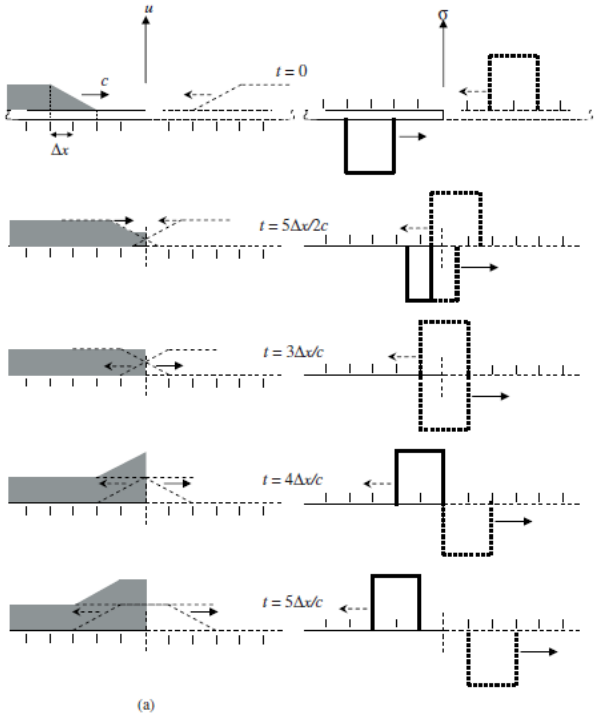


Figure 3.4: Reflection of (a) displacement pulse and (b) stress pulse from a free end (Metrikine and Vrouwenvelder, 2001)

These two situations; free and fixed end draw an analogy with respectively soft and hard soils, see figure 3.5. The compressive stress wave is indicated with red springs and the tensile stress wave with blue springs. As shown in figure 3.5a the pile tip element has no spring underneath and can move freely downwards, which is analogous to

a soft soil. This results in a larger displacement of the pile tip element than the other elements, which results in a tensile stress wave. In figure 3.5b the pile tip element receives a reactionary force from the soil underneath, which is analogous to a hard soil. This causes an even larger compression of the pile tip element spring than the other springs. This results in a force propagating upwards in the form of a compressive wave. Note that toe reactions in practice will behave as a hybrid version of free and fixed end reactions. (Rooduijn and De Gijt, 2017)

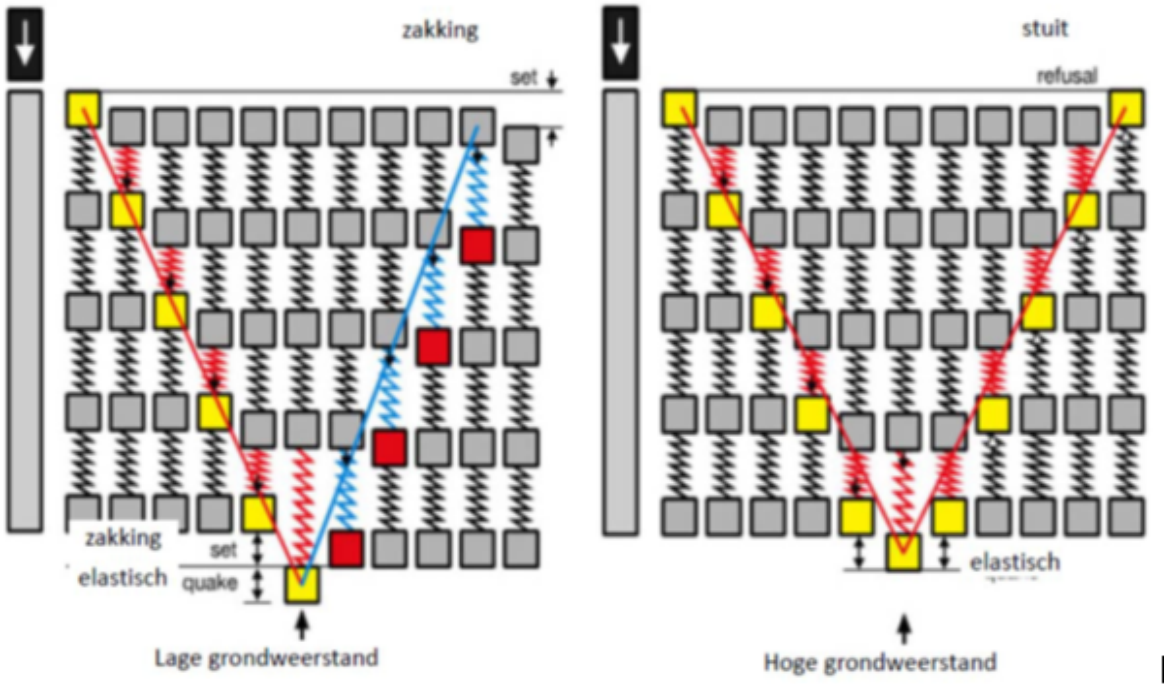


(a) Soft soil

(b) Hard soil

Figure 3.5: Stress wave propagation (Rooduijn and De Gijt, 2017)

### Interlock friction

Interlock (clutch) of two jointed steel sheet piles needs to be considered when driving sheet piles. Publications and documented knowledge about the effects of interlock friction remain rather limited at present. From the experiments done on interlock friction some conclusions can be drawn. The time needed to drive the sheet pile into dry sand has a considerable influence on the shear resistance developed in the interlock. The longer the driving, the greater the amount of sand that is found into the clutch. The interlock resistance is found to be reduced to about 80% when the sheet pile specimen was installed in saturated sand. It is believed that the liquefaction, developed during installation, caused the sand grains to be more mobile and thus able to avoid being jammed into the interlock. Results from the experiment show that the quasi-static amplitude values of interlock friction varied between 2-20 kN/m (Van den Berghe, 2001). Another work on this subject, states that the dynamic interlock resistance can be set to 1.0 kN/m, based on the results of experience. The geometrical shape and size of the interlock gaps (figure 5.5) determine the degree of watertightness. A high degree of water tightness minimizes the undesirable presence of grains in the interlock gap. Not solely the presence of grains determines the interlock friction force that develops. The presence of impurities (such as corrosion) together with permanent deformations of profiles (due to incorrect storage or handling) may also generate non-negligible unfavourable developments of interlock friction. (Viking, 2002)

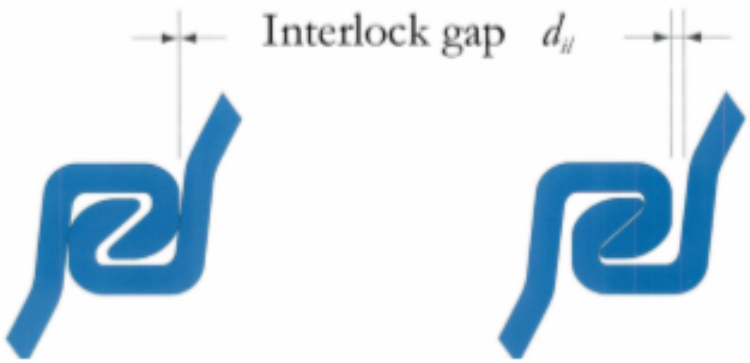


Figure 3.6: Interlock gap (Viking, 2002)

## 3.4. Soil

The soil is the medium which must be penetrated by the foundation element. The force of the vibratory hammer pushes away the soil and makes room for the foundation element. In this section is qualitatively described how the soil behaves and which properties influence this. Broadly, the soil driving resistance can be described by soil fatigue and dynamic resistance. The former causes a reduction of the soil resistance due to cyclic loading, whilst the latter adds extra resistance due to the dynamic character of the loading.

### 3.4.1. Soil fatigue

Decrease of soil friction was first described by E.P. Heerema during driving of piles in stiff clay at Kontich, Belgium. It was found that driving resistance increased only less-than-linearly when the pile progresses. This could be explained by the loss of skin friction as the pile progressed. This is likely to be caused by wear of the slip surface. The clay exerts a peak friction on the pile wall near the tip, where the soil is least disturbed; and to assume that, while the pile progresses downwards, the soil gradually loses its friction effect on the pile wall (Heerema, 1978). The initial shear strength is altered by two soil-related phenomena (Viking, 2002):

- The cyclic motion of grain particles due to vibratory accelerations
- The induced pore-pressure build up (liquefaction)

The influence of each strength reduction mechanism depends especially on the soil type. In non-cohesive soils shear strength reduction can be mainly explained by liquefaction, whilst in cohesive soils the cyclic motion will cause remoulding and reduce friction. In the following sections soil fatigue is discussed in detail.

#### Non-cohesive soils

Due to high frequency and continuous vibration, non-cohesive soils have no time to consolidate in case of vibratory pile driving. This causes increased water pressure, which neutralizes the effective stresses between particles. A loss of effective stress because of increased water pressure is called liquefaction. Liquefaction is a particular effect of cyclic loading that degrades soil resistance further than any other phenomenon (Rooduijn and De Gijt, 2017). Due to the neutralized effective stresses a fluid-like soil state is generated at macroscopic level.

Soil liquefaction is not the only explanation of shear strength reduction, this makes vibrodriving on dry sands possible (Moscoso, 2018). In one experimental attempt to measure penetration velocity, steel balls were placed under a surcharge load in a container filled with air-dried sand. The container was rigidly positioned on a platform and subject to vertical vibrations of specifically selected displacement amplitudes and frequencies, see figure 3.7. This showed that cyclic motion alone can reduce shear strength sufficiently to make penetration possible. (Barkan, 1957)

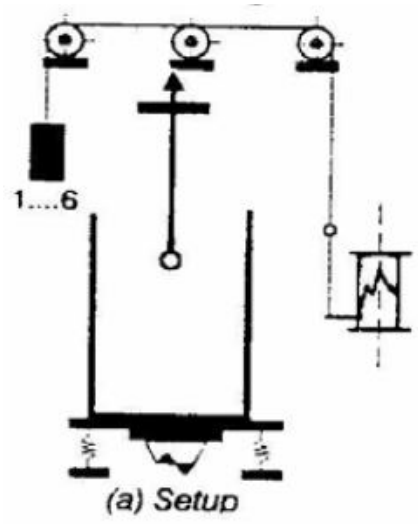


Figure 3.7: Dry sand experiment setup (Barkan, 1957)

In a non-cohesive soil the following parameters affect the strength degradation due to liquefaction and cyclic motion (Viking, 2002):

- **Relative density** The soil parameter that has been reported to have the most significant influence on the driving resistance. The driving resistance has been found to increase with increasing relative density. The volume changes (densification or dilation) induced in the soil have been found to relate to a characteristic driving resistance.
- **Lateral effective stress** Increased confining pressure has been found to proportionally increase the driving resistance. The liquefaction resistance of soil increases with increasing the effective confining stress of the soil, i.e. the soil liquefaction is easier to develop at shallow stratum than that at the deeper stratum (Ni and Fan, 2004). Soils with a high overconsolidation ratio (OCR) are distinguished by a high cone resistance. Due to the vibratory loading the cone resistance and angle of internal friction reduces significantly in soils with a high OCR. (Rooduijn and De Gijt, 2017) (Jonker, 1987)
- **Content of fines** When this fines content (or silt content) is greater than 12%, it usually dictates that the use of vibratory-drivers will not be successful. This has been observed by several authors, but none of them have provided an underlying explanation for it.
- **Degree of saturation** This parameter is already discussed to explain the effect of cyclic motion. Driving resistance is increased for a lower degree of saturation due to the lack of liquefaction.
- **Layers of different relative density** The existence of layers with higher densities has been found to result in a significant increase in driving resistance. It has been concluded from laboratory tests that the dynamic pile-toe resistance increases significantly, while the dynamic pile-shaft resistance increases only slightly when the pile is vibratory driven from a medium-dense sand into a very dense layer of sand.

### Cohesive soils

The cohesive soil displacement at the penetrating pile tip will cause remoulding and create excess pore water pressures. Due to remoulding and the excess pore water pressure the soil shear strength reduces. Remoulding is a process where the clay particles are reorientated parallel to the shearing surface, see figure 3.8. Excess pore water pressure is only measured in overconsolidated clays; in normally consolidated clays the drop in strength is due entirely to particle reorientation.

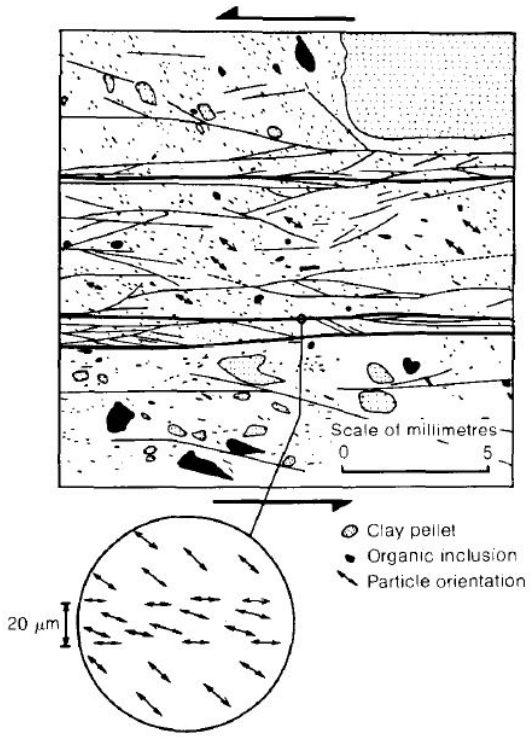


Figure 3.8: Fabric of shear zone and slip surface of clay (Skempton, 1985)

### 3.4.2. Damping

The soil loading during pile driving has a dynamic character. Contrary to most soil testing methods, like CPT or triaxial tests, which have respectively a quasi-static and static character. According to literature the dynamic character results in an additional, velocity-dependent resistance; dynamic resistance or damping (Rooduijn and De Gijt, 2017).

An experiment was carried out by E.P. Heerema by the test apparatus shown in figure 3.9. Against the face of the soil sample, a flat stiff steel plate is pressed which covers the sample face almost completely. The steel plate is moved up and down by an oscillator and all forces and displacements are recorded. Two series of tests were carried out; horizontal load variation tests and velocity variation tests. The results of these tests show that for sand no velocity-dependence was found. For clay the friction is very strongly velocity-dependent at low velocities and very little velocity-dependent at high velocities. Dynamic soil shear strength is proportionate to velocity to the power 0.2. ($v^{0.2}$) (Heerema, 1979). The results of these tests were criticized in another report. Namely, these tests did not duplicate actual field conditions, since the inertial force affecting the sand grains was not present during the laboratory test (Viking, 2002).

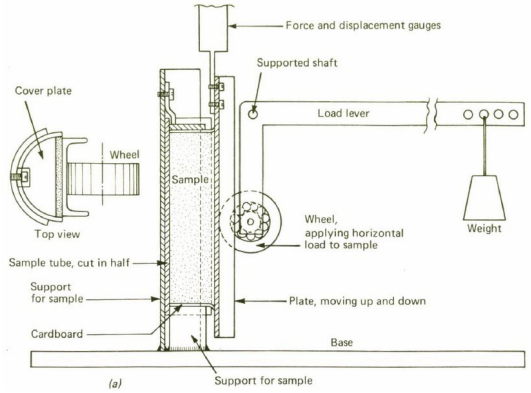


Figure 3.9: Experiment setup Heerema (Heerema, 1979)

Another experiment was carried out by P. Middendorp and P.J. van Brederode to model the dynamic response of the soil. This was done by placing a long steel rod (length = 10 m and diameter = 20 mm) in a plastic tube filled with sand. In this tests is shown that damping is present at a constant value for all velocities. (Middendorp and van Brederode, 1984)

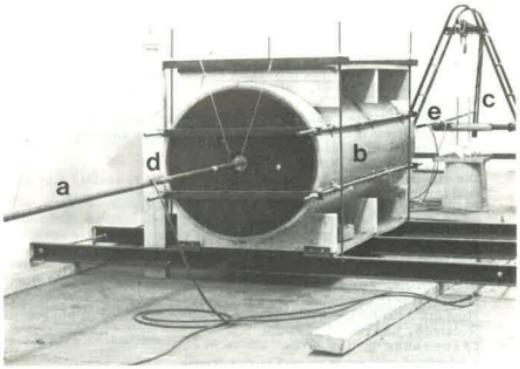


Fig.1 Experimental set up
a = steel rod
b = tube with sand
c = impact rod
d = straingage, station 2
e = straingege, station 1

Figure 3.10: Experiment setup Middendorp (Middendorp and van Weele, 1986)

Coyle & Gibson tested the dynamic resistance of soils, both for clays and sands. The dynamic soil shear strength of sand and clay is proportionate to velocity to the power 0.20 and 0.18 respectively ($v^{0.20}$ and $v^{0.18}$) (Coyle and Gibson, 1970). For clay this was confirmed by other research as exponents in the region of 0.2 were found both for side and tip resistance (Litkouhi and Poskitt, 1980).

## 3.5. Conclusion

A pile driving system consists of a pile, hammer and soil. The vibro hammer excites the pile in a sinusoidal way. The forcing of a vibro hammer is caused by rotating eccentric masses. The driving force is a function of the eccentric moment and frequency. The frequency is reduced due to soil resistance. This has significant impact on the driving force.

The forcing travels trough the pile in a wave-like motion. The forcing on the pile cannot be solved directly by Newton's laws. The applied force cannot be transmitted from one point to another instantaneously. The wave theory is used to describe stress waves in piles. Depending on the toe resistance of the soil, a compressive or tensile wave forms.

The resulting movement of the pile results in resistance caused by pile inertia and soil friction. Vibro driving is an efficient way to install sheet piles and open-ended pipe piles. Soil resistance behaviour is characterized by soil fatigue and damping. Soil fatigue occurs as a result of cyclic loading. Fatigue is caused by cyclic motion of grain particles and induced pore-pressure build up. The former dominates the fatigue behaviour in cohesive soils, whilst the latter does in non-cohesive soils. Soil damping is the velocity-dependent resistance. The experimental results on soil damping led to different results. In general, it can be concluded that damping is linearly related to velocity or to the power 0.2. Additional resistance is caused by the locks connecting neighbouring sheetpiles. Knowledge of interlock friction is limited. Recommended values for interlock friction range from 1 to 20 kN/m.

# 4

# Driveability prediction methods

## 4.1. Introduction

Various driveability prediction methods are around. Logically, all these methods are claiming to give a valid prediction. In this research this will not be questioned. In this chapter will be reviewed how well prediction methods take into account the physics of pile driving. The physics of pile driving have been discussed in the previous chapter. Although it is self-evident that design equations and empirical formulas do not correctly describe the relevant mechanisms (e.g. soil fatigue and wave propagation), these prediction methods will be shortly discussed. Much attention will be given to the Smith model, as this model was the first to incorporate wave theory to driveability predictions. Consequently, variations in the Smith model will be elaborated on. Finally, this chapter will lead to selection of a driveability prediction method which will function as the deterministic basis for a probabilistic model. As CPT is the standard soil test in the Netherlands and gives a relatively complete picture of the geotechnical characteristics of the soil profile compared to other soil tests (SPT), a driveability prediction method using CPT data as input parameters for the soil model is selected.

## 4.2. Empirical methods

The most simple methods to predict driveability are analytical equations and empirical rules. In this research a rule of thumb from CUR (the Dutch centre for research, rules and regulations in civil engineering practice) and EAU. Also a design rule based on Hypervib-I is presented.

### 4.2.1. CUR

This formula calculates the free displacement amplitude ($d$), that is used to determine the appropriate vibration equipment: (CUR, 2012)

$$d = \frac{m_r}{m_{dyn}} \tag{4.1}$$

where

| | | |
|---|---|---|
| $m_r$ | = | eccentric moment (kgm) |
| $m_{dyn}$ | = | dynamic mass (kg) |
| $d$ | = | displacement amplitude (m) |

The chosen vibrator must have $m_r$ large enough to fulfill the required displacement ampltidue (larger than 0.005 m). If so the sheet piles will reach the pre-determined depth according to the formula. Remarkably, there is no soil involved in this formula. The idea behind this formula is that with an amplitude of 5 mm the sheet pile is able to degenerate the strength of the soil to relatively low values and as a consequence the original strength of the soil is not involved anymore. (Korff and van Tol, 2012)

### 4.2.2. EAU

The German design rule (EAU 1990) calculates the minimum required vertical force using only the length of the pile and the dynamic mass: (Korff and van Tol, 2012)

$$F_{c,EAU} = \alpha_E \cdot L + \beta_E \cdot m_d \tag{4.2}$$

where
$\alpha_E$ = $15 \cdot 10^{-3}(m)$
$L$ = pile penetration length (N/m)
$\beta_E$ = $3 \cdot 10^{-4}(N/kg)$
$m_d$ = dynamic mass of hammer and pile (kg)

This rule quantifies the German criteria for their choice of vibratory equipment. For each meter of the pile one requires at least 15 kN vertical cycle force and additionally for each 100 kg dynamic mass one needs 30 kN vertical cycle force. The used force must be more than the calculated force to obtain a succesfull installation. This empirical formula considers the soil resistance in every soil type identical. Thus, soil variation is neglected.

### 4.2.3. Azzouzi

This formula is based on numerical method of Hypervib-I. 180 calculations with this method result in the formula: (Azzouzi, 2003)

$$F_{c,Azzouzi} = \alpha_A \cdot L \cdot \chi \cdot f_A(q_c) + \beta_A \cdot A_t \cdot g_A(q_c) \tag{4.3}$$

where
$\alpha_A$ = $1.92 \cdot 10^{-3}(-)$
$L$ = pile penetration length (m)
$\chi$ = perimeter of the sheet pile (m)
$f_A(q_c)$ = mean cone resistance (N/m$^2$)
$\beta_A$ = $1.2 \cdot 10^{-2}(-)$
$A_t$ = cross-sectional area of sheet pile (m$^2$)
$g_A(q_c)$ = displacement amplitude (m)

The force given by the formula must be smaller than the force of the vibratory hammer. In theory, this would result in succesfull sheet pile installation. In this formula the average cone resistance is used. This simplifies the soil profile and leads to uncertainty in the prediction. Next to that, Hypervib-I uses a Newtonian approach instead of the wave equation to model the behaviour of the pile, which is a simplification of reality.

### 4.2.4. NVAF-PSD design charts

In 2002 design charts were published to predict driveability. The prediction is based on three input parameters:

- Sheet pile profile
- Method of driving
- Soil profile

The soil profile must be selected from 13 default profiles. The profiles represent typical conditions in various parts of the Netherlands. A design chart for a typical soil profile in Rotterdam is given as an example. The horizontal axis shows the section modulus, whilst the vertical axis shows the pile length. For example, to drive a sheet pile of 30 m length with section modulus of 2500 cm$^3$/m a hammer with a centrifugal force of 2300 kN is required. (CUR, 2012)

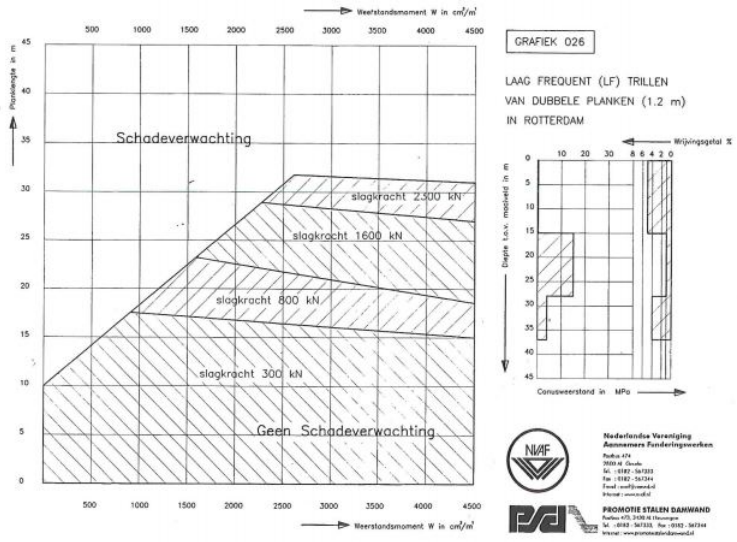


Figure 4.1: NVAF-PSD design chart of Rotterdam (CUR, 2012)

## 4.3. Numerical methods

In this section four methods are discussed that predict driveability of specifically sheet piles. These methods take into account all important elements of a pile driving system; pile, hammer and soil.

### 4.3.1. Vibdrive

The Vibdrive takes into account two soil-related phenomena that alter the characteristics of initial shear strength:

- **Fluidisation** The cyclic motion of grain particles due to vibratory accelerations
- **Liquefaction** The induced pore-pressure build up

The residual shear strength is given by the following formulas:

$$q_l = q_s[(1-\psi)e^{\frac{-1}{FR}} + \psi] \tag{4.4}$$

$$q_d = (1-e^{-\alpha})q_l + q_s \cdot e^{-\alpha} \tag{4.5}$$

$$\tau_l = \tau_s[(1-\psi)e^{\frac{-1}{FR}} + \psi] \tag{4.6}$$

$$\tau_d = (1-e^{-\alpha})\tau_l + \tau_s \cdot e^{-\alpha} \tag{4.7}$$

where

| | | |
|---|---|---|
| $q_d$ | = | vibratory toe resistance [MPa] |
| $q_l$ | = | liquefied toe resistance [MPa] |
| $q_s$ | = | static toe resistance (CPT) [MPa] |
| $\tau_d$ | = | vibratory shaft resistance [kPa] |
| $\tau_l$ | = | liquefied shaft resistance [kPa] |
| $\tau_s$ | = | static shaft resistance (CPT) [kPa] |
| $\psi$ | = | empirical liquefaction factor ($4<(1/\psi)<10$)[−] |
| $FR$ | = | friction ratio [%] |
| $\alpha$ | = | degree of acceleration (a/g) [-] |

Vibratory toe and shaft resistance is calculated by respectively the product of $q_d$ and perimeter area and the product of $\tau_d$ and cross-sectional area. The dynamic mass is considered as a rigid body and is dealt with by Newton's second law. This is shown in figure 4.2, where the following parameters are used:

$m_0$ = bias mass [kN]
$m_v$ = mass of exciter block [kN]
$m_p$ = mass of sheet pile [kN]
$F_v$ = centrifugal force [kN]
$R_s$ = shaft resistance [kN]
$R_c$ = clutch friction [kN]
$R_t$ = toe resistance [kN]

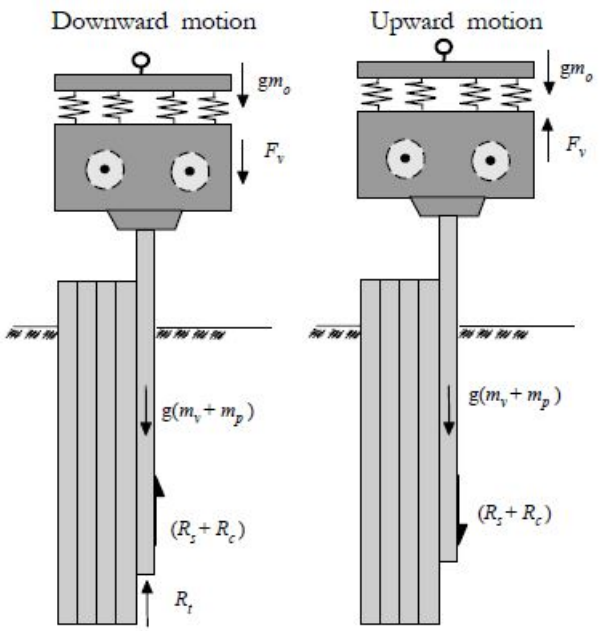


Figure 4.2: Vibdrive model (de Cock, 1998)

### 4.3.2. Vipere

The Vipere model assumes that vibrations propagate in a cylindrical symmetrical way and that these are only in vertical direction. The sheet pile is schematized as rigid cilinder. The soil resistance is based on the CPT results. The soil is modeled by cylinder which are interconnected with springs, see figure 4.3. The damping of the shaft only takes place at the widest cylinder. It is not clear how laboratory test results of soil damping can be transformed to this model.

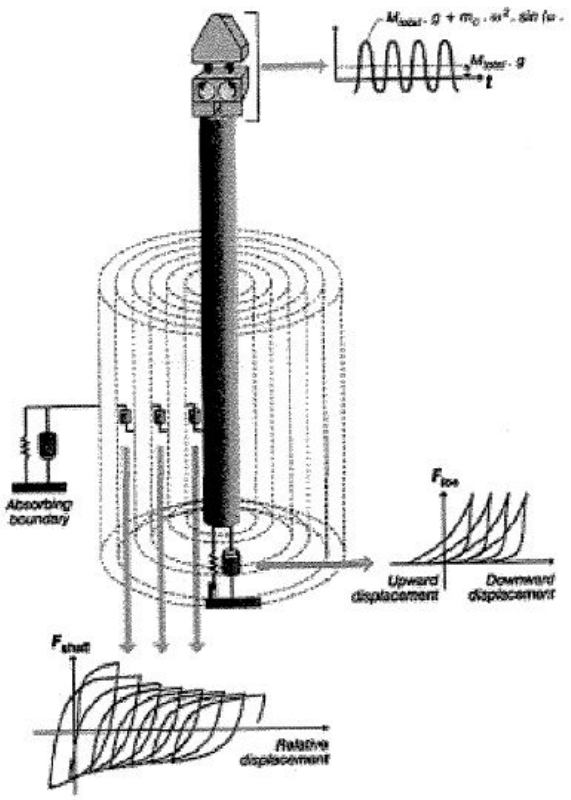


Figure 4.3: Vipere model (Van den Berghe, 2001)

### 4.3.3. Smith model

#### Method

E.A.L. Smith was the first to use the one-dimensional wave equation for pile driving analysis. Prior to that, analyses were carried out using pile driving formulas, which were based on rigid body mechanics. The method by Smith is based on discrete element idealization of the actual hammer-pile-driving system as shown in figure 4.4. All parts involved are represented as a series of weights and springs. The time during which the action occurs is divided into small time intervals. In this way a mathematical determination may be made of stresses, pile penetration blow or permanent set per blow, against any amount or kind of ground resistance. The ram, hammer cushion, pile helmet, pile cushion and pile are shown in figure 4.4 as appropriate discrete weights and springs. The distributed mass of the pile is divided into a number of concentrated weights, which are connected by weightless springs. The frictional soil resistance on the side of the pile is represented by a series of side springs; the point resistance is accounted for by a single spring at the point of the pile. (Smith, 1960)

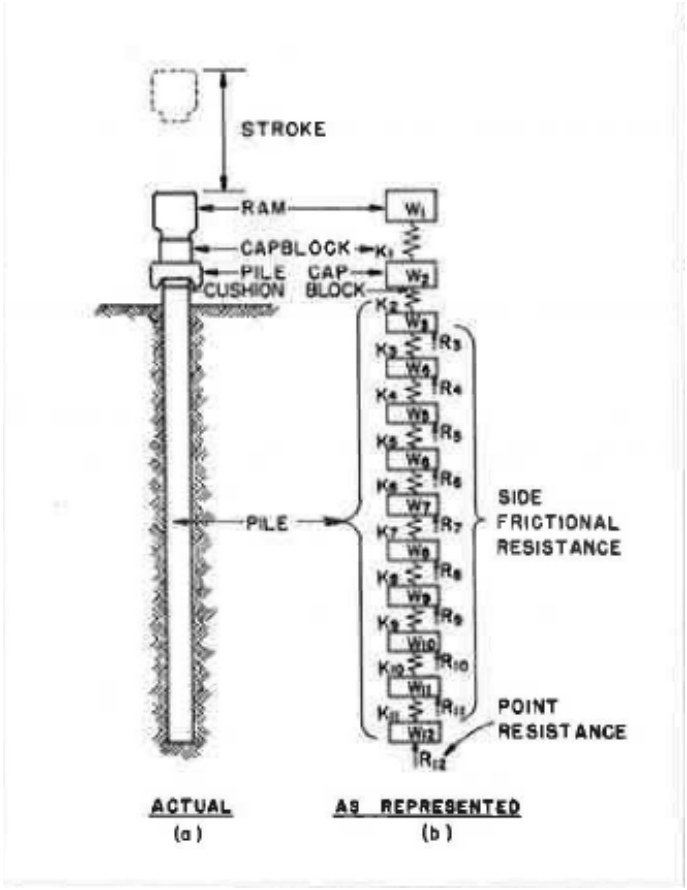


Figure 4.4: Model of the pile system (Smith, 1960)

### Load-deformation properties

The resistance to dynamic loading afforded by the soil in shear along the outer surface of the pile and in bearing at the point of the pile is extremely complex. Figure 4.5a shows the load-deformation characteristics that the soil is assumed to have, exclusive of damping effects. The path OABCDEFG represents loading and unloading in side friction. For the point, only compressive loading may take place and the loading and unloading path would be along OABCFG. These characteristics are defined essentially by the quantities $Q$ and $R_u$. $Q$ and $R_u$ are respectively the elastic ground deformation or quake and the ultimate ground resistance.

The introduction of a dashpot results in a modified load-deformation curve, see figure 4.5b. The magnitude of this dashpot is expressed by Smith damping constant, $J$. The product $Jv$ is used to increase the ground resistance so as to produce damping. The damping coefficient is assumed to be constant for a given soil under given conditions. Just like the static shear strength of the soil from which $R_u$ on a pile segment is determined. It should be kept in mind that at the tip of the pile the soil is loaded in compression or bearing. The damping coefficient in bearing is assumed to be larger than the damping coefficient in friction along the side of the pile. The total soil resistance to plastic deformation is given by:

$$R_t = R_u(1 + Jv_p) \tag{4.8}$$

where

| | | |
|---|---|---|
| $R_t$ | = | Total soil resistance [kN] |
| $R_u$ | = | Ultimate soil resistance of spring [kN] |
| $J$ | = | Smith damping constant [s/m] |
| $v_p$ | = | pile velocity [m/s] |

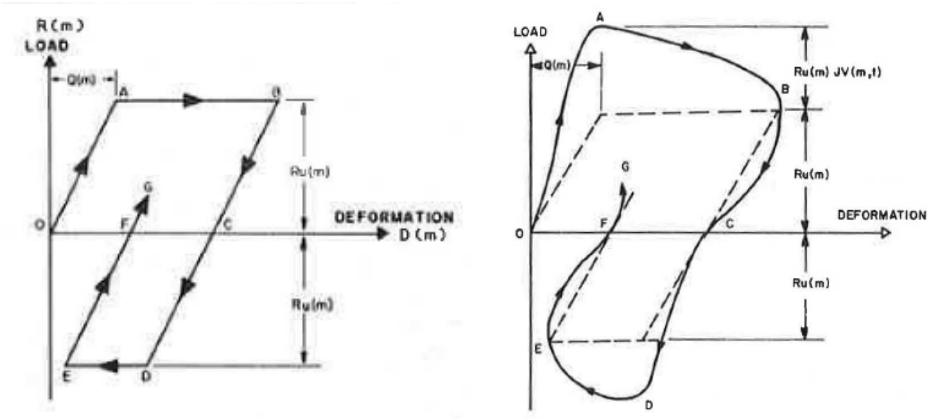


(a) Without damping (b) With damping

Figure 4.5: Load-deformation characteristics (Hirsch et al., 1970)

The behaviour of the soil can be described by a mechanical (rheological) model as shown in figure 4.6. Due to the applied load the spring will want to stretch, but is held back by the dashpot, which cannot react immediately. Since the spring does not change length, the stress is initially taken up by the dashpot. The friction link limits the load in the spring. This results in plastic deformation when the elastic resistance is exceeded.

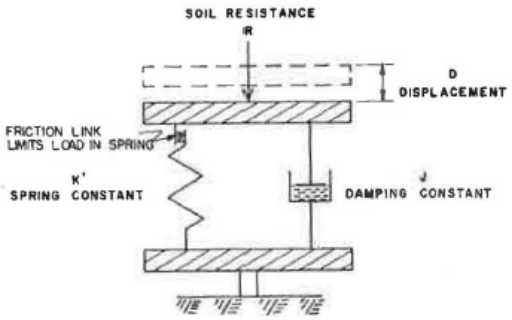


Figure 4.6: Rheological model describing soil resistance (Hirsch et al., 1970)

### 4.3.4. TNOWAVE

In the 1960's TNO, the second largest R&D organization in Europe, started basic research in the area of pile foundations. TNO wanted to develop its own wave equation program; TNOWAVE. It was considered to use Smith's algorithm, which gives a theoretical solution by solving the differential equations by numerical integration, as the basis for such a program, Eventually, it was decided to use the method of characteristics instead (De Saint-Venant, 1867). In the United States WEAP was developed parallel under sponsorship of the Federal Highway Administration (Hussein et al., 1988).

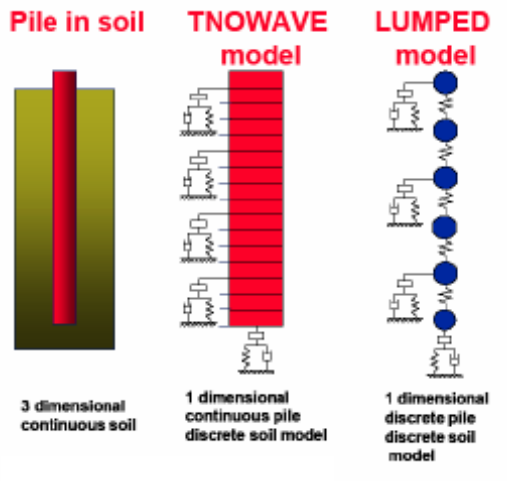


Figure 4.7: Wave equation pile models (Middendorp, 2004)

A general feature of wave phenomena is the transmission of information and energy through a physical system at a finite speed. The so-called method of characteristics lends itself particularly well for this purpose because it makes clear how the disturbances travel through the system, and it enables their computation. The choice for this method by the creators of TNOWAVE is based on the following reasons:

- The elegance of the method;
- The insight it gives in wave mechanics;
- The lack of numerical stability problems.

The method is based on the phenomenon that stress waves in a frictionless pile propagate unaltered with a characteristic velocity. In 1974 the method was extended to piles with skin friction and toe resistance by Voitus van Hamme. He assumed that the skin friction, which in reality acts continuously along the pile, can be substituted by skin friction acting at discrete points along the pile. Between two of these points, the pile remains frictionless and so the propagation of the waves will be undisturbed, as in a free rod. The pile model of TNOWAVE is shown in figure 4.7 Hence waves leaving at one of the the discrete points will propagate undisturbed to the next discrete point. Arriving at the discrete points, a part of the wave will be transmitted, and the other part reflected. The magnitude of transmitted and reflected waves depends on the pile properties and the skin friction. The equations for transmitted and reflected waves are derived from the fulfillment of equilibrium and continuity conditions at the discrete point. The obtained equations are presented below and are visualized in figure 4.8. In figure 4.9 the successive propagation of waves in time is shown. In this figure $\Delta l$ and $\Delta t$ are equal to figure 4.8.

$$f^{-}_{n,i} = f^{+} \cdot -\frac{Z_N - Z_{N+1}}{Z_N + Z_{N+1}} + (2 \cdot f^{-} - W_{n,i-1}) \cdot \frac{Z_N}{Z_N + Z_{N+1}} \tag{4.9}$$

$$f^{+}_{n,i} = f^{-} \cdot \frac{Z_N - Z_{N+1}}{Z_N + Z_{N+1}} + (2 \cdot f^{+} + W_{n,i-1}) \cdot \frac{Z_{N+1}}{Z_N + Z_{N+1}} \tag{4.10}$$

where

| | | |
|---|---|---|
| $f^{+}$ | = | incident downward travelling wave (=$f^{+}_{n-1,i-1}$) |
| $f^{-}$ | = | incident upward travelling wave (=$f^{-}_{n+1,i-1}$) |
| $f^{+}_{n,i}$ | = | transmitted downward travelling wave |
| $f^{-}_{n,i}$ | = | transmitted upward travelling wave |
| $Z_N$ | = | impedance of pile element N [kNs/m] |
| $Z_{N+1}$ | = | impedance of pile element N+1 [kNs/m] |
| $W_{n,i-1}$ | = | friction force acting on node N [kN] |
| $n$ | = | discrete point or node number |
| $N$ | = | pile element number |
| $i$ | = | time step number |

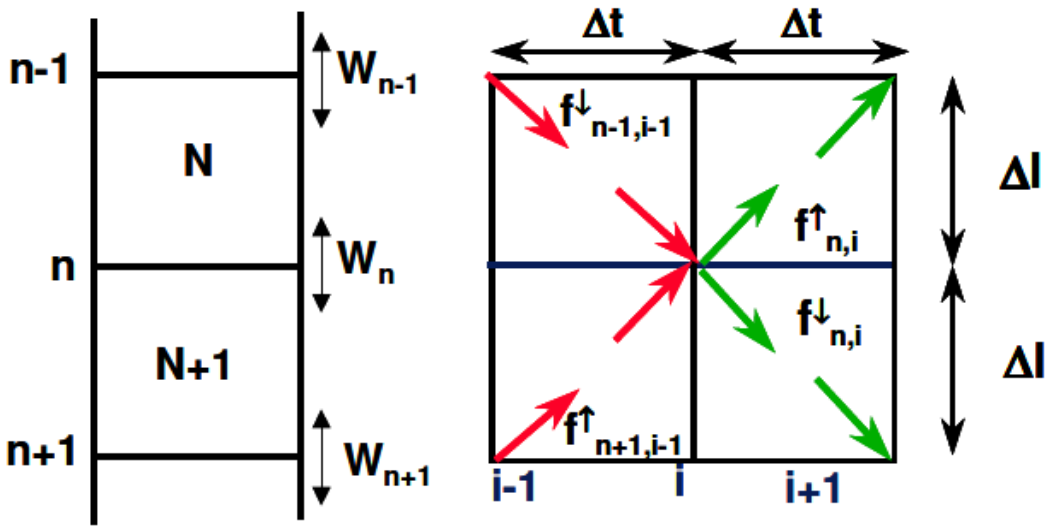


Figure 4.8: TNOWAVE algorithm (Middendorp, 2004)

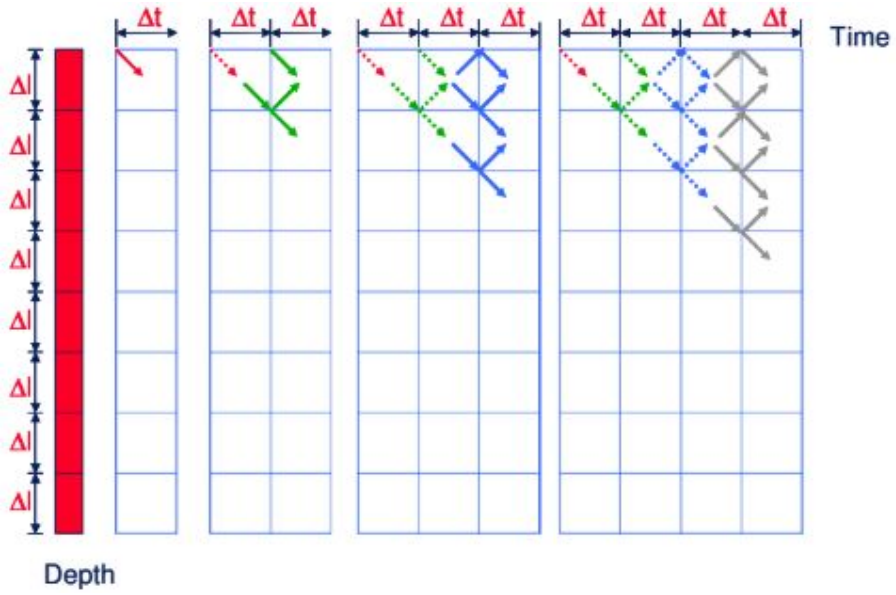


Figure 4.9: Successive propagation of waves in time (Middendorp, 2004)

The TNOWAVE model for vibro driveability is shown in figure 4.10. The continuous soil friction is replaced by a number of concentrated frictional forces. The vibro hammer is rigidly connected to the pile. The applied force is of sinusoidal shape.

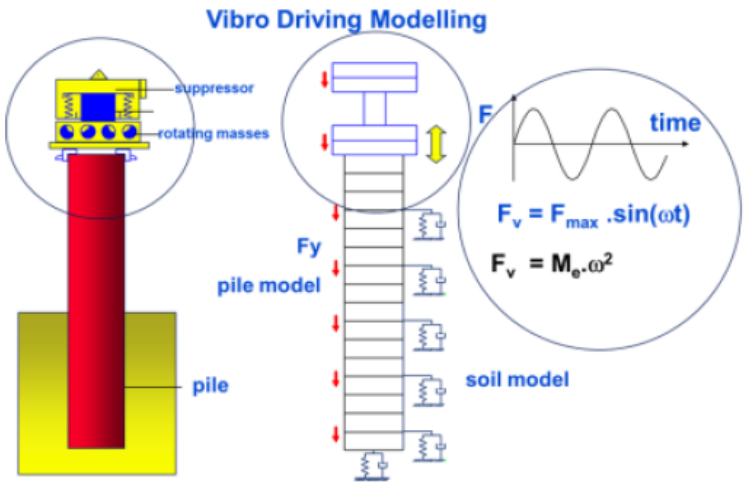


Figure 4.10: Vibro driveability model set up (Middendorp and Verbeek, 2012)

### Soil behaviour

The spring-damper system as used by Smith model (figure 4.6) is also used to model the soil resistance in the TNOWAVE software. However, in the Smith model dynamic and static resistance are coupled by factor $J$ whilst in TNOWAVE the damping is modeled as an independent factor. The soil fatigue is modeled by a $\beta$-factor. The following sections elaborate on how is dealt with damping and fatigue in TNOWAVE.

### TNOWAVE damping

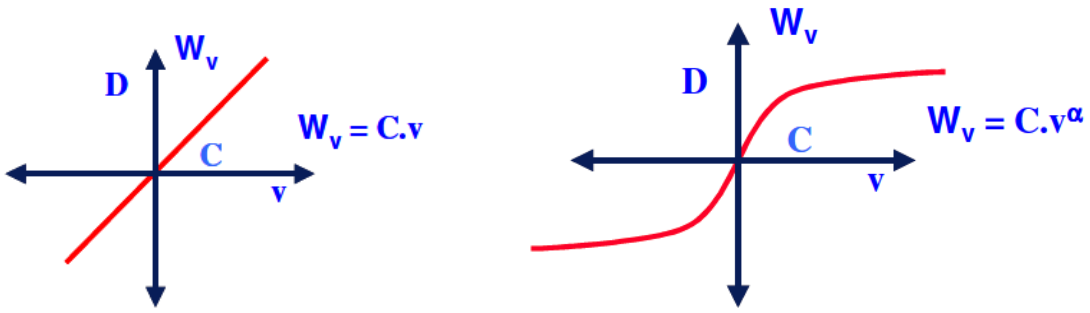


(a) Linear damper model

(b) Exponential damper model

Figure 4.11: Damper models (Middendorp, 2004)

Analogous to equation 4.8 the total resistance consists of static and dynamic resistance in the TNOWAVE model. However, the dynamic resistance is not coupled to the static resistance:

$$R_t = R_s + C v^{\alpha} \tag{4.11}$$

where
$C$ = damping constant [Ns/m]
$\alpha$ = damping exponent [-]

The following formulas are proposed for damping constant at respectively shaft and toe (Moscoso, 2018):

$$C = \sqrt{G \cdot \rho} \tag{4.12}$$

$$C = \frac{1.09 \cdot \sqrt{G \cdot \rho}}{1 - \nu} \tag{4.13}$$

where
G = shear modulus [MPa]
$\rho$ = soil density [kg/m$^3$]
$\nu$ = Poisson's ratio [-]

The shear modulus (G) is linked to the cone resistance ($q_c$) by the following formula:

$$G = 10 \cdot q_c^{0.61} \tag{4.14}$$

For $\alpha = 1$, a linear (viscous) damping is generated while for $\alpha < 1$ a parabolic one is generated. $\alpha$-values of 1 (figure 5.9a) and 0.2 (figure 5.9b) are used for respectively clay and sand by Allnamics. In other literature the $\alpha$-value for clay vary from 0.17 to 0.32 (Moscoso, 2018).

### 4.3.5. $\beta$-method

Cyclic loading stresses the soil periodically, reducing its resistance at each applied cycle, see figure 4.12. A loaded soil has a particular initial yield stress, $F_{initial}$. When several loading cycles are applied to a soil, a change in its microstructure will occur. This hysteresis behaviour will decrease from initial yield stress to a residual one, $F_{residual}$, quantified by the $\beta$-factor, thus: (Jonker, 1987)

$$\beta = \frac{F_{residual}}{F_{initial}} [-] \tag{4.15}$$

The $\beta$-factors are based on a microscopic scale:

- Angular particles interact between them with higher friction. When cyclically loaded, higher $\beta$-factors than rounded particles will be in place. Thus high roundness should be related to a high liquefaction potential, and therefore to low $\beta$-values.
- Cohesion will be directly correlated to the $\beta$-factor. By maintaining contact between particles, higher $\beta$-factors will be in place, especially for clays.

Those microscopic phenomena, defined by particle shape and size parameters, will define the macroscopic response of a cyclically loaded soil. Some proposed values can be seen in table 4.1

| Type of soil | Fatigue factor $\beta$ |
|---|---|
| Round coarse sand | 0.10 |
| Soft loam/Marl, Soft Loess, Stiff Silt | 0.12 |
| Round Medium Sand, Round Gravel | 0.15 |
| Fine Angular Gravel, Angular Loam, Angular Loess | 0.18 |
| Round Fine Sand | 0.20 |
| Angular Sand, Coarse Gravel | 0.25 |
| Angular/Dry Fine Sand | 0.35 |
| Marl, Stiff/Very Stiff Clay | 0.40 |

Table 4.1: $\beta$-factor values for different soil types, (Tara et al., 2014)

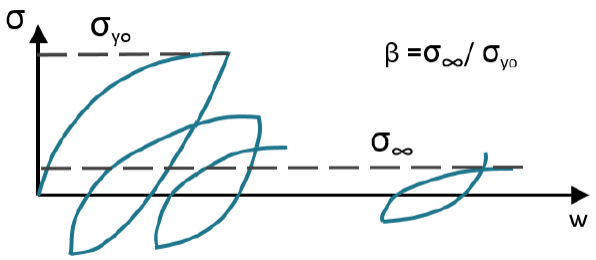


Figure 4.12: Soil fatigue model (Tara et al., 2014)

Vibratory hammers typically operate in the range of 20 to 40 Hz. As such, soil situated along a pile shaft can be subjected to a very high number of cycles in a matter of a few minutes. Therefore, $\beta$-factor is usually considered as a constant due to high frequencies. (Tara et al., 2014)

Very few investigations have been carried out to quantify the $\beta$-factors. The factors may differ for open and closed end piles. Also $\beta$-values may be different for driving and extraction conditions and $\beta_o$ (outside) and $\beta_i$ (inside) may differ in the same layer (Jonker, 1987).

Compared to other methods to take fatigue into account, this method is very simple as only one factor is used. This gives room to use other research to quantify the $\beta$-factor. For example, Alm & Hamre have done extensive research on this topic (Alm and Hamre, 2001).

## 4.4. Conclusion

In this chapter is elaborated on various methods to predict driveability. These methods vary in complexity; from empirical formulas to numerical methods. Some methods are specifically designed for vibro-driving of sheet piles. Other methods are more general and also be applied to impact driving.

Most driveability prediction methods are empirically determined. However, some numerical methods consider the physical mechanisms that occur during the pile driving process. These physical mechanisms are described in the previous chapter. These comprise amongst others wave propagation in the pile and soil fatigue. It is essential that all pile driving system elements (pile, hammer and soil) are described in a driveability model.

Numerical methods are able to consider the geotechnical data in a continuous vertical profile in the form of a CPT. Empirical formulas are only able to use a limited number of parameters to describe the soil. It is essential to incorporate soil properties as accurate as possible.

The probabilistic model, which is developed in this thesis, is based on the Allwave-PDP software. This software uses the TNOWAVE method. Therefore, the functioning of TNOWAVE is elaborately explained. This method is selected because the commercial software was accessible by the author in contrast to other numerical prediction methods. Next to that, this method is well-documented and relevant mechanisms are described correctly. In engineering practice Allwave-PDP is one the most widely accepted and advanced driveability prediction methods.

# 5

# Stochastic model parameters

In this chapter is described how stochastic model parameters for the pile driving system (pile, hammer and soil) are established. In a stochastic model parameter the variability must be quantified. The variability of hammer and pile parameters can be defined straightforward as these parameters are so-called point statistics (section 5.1). The soil parameters are more complex to define due to their one-dimensional character. The variability of these parameters is caused by transformation uncertainty (section 5.2) and soil heterogeneity (section 5.3). It is explained how the variability is incorporated in the one-dimensional profile of each soil model parameter (section 5.4).

## 5.1. Point statistics

Pile and hammer properties are modelled as point statistics. This means that these properties are spatially independent. A mean and a standard deviation describe the variation of these properties. In this section is elaborated on the variation of the point statistics.

### 5.1.1. Hammer

A vibro hammer is defined by various properties. These are static properties (e.g. geometry and weight) and dynamic properties (e.g. frequency and amplitude). The static properties are unlikely to vary throughout the driving process. For example, the eccentric moment, which is defined by geometry and weight of eccentric masses, can only vary due to damage or wear and tear. Next to that, vibro hammers are manufactured under strict tolerances. Therefore, the static properties are assumed to be deterministic properties. The static mass is an exception to this. This property is defined as the mass that does not move in the same axial direction as the pile. Due to the effect of hook load and driving speed on the static mass, its value is hard to define. In this section is explained how this property will be incorporated in the probabilistic method.

Dynamic properties of the hammer are influenced by the soil resistance. As soil resistance varies largely throughout the driving process, dynamic properties also vary significantly. Frequency is the only dynamic property used as an input parameter. Namely, amplitude and driving force of the hammer are a function of frequency and not an input parameter. In this section is discussed how frequency will be incorporated in the probabilistic method.

#### Frequency

Frequency reduces during driving due to inertial resistance from the pile and due to soil resistance. Due to high resistance, hydraulic flow is reduced by an overflow valve and reduces frequency. In literature is stated that frequency will turn out to be 5 to 10 percent lower than the maximum frequency given by the manufacturer. To find out how this process evolves and to what extent reduction takes place, measurements are done at a project of Hakkers B.V. This project takes place in Den Oever, Netherlands. A sheet pile wall had to be driven in heavily overconsolidated sandy soils. This resulted in hard driving conditions. Vibration sensors are attached to nearby buildings to measure vibrations caused by pile driving activities.

The sensors measure the dominant frequency and vibration velocity every 5 second interval. The vibration velocity is related to soil resistance. Namely, when soil resistance increases more soil is brought into vibratory

movement. This movement results in a measured vibration velocity. The causal relationship might also be explained by resonance phenomena. Namely, a lower frequency might be closer to the natural frequency of the building. In this case a lower frequency will result in a higher vibration velocity. However, explaining the causal relationship by resonance phenomena is illogical as frequency drops near end of driving when soil resistance is highest. In figure 5.1 vibration velocity and frequency are plotted against time. In this example relifting is applied twice (at 9:02:30 and 9:03:20). Near end of driving the relation between vibration velocity and frequency becomes unclear. This might be caused by turning off the hammer or because the pile is relifted to place the sheet pile at precise depth.

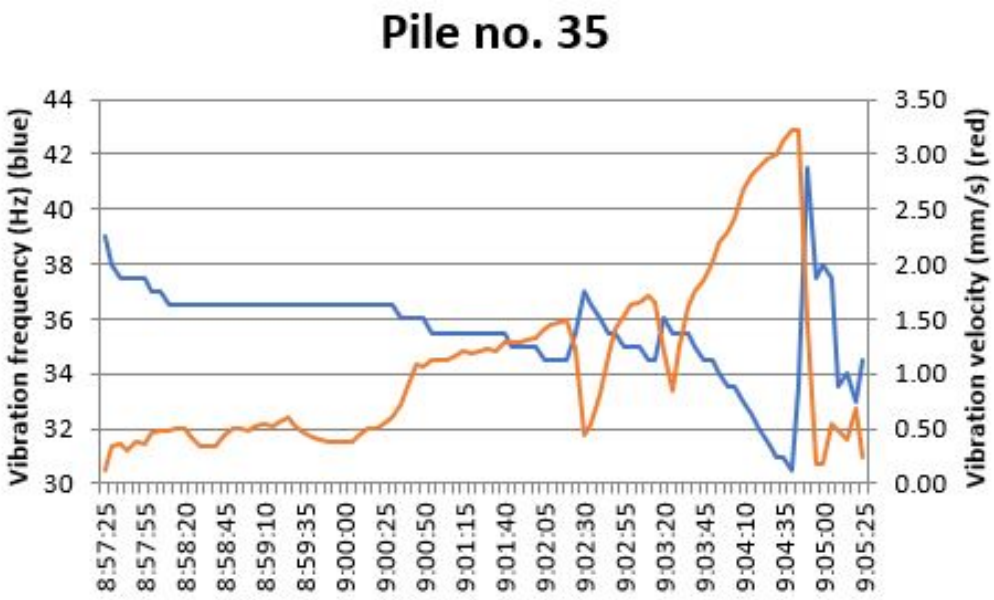


Figure 5.1: Vibration velocity/frequency-time-graph

In annex C vibration velocity and frequency are plotted against time for 38 piles. Various results are found after analysis of this data. The measured frequency has a mean of 36.1 Hz and a standard deviation of 1.4 Hz, see also the histogram in figure 5.2. A strong, negative correlation between vibration velocity and frequency is found. A Pearson's correlation coefficient of -0.70 is found for the full driving time. When the last 15 seconds are left out of the data, the correlation is stronger (-0.78). During the last 15 seconds of driving the relation between frequency and vibration velocity becomes unclear. Possibly the crane operator is lifting the pile to a specific level or the vibro hammer is turned off.

A strong correlation between frequency and soil resistance is found. However, Allwave-PDP has no feature to relate soil resistance and frequency and only uses a single value input for frequency. Therefore, a representative deterministic value is selected from the measured data. Based on results of the measurements, as shown in figure 5.2, a frequency of 36 Hz is chosen as deterministic value for pile driveability predictions. Although lower frequencies than 36 Hz are measured, it is reasonable to assume 36 Hz. This is because the crane operator often re-lifts the pile at a low frequency. This lets the hammer regain driving force. The default frequency of the hammer used in project in Den Oever is 38.3 Hz (2,300 rpm). This means that frequency is reduced by 6%.

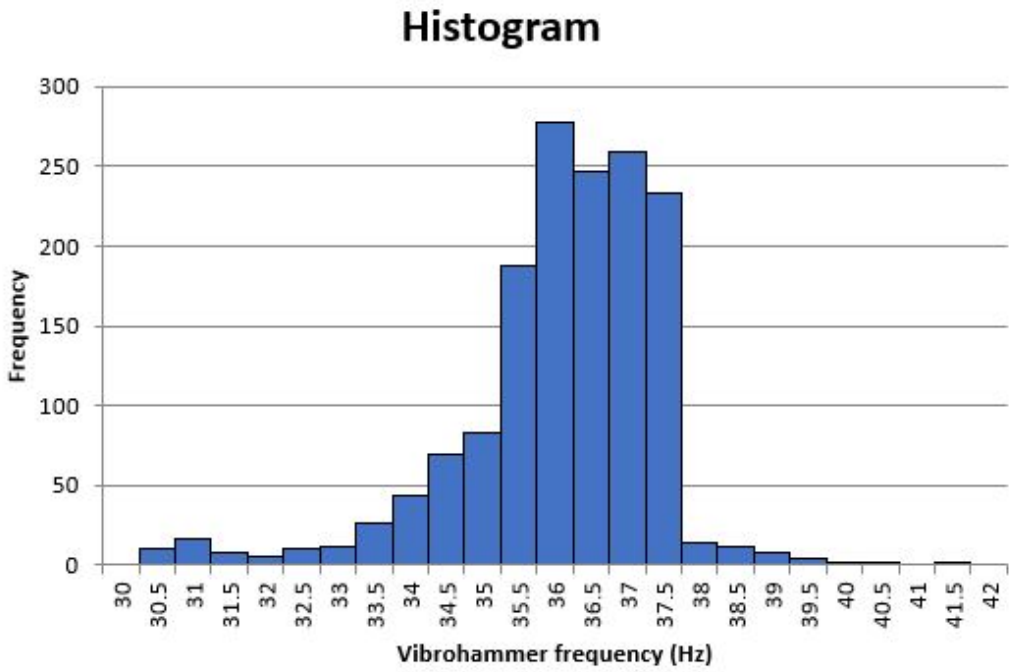


Figure 5.2: Vibro hammer frequency histogram (1 count is 5 s interval)

### Static mass

The static mass is the non-vibrating part of the vibro hammer. By springs vibratory movement is isolated in this part of the hammer. The static mass is connected to the dynamic system (dynamic part of hammer and pile) on the bottom side of the static part. The crane's hook is connected to the upper part of the static part. Weight of the static mass is distributed over the crane's hook and dynamic system. Loading of the dynamic system by a static mass is advantageous to driveability.

The distribution of the static mass over the crane's hook and dynamic system depends on the penetration speed and crane operator's behaviour. The crane operator is able to release the hook, so that the cable is not under tension, see also figure 5.3. This is observed at a project of Hakkers B.V.. Tensioning of the cable can only be prevented to a certain extent. If the sheet pile's driving speed is too high, the winch of the crane cannot keep up with the speed. Therefore, the static mass is most likely fully applied to the dynamic system towards the end of the driving process. In this stage of the process driving speed is lowest. This is also shown in figure 5.4. The so-called holding back force is measured by a force transducer installed in the crane hook. This force must be subtracted from the total static mass to obtain the static mass applied to the dynamic system. The graph shows the driving time and holding back force during installation of a sheet pile AZ26-700N of 22 meter length by vibro hammer PVE 40VM (Denies et al., 2017). It can be concluded that at the start of driving free sinking is prevented by the hook load. Near the end of driving free sinking is prevented by soil resistance. In the middle of the driving process both soil resistance and hook load are low, which results in a high penetration speed.

The full static mass is applied to the dynamic system in critical driving conditions. This is concluded from observations and measurements on the static mass. The probabilistic driveability method is intended to predict refusal. Thus, it is a logical step to model conditions in a refusal or near-refusal situation. As penetration speed in this situation is low, the full static mass is applied to the dynamic system.

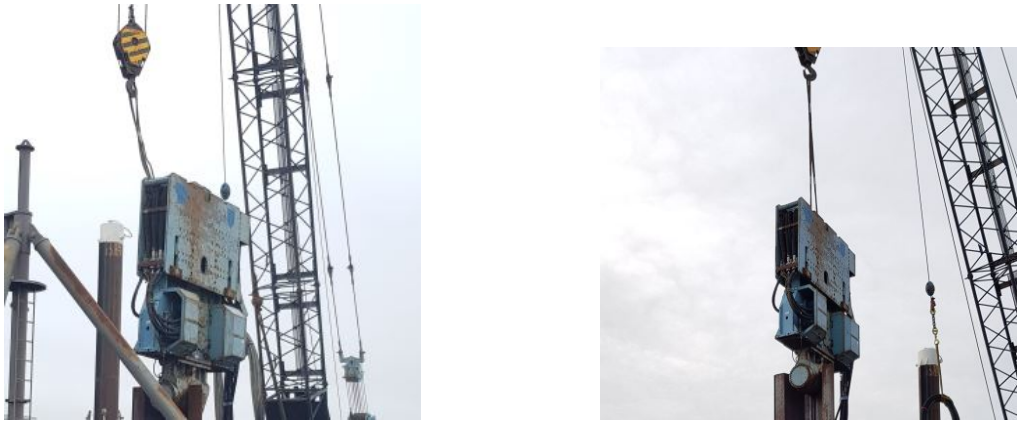

(a) No hook load (b) Hook load present

Figure 5.3: Static mass

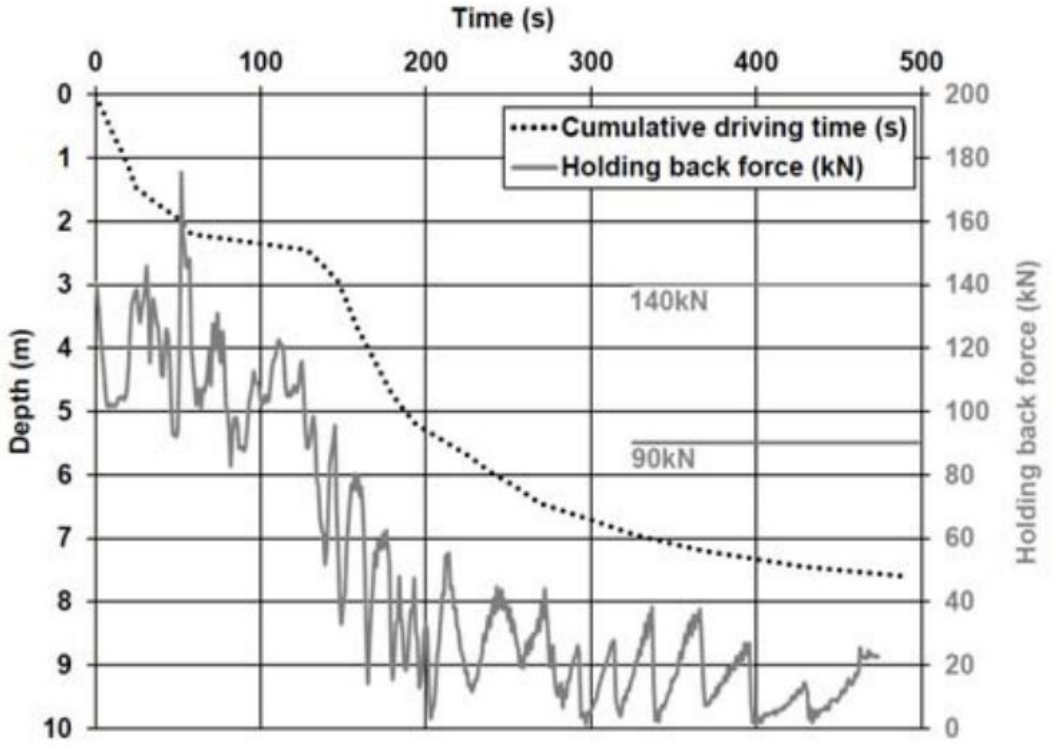


Figure 5.4: Influence of the hook load force on the shape of the penetration log (Denies et al., 2017)

### 5.1.2. Pile

#### Dimensions

In Eurocode 3 coefficients of variation (COV) for geometric and material properties of structural steel are respectively valued as 0.07 and 0.03. All variables are assumed to approximate a log-normal distribution and it is assumed that no correlation exists between variables. Experiments have shown that variation adopted in Eurocode 3 is conservative (Byfield and Nethercot, 1997). In this research pile property variation is neglected. As manufactured materials can be controlled within a narrow range, it is a reasonable assumption to neglect this variation (Phoon et al., 2016). Especially when compared to the magnitude of variation of soil properties.

#### Interlock friction

Interlock (clutch) of two jointed steel sheet piles needs to be considered when driving sheet piles. Publications and documented knowledge about effects of interlock friction remain rather limited at present. From experiments

on interlock friction some conclusions can be drawn (Van den Berghe, 2001). The time needed to drive the sheet pile into dry sand has a considerable influence on the shear resistance developed in the interlock. The longer the driving, the greater the amount of sand that is found into the clutch. Interlock resistance is found to be reduced to about 80% when the sheet pile specimen was installed in saturated sand. It is believed that liquefaction, developed during installation, caused sand grains to be more mobile and thus able to avoid being jammed into the interlock. Geometrical shape and size of the interlock gaps (figure 5.5) determine the degree of water tightness. A high degree of water tightness minimizes undesirable presence of grains in the interlock gap.

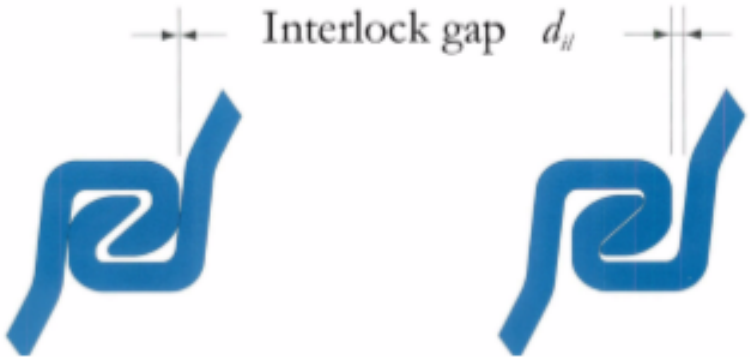


Figure 5.5: Interlock gap (Viking, 2002)

Experimental results show that quasi-static amplitude values of interlock friction varied between 2-20 kN/m (Van den Berghe, 2001). Another work on this subject, states that the dynamic interlock resistance can be set to 1.0 kN/m, based on the results of experience (Ferron, 2001). Both investigations have been done in close co-operation with Arbed, a sheet pile producer. Dynamic interlock resistance is more relevant to installation practice than quasi-static resistance. Therefore, a value of 1.0 kN/m is used in this research. However, it is important to make an informed decision on interlock resistance based on local conditions. Not solely presence of grains determines interlock friction force that develops. Presence of impurities (such as corrosion) together with permanent deformations of brand new profiles (due to incorrect storage or handling) may also generate non-negligible unfavourable developments of interlock friction. (Viking, 2002)

Pile driveability software appears to be insensitive to interlock friction. This was concluded after making various predictions with varying values for interlock friction resistance. Even when interlock friction resistance was set higher than total centrifugal force of the vibro hammer, not even a slight reduction was noticed in penetration speed. Therefore interlock friction is not accounted for in this research.

## 5.2. Transformation variability

A transformation model relates a field measurement (e.g. cone resistance) to a design property (e.g. toe damping). In a typical project field measurements are made by a CPT. This measurement gives a vertical, continuous soil profile of mechanical shaft and toe resistance. The driving process is a system where dynamic and inertial resistance play a role as respectively velocity and acceleration are involved. Next to that the loading is cyclic. This implies that soil resistance decreases during driving due to fatigue. Soil model parameters that describe these properties cannot be directly measured by a CPT. Transformation models have been established to find a value for soil model parameters based on field measurements. Transformation models are found by laboratory experiments or matching of predictions and practice (postdictions). The spread of results of these experiments and postdictions is not taken into account as only a best estimate of results is used in driveability predictions. Furthermore, experiments and postdictions are always a limited representation of soil properties. Therefore, variation in practice will be larger than found in experiments and postdictions.

In this section the transformation model of each soil parameter is described. Consequently, literature is investigated to find statistics on the transformation model. This results in a model error expressed as a coefficient of variation (COV). This error is taken into account in a later stage by multiplying soil parameter values by a randomly sampled value ($N(1, COV)$). Transformation variability is investigated for four soil parameters:

- Quake

- $\beta$-factor
- Damping constant
- Damping exponent

There are additional soil parameters which can be specified in Allwave-PDP. Yield factor is the relation between the plastic value of a spring in compression and tension. This soil parameter is a parameter specifically used in Allwave-PDP. Due to limited information on this parameter, it is taken as a deterministic value. Another parameter, added mass, has a default value of zero. In a typical driveability prediction this default values is used to model the pile's behaviour. Therefore, this soil parameter is not taken into account in this research.

### 5.2.1. Quake model

Quake defines the elastic range of the spring in the soil model. When relative displacement between soil and pile is larger than the quake value, the spring behaves plastically. Loading and unloading quake are dealt with in the same section. In figure 5.6 loading and unloading quake are indicated by respectively $u_{q1}$ and $u_{q2}$. In Allwave-PDP a value of 2 mm is adopted for quake. In case of jumps in cone resistance, quake is larger.

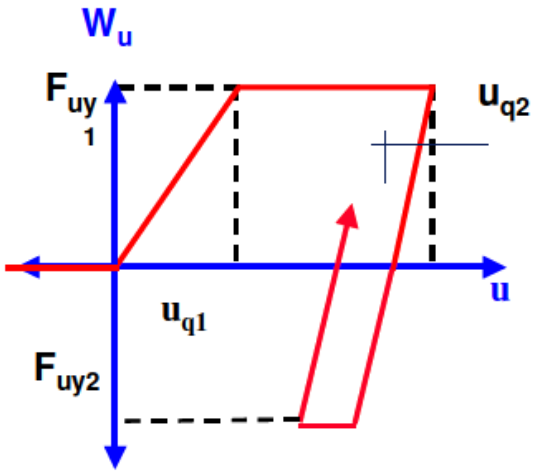


Figure 5.6: Displacement dependent soil model (Middendorp, 2004)

### 5.2.2. Quake variability

Literature on quake values found in vibratory driving measurements is scarce. Therefore, impact driving measurements are used to find variability of quake values. In Allwave-PDP the default value (2 mm) for quake in vibratory driving is copied from impact driving conditions. Loading and unloading quake are discussed in the same section. In this research will be assumed that no correlation exists between loading and unloading quake.

**McVay & Kuo, 1999** A pile database from University of Florida is used as a primary source. The database contains information on pile length and diameter, hammer data, soil properties and driving records. Soil properties include weighted average SPT N-value along pile shaft and at pile tip. Quake and Smith damping are back-calculated by signal-matching analysis (CAPWAP). Scatter found in quake is very wide. Quake is measured at the end of driving (EOD) and beginning of redriving (BOR), see also table 5.1.

Vibratory driving usually does not take place in limestone soils as this soil type is easier to penetrate by impact driving. This research analyses only driveability of closed-ended piles. Toe quake is usually a function of pile diameter for closed-ended piles. This cannot be applied to sheet piles. Only skin quake variability will be derived from this paper.

In Allwave-PDP the quake value is not dependent on soil type. Therefore, the calculated skin quake values are not split out to cohesive or non-cohesive soil types. It is assumed that the measured values represent a 95% confidence interval. Thus boundaries of the confidence interval are 0.5 - 5.1, considering both cohesive and non-cohesive

soil types. Standard deviation and mean are determined as respectively 1.15 and 2.8. This leads to a COV of 41%. (McVay and Kuo, 1999)

| | Non-cohesive | Cohesive | Limestone |
|---|---|---|---|
| EOD skin quake (mm) | 1.3-4.8 | 0.5-3.6 | 0.7-3.8 |
| BOR skin quake (mm) | 1.4-4.0 | 1.3-5.1 | 0.5-5.1 |

Table 5.1: Skin quake data scatter (McVay and Kuo, 1999)

**Additional literature** One study found that toe quake can reach values up to 20 mm. However, these values were measured on displacement piles, closed-end steel pipe piles and concrete piles. The author of this paper believes that large quakes occur more often than one at first would think. (Authier and Fellenius, 1980)

In a study on the driveability of open-ended pipe piles in offshore conditions also high quake values were found. For the shaft quake GRLWEAP (signal-matching software) recommended values of 2.5 mm were selected. Toe quake in clay deposits was taken as 28.0 mm, while values of 14 mm and 21 mm were selected respectively for sand and silt layers. (Moghaddam et al., 2018)

Dutch CUR handbook 'Hei- en Trilbaarheid palen en damwanden' advises values between 0.0 and 2.5 mm for both shaft and toe quake of steel non-displacement piles, see also table 5.2. If it assumed that the 95% confidence interval is between 0.0 and 2.5, which results in a COV of 50%. (Rooduijn and De Gijt, 2017)

NEN 9997-1 2.4.5.2 table 2.b provides a variation coefficient of 10% for the Young's modulus of soil (NEN, 2017). This parameter defines the relationship between stress and elastic strain. As quake is defined as the elastic range of the soil, the Young's modulus is in some sense analogous to quake.

| Pile type | Property | Location | Unit | Symbol | Sand | Silt | Clay |
|---|---|---|---|---|---|---|---|
| Steel non-displacement | Quake | Shaft | [mm] | $Q_s$ | 0.0-2.5 | 0.0-2.5 | 0.0-2.5 |
| | Damping | Shaft | [s/m] | $J_s$ | 0.15 | 0.15-0.6 | 0.3-0.6 |
| | Quake | Tip | [mm] | $Q_t$ | 0.0-2.5 | 0.0-2.5 | 0.0-2.5 |
| | Damping | Tip | [s/m] | $J_t$ | 0.5 | 0.5 | 0.5 |
| Steel displacement | Quake | Shaft | [mm] | $Q_s$ | 0.0-2.5 | 0.0-2.5 | 0.0-2.5 |
| | Damping | Shaft | [s/m] | $J_s$ | 0.15 | 0.15-0.6 | 0.3-0.6 |
| | Quake | Tip | [mm] | $Q_t$ | 0-1%D | 0-1%D | 0-1%D |
| | Damping | Tip | [s/m] | $J_t$ | 0.5 | 0.5 | 0.5 |
| Concrete displacement | Quake | Shaft | [mm] | $Q_s$ | 0.0-2.5 | 0.0-2.5 | 0.0-2.5 |
| | Damping | Shaft | [s/m] | $J_s$ | 0.15 | 0.15-0.6 | 0.3-0.6 |
| | Quake | Tip | [mm] | $Q_t$ | 0.5-1%D | 0.5-1%D | 0.5-1%D |
| | Damping | Tip | [s/m] | $J_t$ | 0.5 | 0.5 | 0.5 |

Table 5.2: Wave equation parameters (Smith model) (Rooduijn and De Gijt, 2017)

**Conclusion** The research on quake values is limited. Only the research of McVay & Kuo analyses quake values on a large scale. Remaining research only defines quake values with pile driving analysis on case studies. This does not provide statistics on quake values.

Also research of McVay & Kuo has only limited applicability to this research as displacement piles are analyzed. However, shaft friction is largely the same phenomenon in both open and closed-ended pipe piles. Therefore, the COV of 41% is adopted. Mean of shaft quake is taken as 2 mm and adopted from Allwave-PDP as it is believed that the extensive database of Allnamics has led to the most reliable mean value.

In literature high toe quake values, up to 28 mm, are found for specific case studies of displacement piles. However, it is assumed that quake of sheet pile driving is much lower due to the knife-effect of sheet piles.

As statistics on toe quake of open-ended pipe piles or sheet piles cannot be found in literature, the COV of 10% from soil Young's modulus, $E$, in NEN 9997-1 is adopted. The mean is, just like the shaft quake, 2 mm.

### 5.2.3. $\beta$-factor model

The $\beta$-factor of a soil type indicates until what extent soil resistance degrades as a result of vibratory loading. These values are derived from Allwave-PDP software, see table 5.3. The soil type is derived from CPT results of cone tip and shaft resistance based on research by Robertson et al. (1986).

| Soil type | Estimated range of FR | $\beta$-factor shaft | $\beta$-factor toe |
|---|---|---|---|
| Sand | 0-1.1 | 0.10 | 0.50 |
| Silty sand | 1.1-1.8 | 0.18 | 0.40 |
| Loam | 1.8-2.2 | 0.18 | 0.20 |
| Silt | 2.2-2.9 | 0.12 | 0.20 |
| Clay | 2.9-6.1 | 0.40 | 0.20 |
| Peat | >6.1 | 0.12 | 0.12 |

Table 5.3: Allwave-PDP $\beta$-factors

### 5.2.4. $\beta$-factor variability

**Introduction** The $\beta$-factor must be determined both for toe and shaft. These are fundamentally different as toe resistance is overcome by a more complex failure mechanism than shaft resistance. Namely, shaft resistance is overcome by loading along the shear plane between pile and soil. The $\beta$-factor of shaft resistance can simply be calculated by dividing residual/remoulded shear strength by its initial shear strength. Toe resistance is overcome by shear failure of a slip plane of a logarithmic spiral shape. This results in a more complex failure mechanism. Due to high frequency of vibratory hammers it can be assumed that residual shear strength is normative during driving.

In Allwave-PDP $\beta$-factors as shown in table 5.4 are used. These depend on soil type. In Allwave-PDP soil types are automatically selected based on friction ratio (FR). The range is estimated as these values are obtained by reverse engineering.

In general can be stated that shaft fatigue has a larger effect in sandy soils than in clay soils as sand and clay have $\beta$-factors of respectively 0.10 and 0.40. The intermediate soil types, silty sand, loam and silt, have intermediate $\beta$-factors as well.

The effect of fatigue on toe resistance is inverse to that of the shaft; fatigue has a smaller effect on sand than on clay.

Peat, an organic soil, is affected heavily by fatigue both in case of shaft and toe resistance.

| | Estimated range of FR | $\beta$-factor shaft | $\beta$-factor toe |
|---|---|---|---|
| Sand | 0-1.1 | 0.10 | 0.50 |
| Silty sand | 1.1-1.8 | 0.18 | 0.40 |
| Loam | 1.8-2.2 | 0.18 | 0.20 |
| Silt | 2.2-2.9 | 0.12 | 0.20 |
| Clay | 2.9-6.1 | 0.40 | 0.20 |
| Peat | >6.1 | 0.12 | 0.12 |

Table 5.4: Allwave-PDP $\beta$-factors

**Moghaddam, Rausche and Webster, 2018** Traditionally, driving resistance is determined by dividing long-term static resistance by the soil setup factor. For example, if the soil setup factor was 2 then driving resistance was assumed to be 50% of long-term resistance. This approach has been satisfactory for land piles with moderate pile penetrations. Unfortunately, the setup factor was not well defined for marine clays, and varied between 2 and 10. This implies a $\beta$-factor varying between 0.1 and 0.5. Experience in certain geology was needed to select the correct value. (Moghaddam et al., 2018)

**Heerema, 1978** The friction decrease along the pile wall cannot be caused by remoulding only. Also the horizontal stress decrease plays a role. This may be explained to be caused mainly by irregularities of the pile wall

pushing the soil outwards and taking some soil downwards, and by elastic expansion and transverse vibration of the pile. The soil is thus believed to form a temporary horizontal arch around the pile.

**Schneider, 2010** The ratio of end bearing of statically loaded closed ended displacement piles to CPT tip resistance ($q_b/q_t$) is often considered to vary from 0.6 to 1.0. The normalized annular end bearing during installation is estimated to range from 0.35 to 0.55

**Robertson, 2010** Liquefaction can be triggered by both static or cyclic loading. Many papers have been written on liquefaction potential; whether liquefaction occurs or not occurs. Also papers on liquefied residual shear strength have been published. A number of these papers are summarized. In the paper back-calculated liquefied shear strength values are given. A stability analyses was performed considering kinetics of the failure mass Robertson (2010). The best estimates are used to find a stochastic value for the $\beta$-factor. Namely the best estimate is a ratio between initial shear strength and liquefied shear strength. The mean and COV of the best estimates for liquefied residual shear strength are respectively 0.08 and 0.32.

**Yasuhara, 1992** It is generally recognized that clay exhibits a larger resistance to cyclic loading than sand does. This is particularly true for clay in the case of short-term cyclic loading such as in earthquakes. However, once a cyclic load is applied to clay and then continues for a long-term period, the situation becomes different. In case of vibratory driving a large number of loading cycles is applied in a short period. Therefore, strength degradation of clay must be considered.

In clay soils a rise in pore pressure is also measured during cyclic loading. However, this does not directly lead to liquefaction as there is cohesion in clay to prevent this.

Clay behaviour under undrained cyclic loading is more complex than sand behaviour, because of its dependency on such factors as time-dependent creep and preconsolidation periods which can be overlooked for the cyclic behaviour of sand. In spite of there being many case histories for clay which are concerned with settlement and stability induced by cyclic loading situations such as earthquakes, offshore structures under wave actions and road pavements or railway subgrades under traffic loading conditions, few systematic research has been carried out. (Yasuhara et al., 1992)

**Conclusion** Saturated, sandy soils fail solely under the influence of liquefaction. Therefore a COV of 0.32 is selected for the $\beta$-factor of sand is used. In case of clayey soils the cyclic loading behaviour is more complex. In literature no conclusive research on scatter of residual shear strength of clay can be found. The COV of $\beta$-factor for clay is chosen as 0.64, double the magnitude of sand. Namely, it is assumed that a more complex failure mechanism introduces more variability of fatigue. Also the rise in pore pressure impacts the clay, although it cannot solely lead to failure as in the case of sand.

The COV of the $\beta$-factor for the remaining soil types that are used in Allwave-PDP, loam and peat, are classified by linear interpolation. This is shown in figure 5.7 for respectively toe and shaft. Indirectly, the variation becomes larger when Friction Ratio (FR) increases. As FR is a measure for cohesion, liquefaction becomes less influential in more clayey soils.

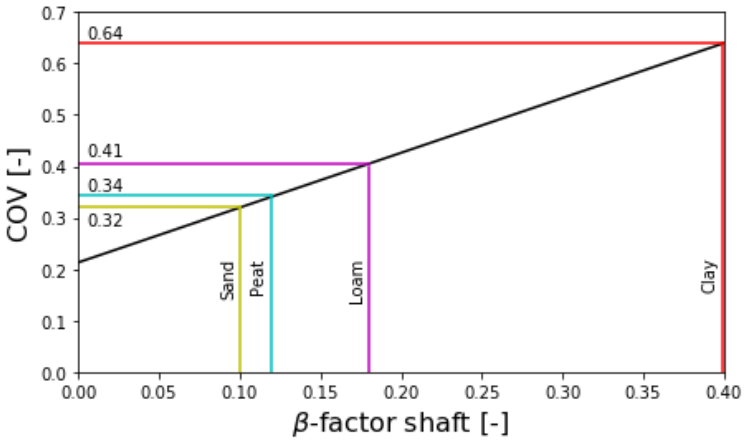


Figure 5.7: Shaft

Figure 5.8: Linear interpolation of $\beta$-factor, COV-plot

For the $\beta$-factor of the toe, even less literature is available. Based on the range found by Schneider, which broadly agrees with the values found in Allwave-PDP, a standard deviation of 0.10 is selected. This implies a COV of 50% for clay and 25% for sand. The remaining soil types are interpolated based on the toe $\beta$-factors

### 5.2.5. Damping model

In Allwave-PDP the damping is not directly related to the static resistance. The following formulas are proposed for damping constant at respectively shaft and toe (Moscoso, 2018):

$$C = \sqrt{G \cdot \rho} \tag{5.1}$$

$$C = \frac{1.09 \cdot \sqrt{G \cdot \rho}}{1 - \nu} \tag{5.2}$$

where

| | | |
|---|---|---|
| G | = | shear modulus [MPa] |
| $\rho$ | = | soil density [kg/m$^3$] |
| $\nu$ | = | Poisson's ratio [-] |

The dry density as used by the Allwave-PDP software is shown in table 5.5.

| Soil type | Dry density [kg/m$^3$] |
|---|---|
| Sand | 2000 |
| Silty sand | 2000 |
| Loam | 1800 |
| Silt | 1800 |
| Clay | 1500 |
| Peat | 1100 |

Table 5.5: Dry density

Based on back-calculation of Allwave-PDP soil model parameters by equation 5.2 a value of 0.244 is found for $\nu$.

The shear modulus is linked to the cone resistance ($q_c$) by the following formula:

$$G = 10 \cdot q_c^{0.61} \tag{5.3}$$

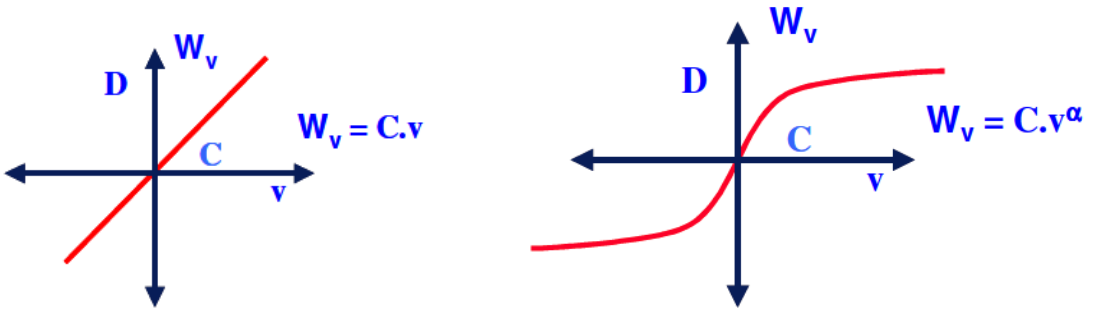


(a) Linear damper model

(b) Exponential damper model

Figure 5.9: Damper models (Middendorp, 2004)

For $\alpha = 1$, a linear (viscous) damping is generated while for $\alpha < 1$ a parabolic one is generated. $\alpha$-values of 1 (figure 5.9a) and 0.2 (figure 5.9b) are used for respectively clay and sand by Allwave-PDP.

### 5.2.6. Damping variability

In Allwave-PDP the damping is modeled according to the TNOWAVE model. This implies that the dynamic component of the total resistance is not related to the static resistance: (Allnamics, 2017)

$$R_t = R_s + R_d = R_s + C v^{\alpha} \tag{5.4}$$

where
$R_t$ = total resistance [kN]
$R_d$ = dynamic component of resistance [kN]
$R_s$ = static component of resistance [kN]
$C$ = damping constant [Ns/m]
$\alpha$ = damping exponent [-]

In most papers on soil damping the method introduced by Gibson & Coyle is applied: (Coyle and Gibson, 1970)

$$R_d = R_s J v^{\alpha} \tag{5.5}$$

where
$J$ = Smith damping constant [s/m]
$\alpha$ = damping exponent [-]

This method is an extension on the Smith model as the damping can be modeled with a non-linear nature. An analogy is drawn between between $C$ in the TNOWAVE model and $R_s J$ in the Gibson & Coyle method. The variability of $R_s$ is incorporated by the random field. Therefore, the variation of $J$ in the Smith/Coyle & Gibson method is equal to the variation of $C$ in the TNOWAVE method.

**Litkouhi & Poskitt, 1980** In these tests the goal is to measure damping. This is done by the set-up as shown in figure 5.10. Toe and shaft forces are measured simultaneously. To identify the resistance of toe and shaft separately, a cone of identical geometry to the pile point is used. The resistance so obtained is then subtracted form the total resistance. The error resulting from the lack of lateral support in this conditions results in a negligible error since the point resistance is only 10% of the side resistance.

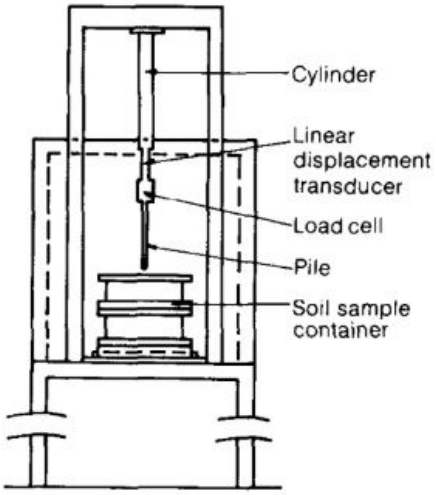


Figure 5.10: Model pile test rig (Litkouhi and Poskitt, 1980)

The tests have been done on remoulded samples of London, Forties and Magnus clay. Forties clay is a normally consolidated or lightly overconsolidated silty clay and Magnus clay is a very stiff clay with shell fragments and scattered gravel.

To obtain the static resistance, $R_s$, the test pile is pushed into the sample at 0.3 mm/s. Five speeds are selected and the test pile is pushed in at this speed to give the dynamic resistance, $R_d$.

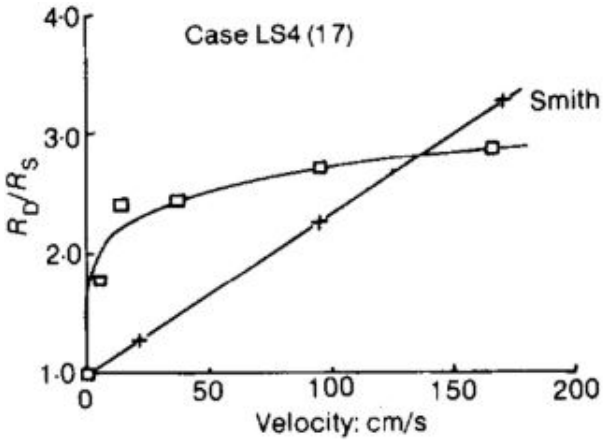


Figure 5.11: Test on London clay (Litkouhi and Poskitt, 1980)

Fitting of the test results (square dots) delivers a non-linear trend as shown in figure 5.11. The Smith damping for shaft resistance is much higher than that for toe resistance. The experiment is repeated 26 times for the shaft tests and 12 times for the toe tests. From the results of these tests the information as shown in table 5.6 is derived.

| Property | $\mu$ | $\sigma$ | COV [%] |
|---|---|---|---|
| $J_{toe}$ | 0.235 s/m | 0.078 s/m | 33.99 |
| $N_{toe}$ | 0.247 | 0.073 | 29.76 |
| $J_{shaft}$ | 0.598 s/m | 0.326 s/m | 54.53 |
| $N_{shaft}$ | 0.248 | 0.143 | 57.57 |

Table 5.6: Statistical damping parameters (Litkouhi and Poskitt, 1980)

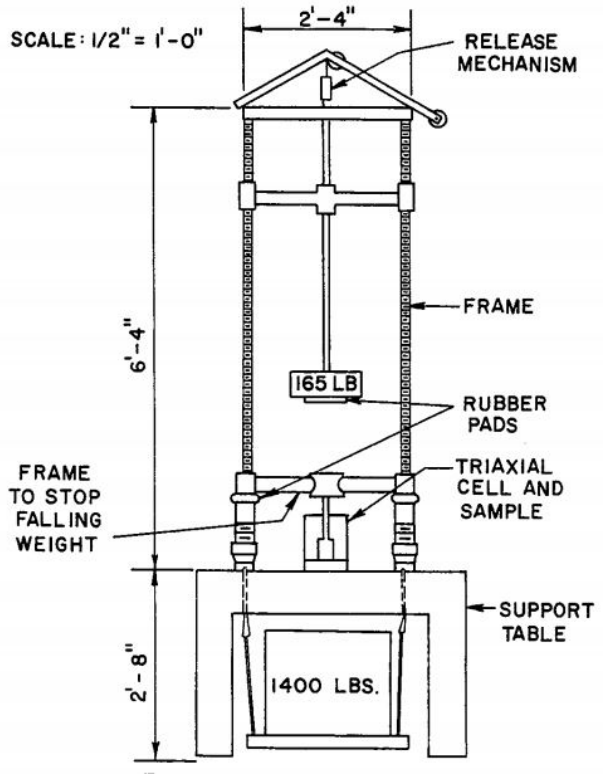


Figure 5.12: Coyle & Gibson test set-up (Coyle and Gibson, 1970)

**Coyle & Gibson, 1970** In the soil tests in the research of Coyle & Gibson the soil specimen is impacted by a falling load, see figure 5.12. With an increasing fall height the velocity of deformation increases. This type of loading resembles the loading by the tip of the pile.

The tests are done both on sand and clay. Three sand types are used; Ottawa, Arkansas and Victoria sands. Ottawa sand has uniform smooth grains, Arkansas sand has fine, angular grains, and Victoria sand has very fine and extremely angular grains. In the results, shown in figure 5.13, a large difference in damping constant can be noticed between Ottawa and Victoria and Arkansas sands. The COV is 32%. This can probably be explained by the difference in uniform smooth grains and fine angular grains. The damping constant in TNOWAVE is solely determined by $q_c$ of the CPT and soil density. So the grain type is not taken into account and its caused variation must be incorporated in the transformation uncertainty.

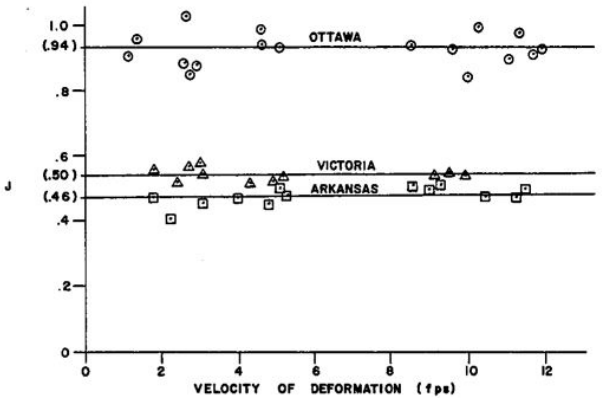


Figure 5.13: Damping constant of sand versus velocity of deformation (N=0.20) (Coyle and Gibson, 1970)

Three of the tested clays in figure 5.14 are classified as high plasticity clays; OR, EA and VE. The clay with low plasticity is CE. The dynamic loads in the clay increase rapidly and then level off to an essentially straight line

with a slight slope. The Smith damping constant for clay soils vary between 0.67 and 1.26. The COV of the results is 16%. (Coyle and Gibson, 1970)

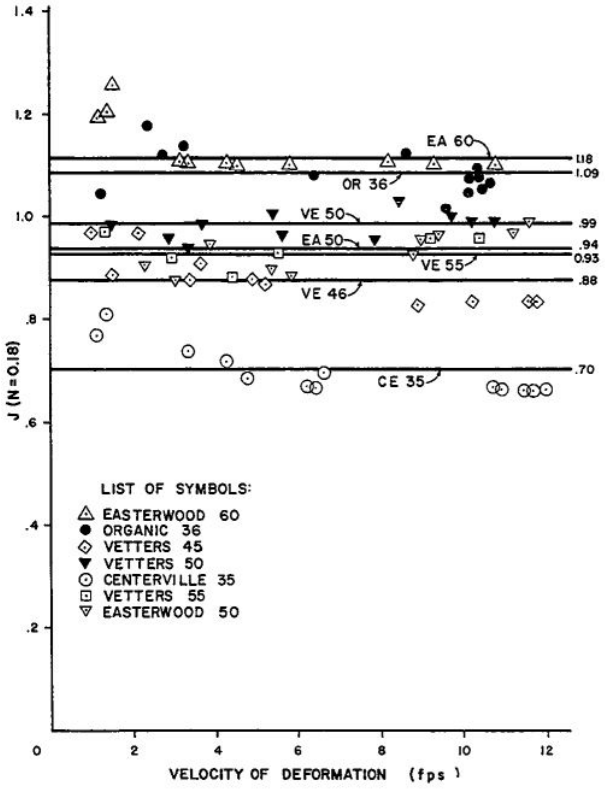


Figure 5.14: Damping constant of clay versus velocity of deformation (N=0.18) (Coyle and Gibson, 1970)

**Additional literature** The damping exponent lies between 0.17 and 0.37 according to Lee et al. (1988) and the Allwave-PDP manual (Allnamics, 2017).

**Conclusion** The damping constant $C$ as used in the TNOWAVE method is analogous to the Smith damping constant, $J$, multiplied with the static resistance. The static resistance variability is incorporated by the random field . Therefore, the variance of $J$ is assumed to be equal to $C$. In the majority of literature on damping the Smith damping is used to expresses the magnitude of damping.

The test set-up of Coyle & Gibson only measures the toe damping both on clay and sand samples. For clay the COV is 16%, whilst for sand the COV is 32%. Lithouki investigates clay samples both on toe and shaft resistance, and gives a COV of 34% and 58% respectively. Thus, only the toe damping constant on clay is measured in both papers. The most conservative value is used in the probabilistic model; 34%. For the shaft damping constant of clay a COV of 58% is adopted and for the toe damping constant of sand a COV of 32%. As there is no data on the shaft damping of sand, the value of clay is used here; 58%.

Statistical data of the damping exponent is only known for clay samples. The COV of the shaft and toe damping exponent is respectively 34% and 58%. These values are also adopted for sandy soils. If the boundaries given by Lee et al., 1988 and Allwave-PDP are considered as the 95%-confidence interval, a COV of 19% is found. As the boundaries of 0.17 and 0.37 are found after extensive back-analysis by Allnamics, these findings are considered to be more reliable. Therefore, a value of 19% is used for the COV of shaft and toe damping exponent in sand and clay.

## 5.3. Spatial variability

### 5.3.1. Introduction

One distinctive feature of geotechnical data is that they vary spatially both in the vertical and horizontal direction. This heterogeneity of the soil leads to uncertainty of the vertical, geotechnical profile at each installation location. Namely, measurements of the vertical, geotechnical soil profile (CPT) are taken only at a horizontal distance of 25-50 m in a typical hydraulic engineering project. In between these measurements vertical, geotechnical profiles vary due vertical and horizontal variability. In this section the vertical variability is quantified based on CPT's. The horizontal variability is considered in section 5.4.

### 5.3.2. Definition of scale of fluctuation

Taking into account spatial variability requires a further statistical parameter, scale of fluctuation ($\theta$) expressed in length. The scale of fluctuation defines the distance beyond which there is no significant correlation. For a weakly correlated material, $\theta$ is small, while, for a strongly correlated material, $\theta$ is large. In figure 5.15 the influence of $\theta$ is illustrated, relative to the domain dimension D, on the spatial variation of the soil property X in two dimensions, in which dark and light zones indicate high and low values of X respectively. For small $\theta/D$, the property values change rapidly over small distances, whereas, for large $\theta/D$, the spatial variation is much more gradual. Note that this is an example of isotropic random fields, which means that the same scale of fluctuation has been used in all directions. (Hicks, 2015)

(a) $\theta/D = 0.1$ (b) $\theta/D = 1.0$

Figure 5.15: Two-dimensional random fields (Hicks, 2015)

### 5.3.3. Soil stratification

As shown in figure 5.16, values of the cone resistance fluctuate over the depth. In this soil profile three geological layers are defined, indicated by the red dotted lines. The stratification of geological layers is based on physical properties of the soil, e.g. soil texture and overconsolidation ratio (OCR). A highly overconsolidated sand layer (-12.0 - -20.5 m N.A.P. in figure 5.16) has a much higher average cone resistance than that of a normally consolidated clay layer (-6.0 - -12.0 m N.A.P. in figure 5.16). This is not considered as random variation. Only the variation around the average value in a geological layer is considered as random variation. To incorporate only the random variation in the scale of fluctuation, the scale of fluctuation is defined for every geological layer.

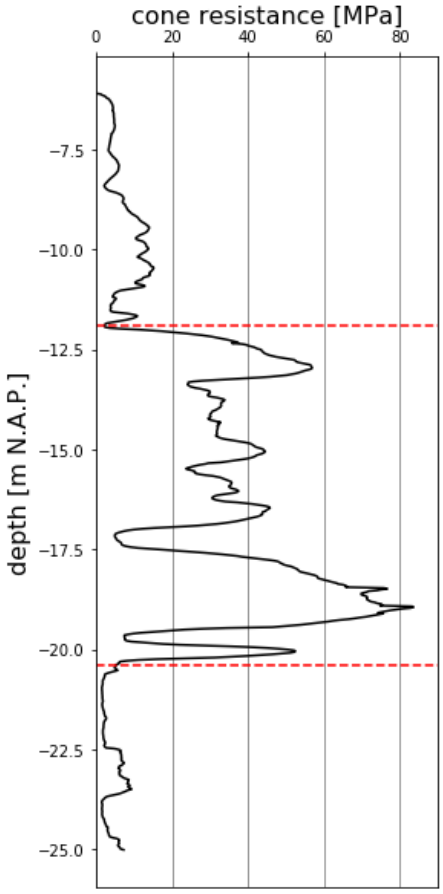


Figure 5.16: DKP-9 with layer division (red dotted lines)

### 5.3.4. Standard normal soil profile

To make a soil profile suitable to extract the scale of fluctuation, the profile must be detrended and normalized (Lloret-Cabot et al., 2014). Detrending implies the removal of the linear depth trend from the data. The linear trend is shown by the red lines in figure 5.17a. The result of detrending is shown in figure 5.17b. Consequently, the residual standard deviation ($\sigma_{res}$) of the detrended tip resistances is calculated. The detrended cone resistances are normalised by dividing each value by the corresponding $\sigma_{res}$. The result is a standard normal field ($\mu = 0, \sigma = 1$), see figure 5.17c.

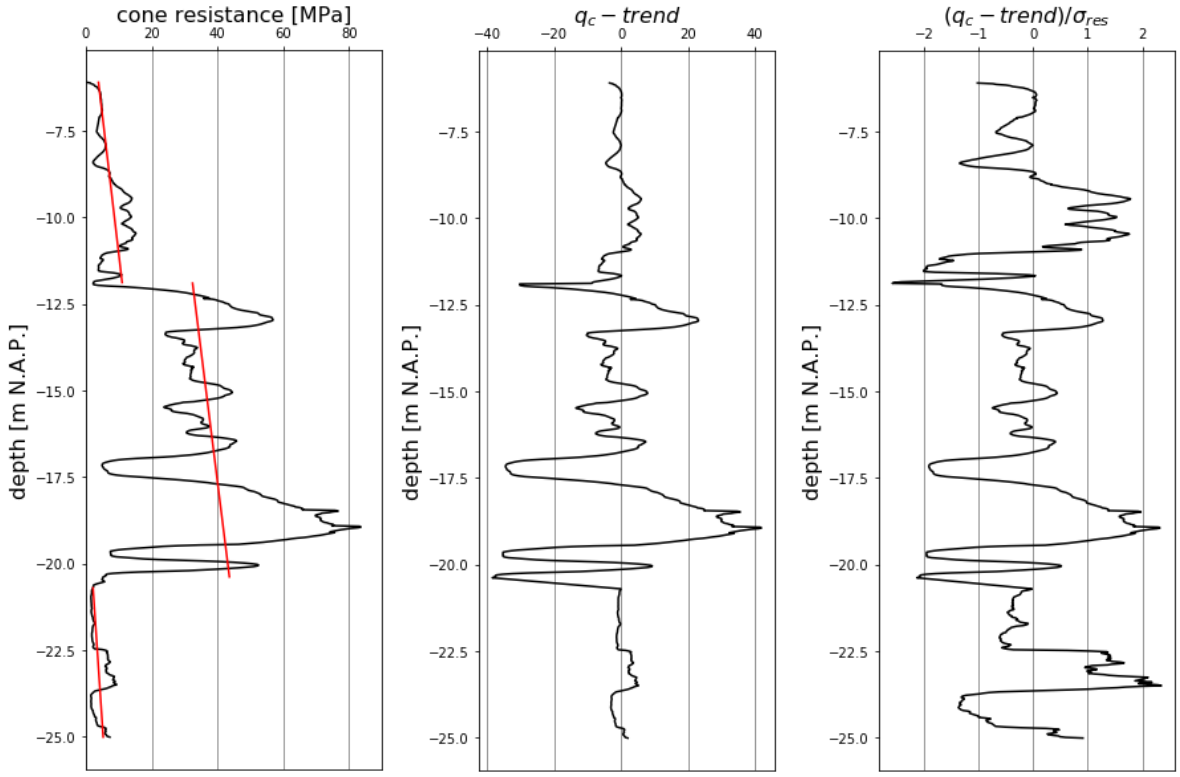


(a) Trend lines (b) Detrended (c) Normalised detrended

Figure 5.17: CPT DKP-9 Woudsend

### 5.3.5. Autocorrelation

To estimate the scale of fluctuation the autocorrelation must be estimated first by formula 5.6. The autocorrelation is found by normalising the autovariance (formula 5.7). The result is a graph where the correlation is a function of the distance between points (lag), see red line in the lag-correlation graph in figure 5.18.

$$\rho(h) = \frac{\hat{\gamma}(h)}{\hat{\gamma}(0)} \tag{5.6}$$

where
$\hat{\rho}(h)$ = experimental autocorrelation at distance $h$
$\hat{\gamma}(h)$ = experimental autocovariance at distance $h$
$\hat{\gamma}(0)$ = experimental autocovariance at zero distance

$$\hat{\gamma}(h) = \frac{1}{n}\sum_{t=1}^{n-|h|}(x_{t+|h|})(x_t), \quad \text{for} - n < h < n. \tag{5.7}$$

where
$\hat{\gamma}(h)$ = experimental autocovariance at distance $h$
$n$ = number of points
$h$ = distance between points
$x$ = value of parameter ($q_c$)
$t$ = location (depth)

### 5.3.6. Fitting of experimental to theoretical curve

The scale of fluctuation is a variable of a theoretical autocorrelation function. The theoretical autocorrelation function is fitted to the experimental autocorrelation function. The theoertical function has an exponential shape.

In figure 5.18 is shown how the theoretical and experimental function are fitted by varying the scale of fluctuation.

is determined by fitting the experimental correlation function to the theoretical correlation function. This is the most simple approach to determine the scale of fluctuation. The fitting is especially important until 1.0 m lag, at larger distances the autocorrelation is influenced by large scale trends (Lloret-Cabot et al., 2014). In this research a correlation function with an exponential shape is used as this shape seems to be most consistent with the experimental line. As shown in figure 5.18 the scale of fluctuation is 0.5, 0.75 and 0.75 for respectively the upper, middle and lower section.

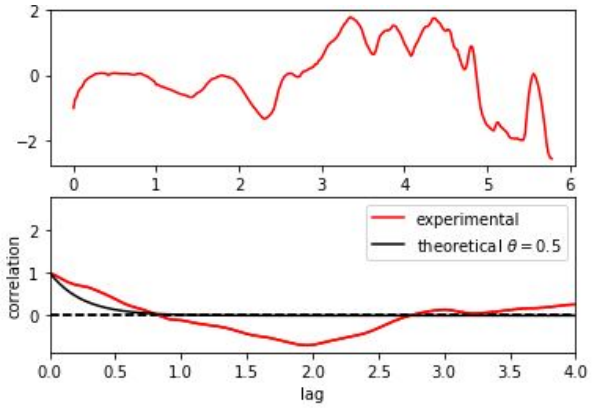


(a) Upper section

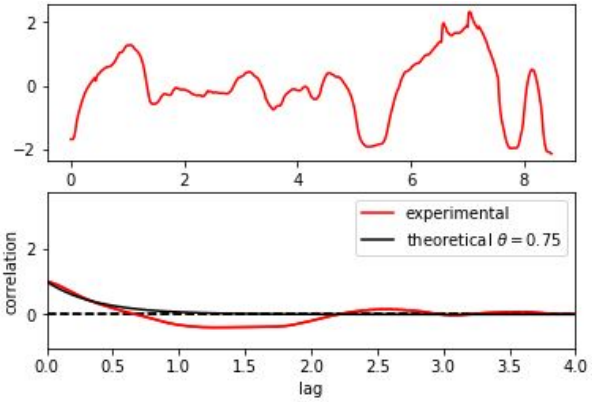


(b) Middle section

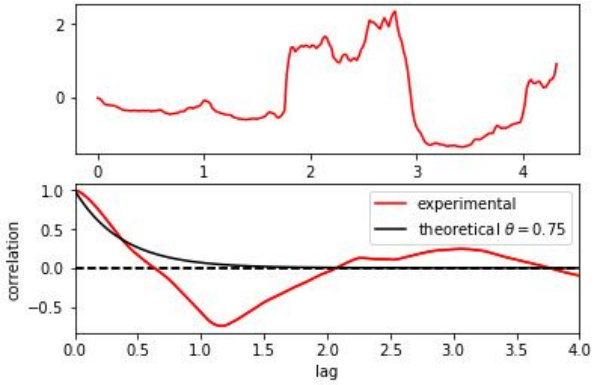


(c) Lower section

Figure 5.18: Correlation CPT DKP-9 Woudsend

## 5.4. Stochastic soil profile composition

In this section a randomly generated soil profile will be composed for all soil parameters. The stochastic soil profile considers the transformation uncertainty and spatial variability. It is explained how variability is incorporated into the soil profile.

### 5.4.1. Representative CPT

A soil investigation of a sheet pile driving project consists typically of multiple CPT's. A representative CPT is selected from the soil investigation as a best estimate (mean of the probability distribution). A CPT with average properties is selected as a representative CPT from the soil investigation. These properties comprise the geological layer division (see figure 5.16), trend lines and residual standard variation ($\sigma_{res}$). The selection of average properties is explained by figure 5.19 where the representative CPT (CPT-9) is indicated by a thick black line. The other CPT's from the soil investigation are plotted as well. It is shown that the representative CPT has an average profile. The layer division is approximately at the same depth as the other CPT's. Also peaks and trends of the values have the same order of magnitude as the other CPT's.

In this research a representative CPT with average properties is chosen 'by hand'. Also a fictitious, average profile could be created by averaging all CPT's from the soil investigation. For convenience an existing soil profile is used to represent the soil in the probabilistic prediction. Next to that, a fictitious profile will result in blurred layer divisions and a disturbed scale of fluctuation.

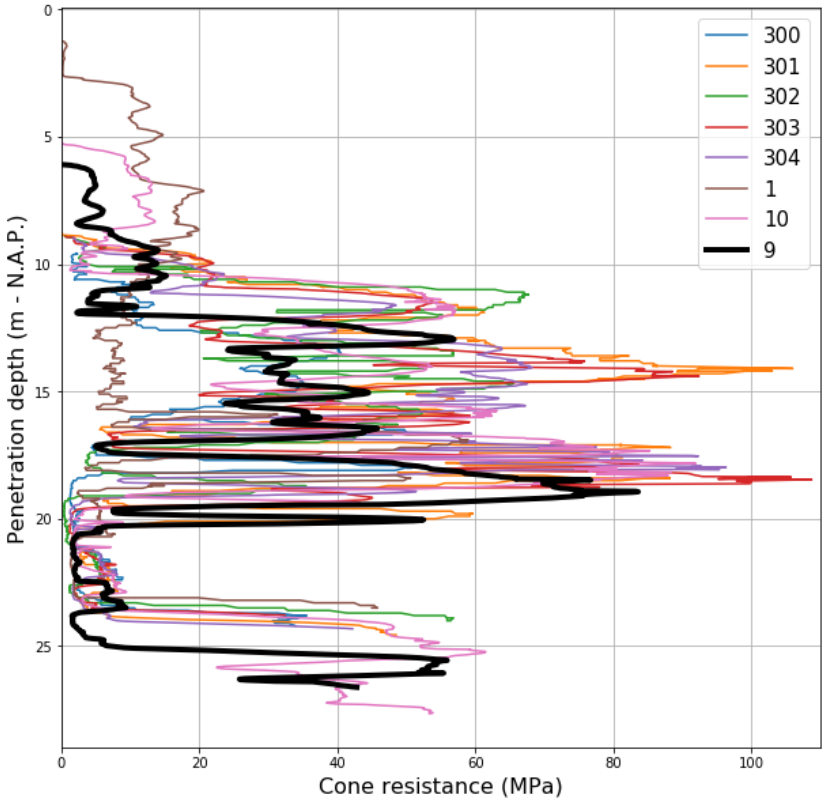


Figure 5.19: Representative CPT

### 5.4.2. Element size of soil profile

The high resolution of the CPT is reduced to speed up computation time. In a CPT a measurement is made every 0.02 m. To speed up computations the element size in Allwave-PDP is chosen as large as possible. The upper bounds for the size of the discrete elements is defined by: $\Delta x \leq (0.25 - 0.5)\theta$, where $\Delta x$ is the finite element size in the same spatial direction as the scale of fluctuation (Phoon, 2008). For a typical vertical scale of fluctuation between 0.5 and 1.0 m, the upper bound for the element size of the soil model parameters is 0.25 m. The elements of the one-dimensional soil profile in Allwave-PDP are determined as 0.25 m to speed up computations as much as possible

### 5.4.3. Horizontal variability

The horizontal spatial variability cannot be determined by CPT data. This data is only sufficient to determine the vertical spatial variability as it gives a vertical soil profile with a measurement resolution of 0.02 m. In a typical foundation project the horizontal distance between CPT's is 25-50 m. With this distance the horizontal scale of fluctuation cannot be accurately estimated. For example, in one research scales of fluctuation varied between 6 and 15 m. (Lloret, 2012)

The horizontal variability is taken into account without quantifying this statistical value. This is done by assuming the geological layer divisions as deterministic and assuming no horizontal correlation in the generation of the random field.

Assuming deterministic geological layer divisions gives less variability in the results of the driveability prediction than would be the case in practice. A deterministic geological layer division implies that start and end of a division are identical in every repetition of the Monte Carlo simulation. In practice, the depth of start and end of a geological layer might vary.

On the other hand, assuming no horizontal correlation gives more variability in the results of the driveability prediction than in practice. The absence of horizontal correlation implies that soil parameter values are not influenced by its horizontally neighbouring values. Two neighbouring vertical soil profiles could be completely different. In reality, neighbouring soil profiles will turn out to be largely identical. For example, a peak in the cone resistance is likely to occur at the same depth at one meter horizontal distance.

The impact of both assumptions is expected to give a result identical to the impact of horizontal variability in practice. The absence of horizontal correlation results in larger variability of driveability predictions, whilst deterministic layer division results in less variability.

### 5.4.4. Spatial variability

Multiple statistical properties are extracted from the representative CPT. Scale of fluctuation, trend lines and residual standard deviations of each geological layer are used for further analysis. All soil parameters are directly or indirectly derived from the CPT. Therefore, it is assumed that the scale of fluctuation derived from the CPT is identical for all soil input parameters in Allwave-PDP. Based on the scale of fluctuation a standardized random field ($\mu = 0, \sigma = 1$) is generated. This process is elaborately described in section 5.3. The trend lines and residual standard deviations are unique for every soil input parameter.

An identical standardized random field is used for all soil parameters. In annex A is explained how standardized random field is generated. The course of the variation around the trend is identical in all soil parameters. In step 3 figure 5.20 is shown that every soil parameter profile is generated with the same standardized random field. For example, a peak in damping occurs at the same depth as a peak in cone resistance. All soil parameters are directly or indirectly related to the CPT. Thus, it is likely that peaks of soil parameter values occur at the same depth.

The standardized random field is turned into a soil parameter-specific random field by multiplying by $\sigma_{res}$. In figure 5.20 this is indicated by step 3. The $\sigma_{res}$ is the residual standard deviation. This is the standard deviation of the variation around the trend line. The $\sigma_{res}$ is defined for every geological layer. In figure 5.20 the $\sigma_{res}$ is highest for the middle layer. This is explained by the large peaks in the overconsolidated sand layer in CPT DKP-9. As the course of the profile of the $\alpha$-factor is linear, there is no $\sigma_{res}$ for this soil parameter.

The trend line of a soil parameter functions as the depth-dependent mean of the probability distribution of the random field. The trend line is derived from each soil parameter profile, see step 1 in figure 5.20. The trend line is added to the the soil parameter-specific random field, see step 2 in figure 5.20. After addition of the trend line of the soil parameter and its soil parameter-specific random field, a randomly generated one-dimensional profile of the soil parameter is the result. Note that the peaks of each profile are located at the same depth.

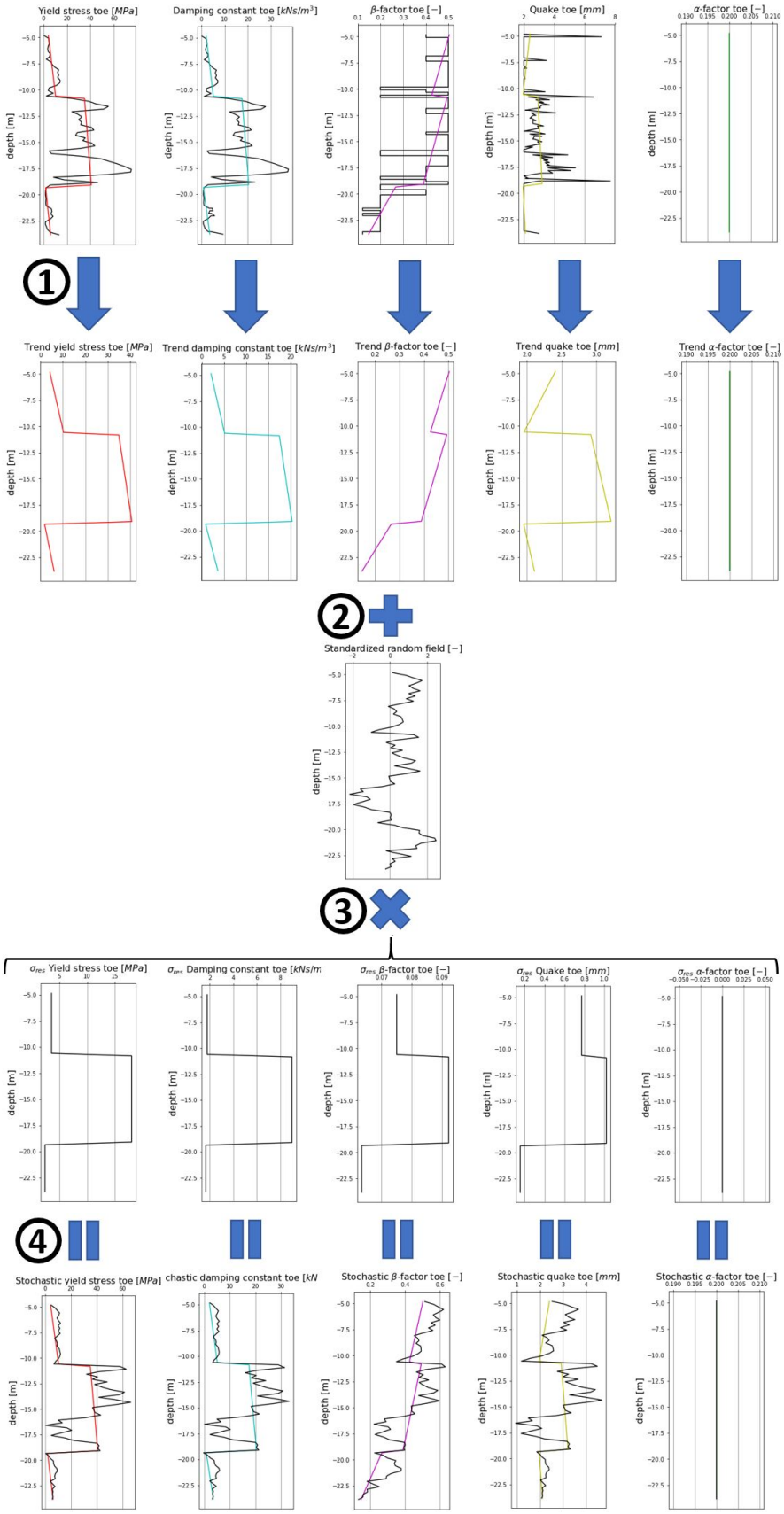


Figure 5.20: Composition random soil profile

### 5.4.5. Transformation variability

The transformation variability is taken into account by shifting the soil parameter values with a depth-constant shift for a geological layer. The amount of this shift is determined by multiplying the soil parameter values by a constant value. The constant value is found by sampling a random value from a normal distribution with a mean of 1 and a specific COV for each soil parameter ($N(1, COV)$). In table 5.8 the values for the COV of soil parameters is given as found in section 5.2. The COV of the $\beta$-factor is dependent on the soil type. The upper value applies to a geological layer consisting of heavy clay and the lower value applies to a geological layer consisting completely of sand. For geological layers with intermediate soil types, the transformation variability is interpolated from the values in the table. In case of a COV of 0%, the transformation variability would be zero. This is the case for the yield stress. This soil parameter is directly copied from the CPT data.

The transformation uncertainty is constant over each geological layer. Soil properties, like grain shape or over-consolidation, are not measured by a CPT. These properties influence the transformation relation. It is likely that the unmeasured properties are not varying much throughout the layer. Therefore, the variability introduced by the transformation relation is assumed to be constant in each geological layer.

An example is given in figure 5.21. Transformation variability is included in step 5. The starting soil parameter profiles are randomly generated with a random field. For each geological layer a constant value is randomly sampled. This constant value has a mean of 1. Dependent on whether the constant value is smaller or larger than 1, the soil parameter values are respectively reduced or increased. The thin black line shows the soil parameter profile before transformation variability is included. The thick black line shows the soil parameter profile after transformation variability is included.

| | **Toe** | **Shaft** |
|---|---|---|
| **Yield stress** | 0% | 0% |
| **Quake** | 10% | 41% |
| **Damping constant** | | |
| Sand | 32% | 58% |
| Clay | 34% | 58% |
| **Damping exponent** | 19% | 19% |
| **$\beta$-factor** | 25-50% | 32-64% |

Table 5.7: COV of transformation variability of soil parameters

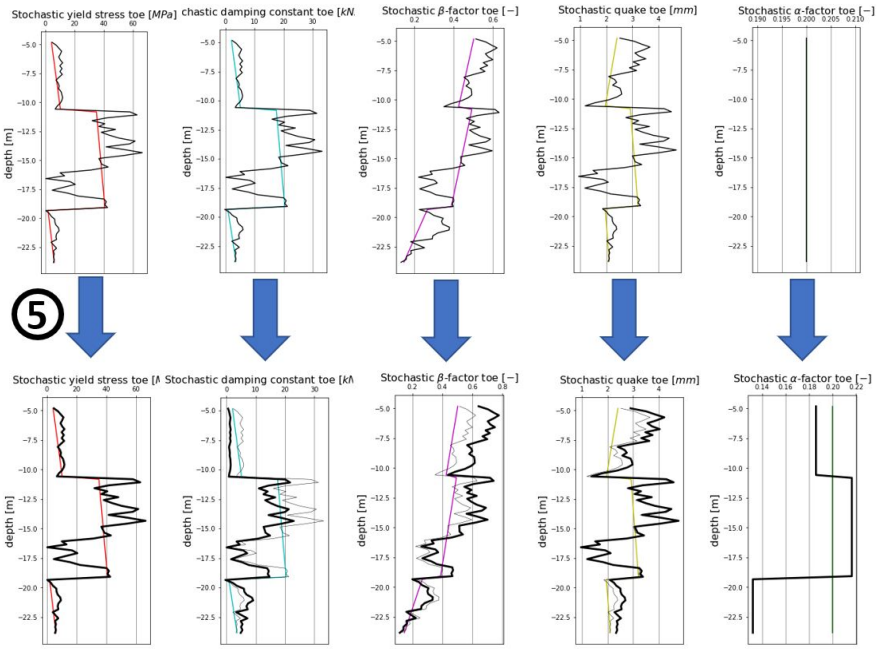


Figure 5.21: Composition random soil profile

## 5.5. Conclusion

All pile and hammer parameters are defined as deterministic values in the probabilistic method. Manufactured materials can be controlled within a narrow range, thus its variation is neglected. Default values as given by manufacturers are used in the probabilistic method, except for the hammer frequency. Field measurements show that a reduction of the hammer frequency by 6% is more realistic. Variability of the soil model parameters is caused by transformation uncertainty and soil heterogeneity. The variability as a result of transformation uncertainty is quantified by a coefficient of variation (COV). A normal distribution is assumed for the transformation variability. The most conservative value found in literature is used to quantify the transformation variability. In table 5.8 the COV for each model parameter are given.

| | **Toe** | **Shaft** |
|---|---|---|
| **Quake** | 10% | 41% |
| **Damping constant** | 34% | 58% |
| **Damping exponent** | 19% | 19% |
| **$\beta$-factor** | 25-50% | 32-64% |

Table 5.8: COV of soil model parameters

In figure 5.22 the steps as written below are visualized. The spatial variability caused by the soil heterogeneity is modelled by a random field. An identical standardized random field (defined by correlation length only) is used for all soil model parameters. A model parameter-specific random field is defined by multiplying correlation length by the residual standard deviation ($\sigma_{res}$). The former is found after analysis of the CPT data, whilst the latter is extracted from the deterministic model parameter values. The trend lines of the model parameters are also derived from the deterministic model parameter values. To these trend lines a soil model parameter-specific random field is added to generate a randomly generated soil profile. Consequently, a transformation model error is added to the randomly generated soil profile. For each geological layer a randomly generated transformation model error is defined by the COV of the transformation uncertainty. The transformation relations for the model parameters as defined by Allwave-PDP are used as best estimates in this research.

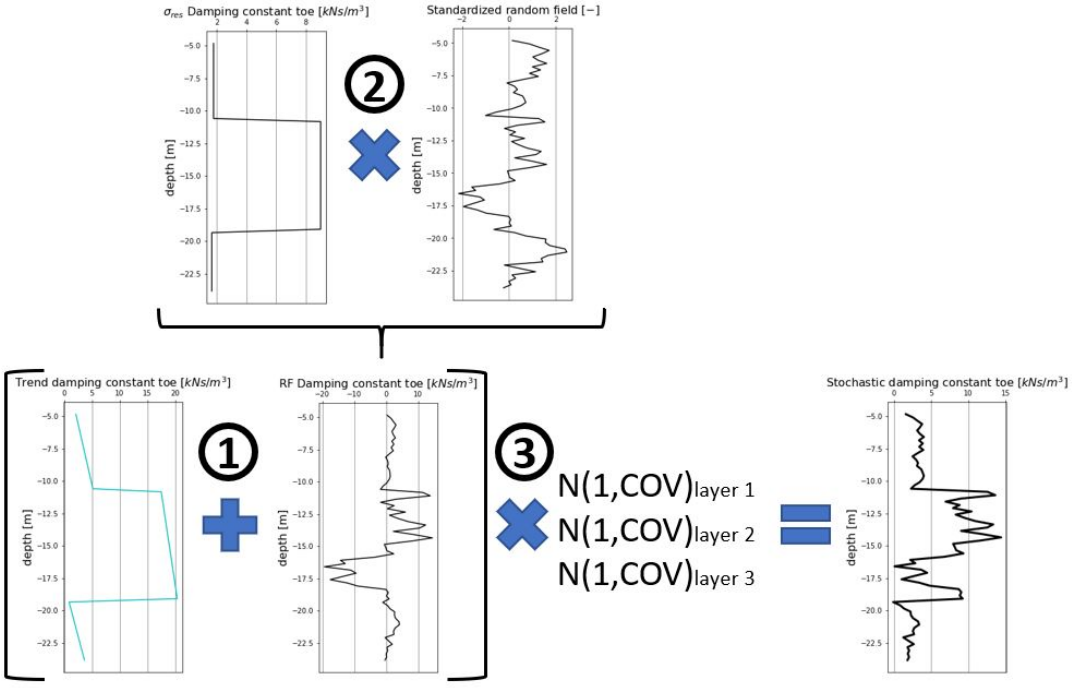


Figure 5.22: Composition of stochastic soil profile (Damping constant)

# 6

# Application to case studies

The probabilistic method which is developed in the previous chapter will be applied to case studies. These case studies are done on sheet pile driving projects. Information on hammer, pile and soil in these projects is collected from contractors, government bodies and databases. Also information on driveability of each project is collected. The predicted and measured driveability are compared and it can be concluded how the probabilistic method performs in the case studies. In section 6.1 is explained what method is used to predict probability of refusal. In section 6.2, 6.3, 6.4 the case study for Woudsend (red), Rotterdam (blue) and Den Oever (green) is given respectively. Between brackets the color of the indicators are given as shown in figure 6.1.

Figure 6.1: Overview map of case study locations

## 6.1. Monte Carlo simulation

In this section is described how the refusal probability of a driving project is predicted. The driveability prediction method Allwave-PDP is used in this research. In Allwave-PDP a deterministic set of input parameters defines pile, hammer and soil properties. This approach does not take into account variability of the properties. By incorporating probability theory the variability of properties is taken into account. A stochastic set of pile, hammer and soil properties is generated by quantifying variability of properties. This set of properties generates a unique output in the form of a penetration speed-depth-curve ($v_p$-z-curve) when entered in Allwave-PDP. The unique output is generated multiple times in a Monte Carlo (MC) simulation. In figure 6.2 the process of a MC simulation is described. Pile driveability is evaluated a number of times with Allwave-PDP and a randomly generated set

of input parameters. In the scope of this research the output is defined as accurate after 40 repetitions. The probability of refusal is defined as the proportion of the total number of simulations in which refusal occurs. Refusal is defined as non-exceedance of the design penetration speed of 1 mm/s in the $v_p$-z-curve. By various automation scripts, as shown in annex E, the probabilistic prediction is accelerated.

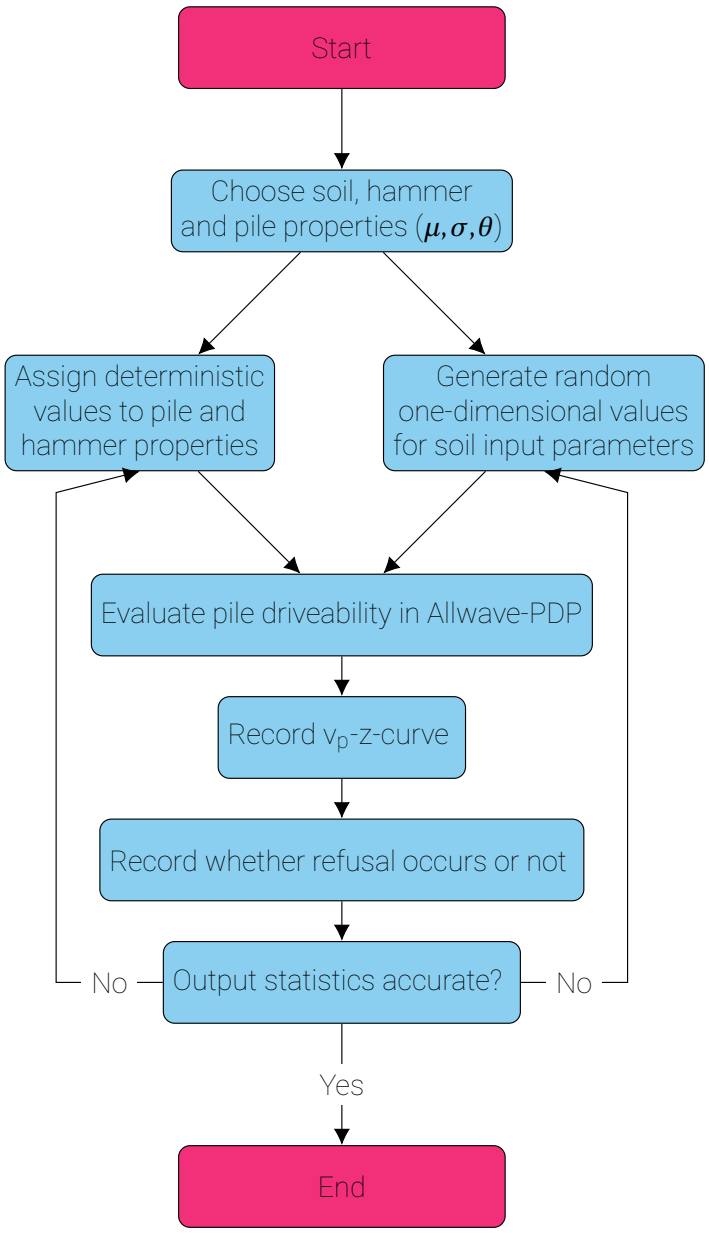


Figure 6.2: Monte Carlo simulation

.

## 6.2. Case study Woudsend

### 6.2.1. Project

In 2006 the construction of a large project to promote tourism in one of the northern provinces in the Netherlands, Friesland, was started. As part of this project five aqueducts were built to remove intersections between waterways and motorways. On one of these aqueducts near the village of Woudsend is being focused in this case study. The final result is shown in an overview photo in figure 6.3.

Figure 6.3: Overview aqueduct Woudsend

This project was selected as a case study due to its well-reported problems and conditions. In a database of Deltares, Geobrain, in which vibratory driving projects are reported, abundant data is available on driving experience (Deltares). In annex D the data on two experiences is described (in Dutch). Also the provincial government has provided the full geotechnical investigation on this project. Next to that, geotechnical experts in driveability studies of Allnamics have used this case for academic purposes and provided additional information on installation details (van Dorp, 2019).

As the ground water level in this area is normally only 0.5 to 1.0 meter below ground level, a watertight bathtub-like construction must be installed to ensure a dry situation. The driven sheet piles were part of this cofferdam in which the aqueduct was constructed. All piles must be interlocked correctly. The piles must also reach the depth specified in the plan to make sure the piles hit the non-permeable layer and the sheet pile wall and non-permeable layer are joined correctly. These conditions should provide a watertight cofferdam.

By the client strict requirements were given with respect to driving of the sheet piles to ensure that the conditions mentioned above were fulfilled. Fluidization was only allowed to a depth of -19 m N.A.P.. Pre-drilling was not allowed and there were strict limits on environmental vibrations. Also damage to buildings in the proximity due to vibrations from installation equipment had to be prevented. This led to strict requirements with respect to environmental vibration levels. (van Dorp, 2019).

These strict conditions on execution and design combined with hard driving conditions resulted in major problems during this project. At many locations the piles did not reach the required depth. Eventually, there was agreed on more lenient driving methods. Impact driving was allowed and fluidization was allowed until larger depths and with higher pressure (water jetting). This increased the risk on lock damage, environmental damage due to vibrations and leaking of the non-permeable layer. The heavy driving resulted in a delay of 34 weeks and a lawsuit where the contractor sued the client for 1.5 million euro (Cobouw, 2007).

### 6.2.2. Conditions

In this case study is looked into conditions when the strict requirements given by the client were still in effect. In the final stage of installation of the sheet piles, when requirements were more lenient, various types of driving equipment are used and remedial measures are taken. The strict conditions are described by the first described experience in Geobrain as shown in annex D. The second experience in Geobrain describes a situation in which an impact hammer is used to drive the sheet piles to a sufficient depth. Impact driving of sheet piles was definitely not allowed when the strict requirements were in effect, so this case is not considered in this case study.

In the sections below, information on pile, hammer and soil is summarized. This information will be used in the probabilistic driveability prediction.

### Hammer

The vibratory hammer that was initially used to drive the piles is a PVE 2335VM hammer. Specifications of this hammer are given in table 6.1. The total dynamic mass consists of the vibrating part of the hammer (4,400 kg) and the clamp (1,200 kg). It is assumed that the full static mass is applied to the pile driving system.

| PVE 2335VM | |
|---|---|
| Ecc. moment | 0-35 kgm |
| Max. frequency | 2,300 rpm (38.3 Hz) |
| Centrifugal force | 0-2000 kN |
| Total static mass | 2,600 kg |
| Total dynamic mass | 5,600 kg |

Table 6.1: PVE 2335VM specifications

### Pile

In this prediction AU16 sheet pile type is used Deltares. In figure 6.4 the geometry of AU16 sheet pile type is shown. The data given in table 6.2 holds for a double pile. The symbol Ω stands for the coating area on one side, excluding inside of interlocks. The length of the sheet piles is 20 m (Deltares).

| | b [mm] | h [mm] | s [mm] | t [mm] | m [kg/m] | A [$mm^2$] | Ω [mm] | $W_x$ [$cm^3$] | $I_x$ [$cm^4$] |
|---|---|---|---|---|---|---|---|---|---|
| AU16 | 750 | 411 | 9.3 | 11.5 | 172.5 | 74.1 | 1,910 | 2,400 | 49,280 |

Table 6.2: Dimensions of AU16 sheet pile profile

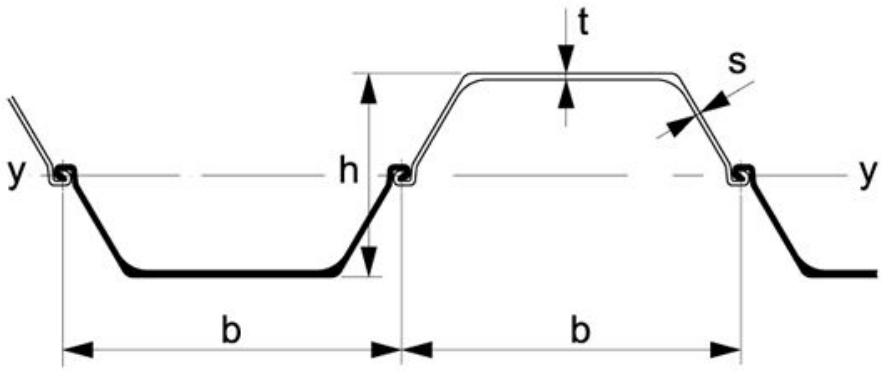


Figure 6.4: Cross-section of AU16 sheet pile profile

### Soil

A total of 15 CPT's is made for this project. Only 8 out of 15 CPT's reached a sufficient depth to be useful to make pile driveability predictions. The non-usable CPT's do not reach the pile toe installation depth of -21 m N.A.P.. The usable CPT's are indicated with a green dot on the map in figure 6.5. Only one land-based CPT reaches the sufficient depth. Most probably, equipment for water-based tests is stronger than land-based tests.

In figure 6.6 and 6.7 respectively the cone resistance and shaft friction are shown for every usable CPT. The sand layers between -11 and -20 m N.A.P. are heavily overconsolidated which results in very high cone resistances; over 100 MPa. The high cone resistance values are caused by overconsolidation. It is expected that the high cone resistance decreases sharply as the vibratory force exerted on the soil releases the horizontal stress. This is why cone resistance and shaft friction are capped at respectively 40 MPa and 200 kPa (van Dorp, 2019). These values are advised by Allnamics and are empirically determined. In figure 6.6 and 6.7 these values are visualized by the red dotted line. This shows the large impact as shaft friction values are reduced down to 15% of their original value and cone resistance is reduced to 40% of its original values.


Figure 6.5: CPT map

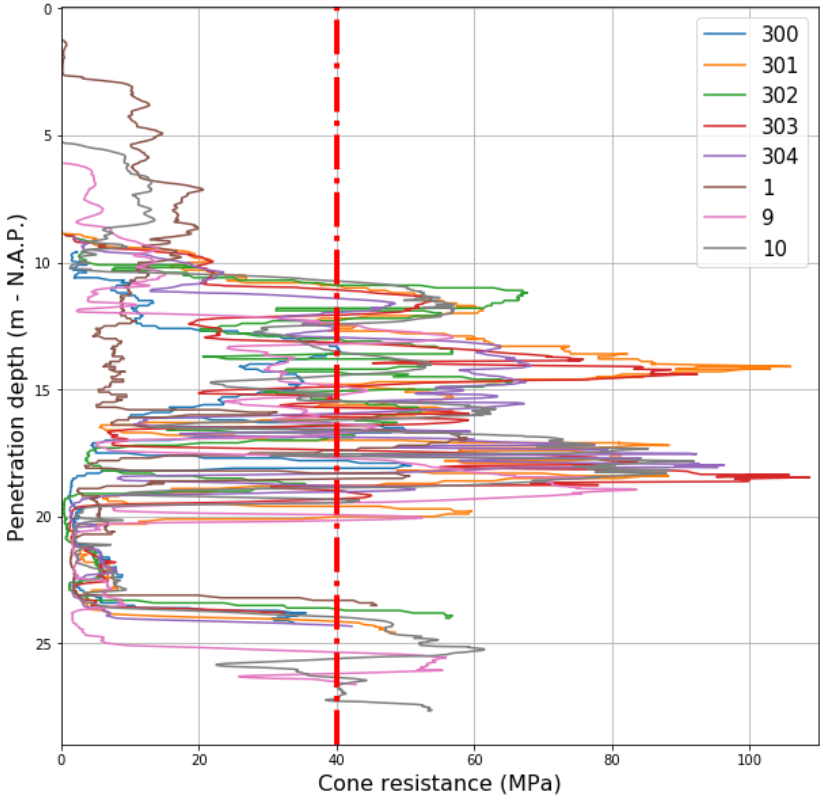


Figure 6.6: Cone resistance of CPT's Woudsend

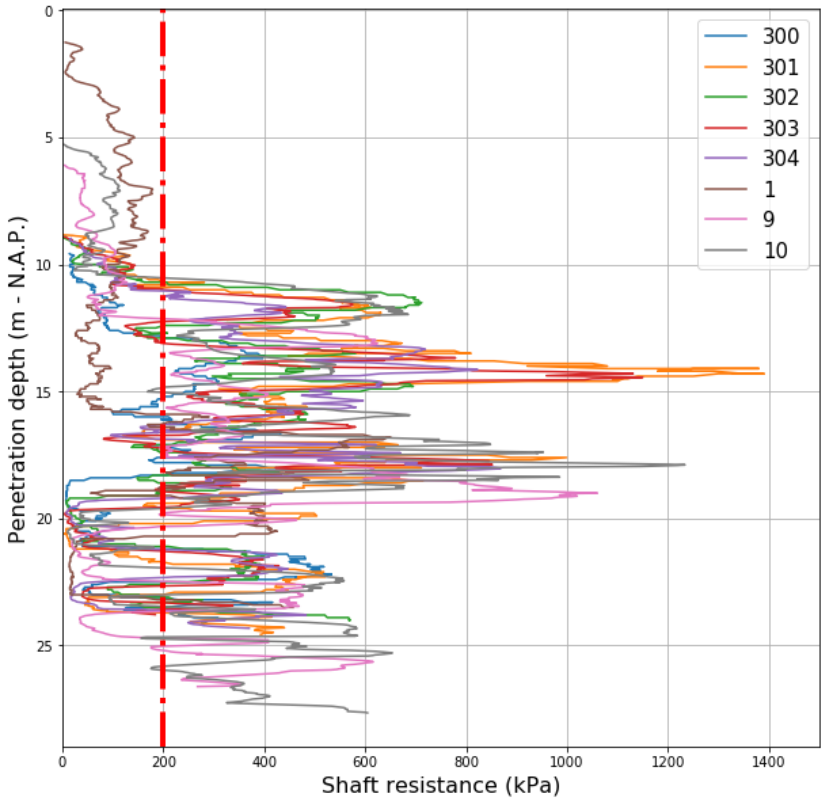


Figure 6.7: Shaft friction of CPT's Woudsend

### 6.2.3. Representative CPT

CPT DKP-9 is selected as a representative CPT based on the outcome of the deterministic prediction for each CPT. In total 8 deterministic predictions are made; one for every usable CPT. In the deterministic prediction default Allwave-PDP parameters are used and TNOWAVE damping is applied. The foundation elements of 20 m length will be placed at a toe depth of -21 m N.A.P. (Deltares). This implies that the sheet piles will not be visible when the project is finished. Namely, the ground level is at approximately -0.5 m N.A.P. The results of the uncapped predictions are shown in figure 6.8. In 3 out of 8 (CPT DKM-1, DKP-300 and DKP-302) succesful installation is predicted. As mentioned before, experts of Allnamics advise to cap soil resistance in case of overconsolidated sandy soils. This results in different outcomes of the deterministic driveability predictions, see figure 6.9. The results of the CPT's is more homogeneous. Based on these results CPT DKP-9 is selected as a representative CPT. The $v_p$-z-curve shows average behaviour compared to other curves. Also the CPT profile has average properties and has the same characteristics as other CPT's, see figure 6.6.

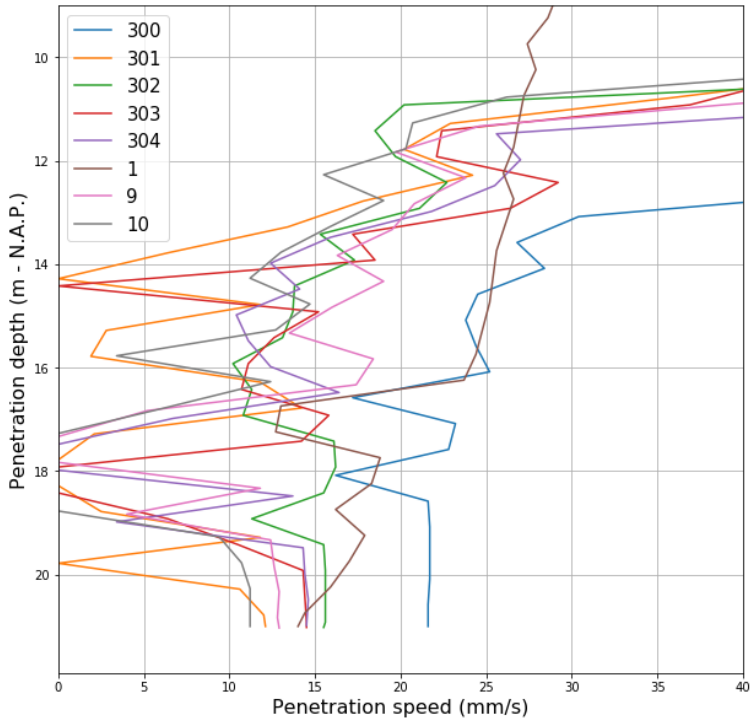


Figure 6.8: Uncapped $v_p$-z-curve Woudsend

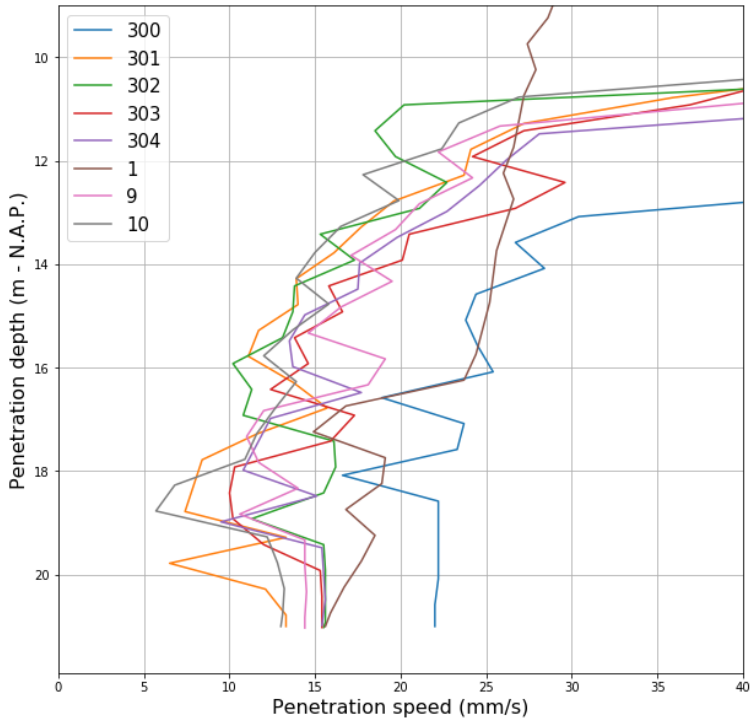


Figure 6.9: Capped $v_p$-z-curve CPT Woudsend

### Layer division

In figure 6.10 CPT DKP-9 is given including its trendlines. These trendlines demarcate the three zones into which the soil profile is divided. These zones are demarcated based on the cone resistance as a function of the depth. The overconsolidated layer can easily be identified between -11 m N.A.P. and -19 m N.A.P.. The third layer ends

at -23 m N.A.P. as a another overconsolidated layer starts below here. For this CPT defining the layer division is a simple task as the divisions are clearly indicated by jumps in $q_c$-values.

The correlation length is established from the normalized, detrended cone resistance. The correlation length is in every zone determined as 0.5 m. This is shown in figure 6.11a, 6.11b and 6.11c. This process is also done for shaft friction. The covariance-lag-graphs of shaft friction and cone resistance are more or less identical. Therefore, the same correlation length will be used for shaft parameters as toe parameters. It is assumed that correlation length of the soil model parameters is identical to that of the CPT. Namely, all soil model parameters are directly or indirectly derived from the CPT.

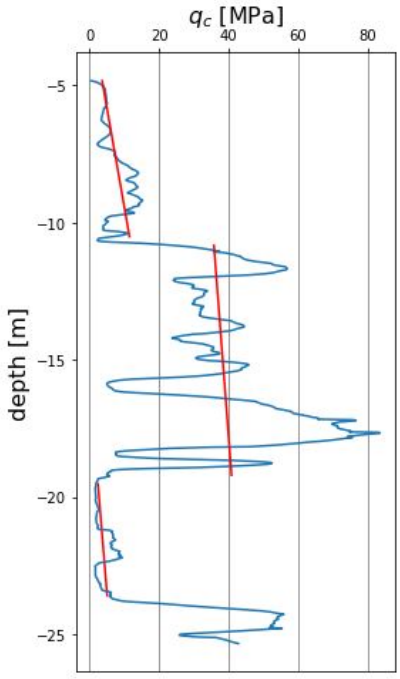


Figure 6.10: CPT DKP-9 including trendlines

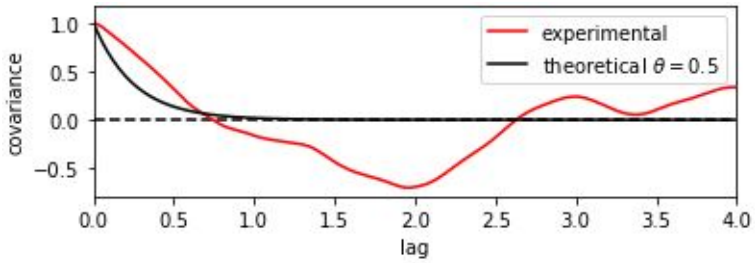


(a) Zone 1

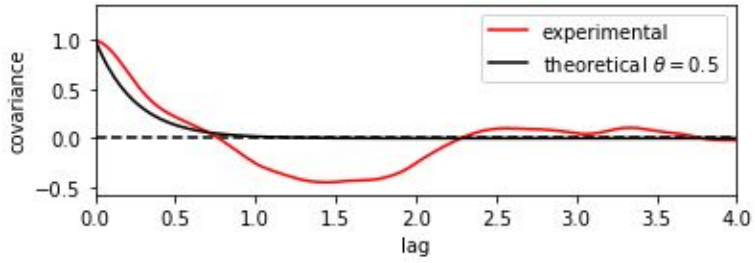


(b) Zone 2

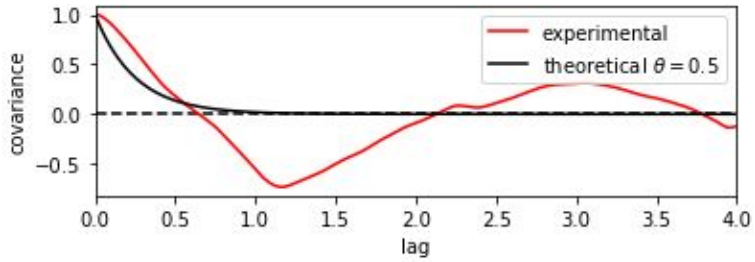


(c) Zone 3

Figure 6.11: Correlation length CPT DKP-9 Woudsend

### 6.2.4. Probabilistic prediction

For the probabilistic driveability prediction CPT DKP-9 is used a representative CPT. The probabilistic prediction method as used in the case study is slightly different as explained in chapter 5. The differences are explained in annex B. Improved insights after the case studies were made, led to changes in the generation of the stochastic soil profile. In table 6.3 the input parameters for the probabilistic prediction are summarized. The driveability prediction is repeated 40 times with the stochastic input parameters in a Monte Carlo simulation.

| | Soil heterogeneity | Transformation uncertainty |
|---|---|---|
| **Hammer** | | |
| Frequency | Deterministic (38.3 Hz) | |
| Excentric moment | Deterministic (35 kgm) | |
| Dynamic mass | Deterministic (5,600 kg) | |
| Static mass | Deterministic (2,600 kg) | |
| **Pile** | | |
| Geometry | Deterministic | |
| Material | Deterministic | |
| **Soil** | | |
| Shaft | | |
| Yield stress | Deterministic (see CPT DKP-9) | |
| Loading quake | $\sigma$ = 0.2 [mm] | - |
| Unloading quake | $\sigma$ = 0.2 [mm] | - |
| Yield factor | Deterministic (Shaft: 1.0, Toe: 0.1) | |
| Damping constant | $\sigma$ = 5.56, 53.5, 45.1 [kNs/m$^3$] | COV = 48.3 % |
| Power alpha | $\sigma$ = 0.18, 0.25, 0.36 [-] | $\sigma$ = 0.038 |
| $\beta$-factor | COV = 0.32 - 0.64 | - |
| Toe | | |
| Yield stress | Deterministic (see CPT DKP-9) | |
| Loading quake | $\sigma$ = 0.2 [mm] | - |
| Unloading quake | $\sigma$ = 0.2 [mm] | - |
| Yield factor | Deterministic (1.0/0.1) | |
| Damping constant | $\sigma$ = 59.1, 100.4, 62.1 [kNs/m$^3$] | COV = 57.6 % |
| Power alpha | $\sigma$ = 0.00, 0.00, 0.00 [-] | $\sigma$ = 0.038 |
| $\beta$-factor | COV = 0.32 - 0.73 | - |

Table 6.3: Allwave-PDP input parameters for probabilistic prediction

### 6.2.5. Results

A Monte Carlo simulation with 40 repetitions is made for both a capped and uncapped situation. In figure 6.12 and 6.13 the deterministic prediction and 40 repetitions with stochastic parameters are visualized for respectively uncapped and capped soil resistance. Only the part below a penetration speed below 40 mm/s and depth larger than -11 m N.A.P. is shown as this is relevant to determine the risk of refusal. The deterministic prediction, shown with the black line in figure 6.12 and 6.9, is the best estimated $v_p$-z-curve. This implies that the prediction is made with the default parameter of Allwave-PDP. The uncapped prediction gives a risk of refusal of 95% and the capped prediction gives a risk of refusal of 22.5% when the design penetration speed is 1 mm/s. The refusal rate of 55 out of 300 or 18% is measured in Geobrain for driving under the strict requirements given by the client (Deltares). Comparing prediction and practice shows that using uncapped values shows no agreement. The risk of refusal in prediction and practice for capped conditions have the same order of magnitude.

The pile driving system parameter values of the deterministic $v_p$-z-curve are used as the mean values of the probabilistic driveability prediction. The distribution of simulations with respect to the deterministic $v_p$-z-curve is therefore expected to be symmetrical. However, peaks are more extreme towards lower penetration speeds (visible at depths between -16 and -19 m N.A.P.). This implies that it is harder to regain penetration speed than to lose penetration speed.

When the pile regains penetration speed the $v_p$-z-curves converge (visible at a depth of -18 and -19 m N.A.P. in figure 6.9). This is expected to be caused by additional resistance in the form of damping when penetration speed increases. When penetration speed decreases a reduction of damping resistance occurs.

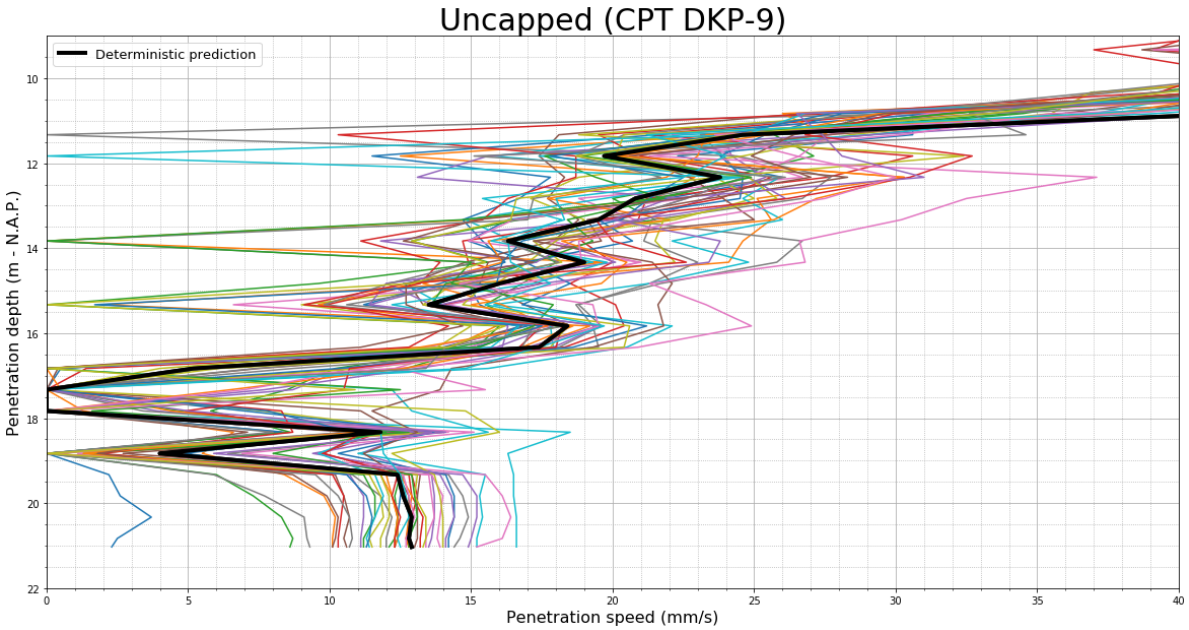


Figure 6.12: Probabilistic $v_p$-z-curve uncapped CPT Woudsend

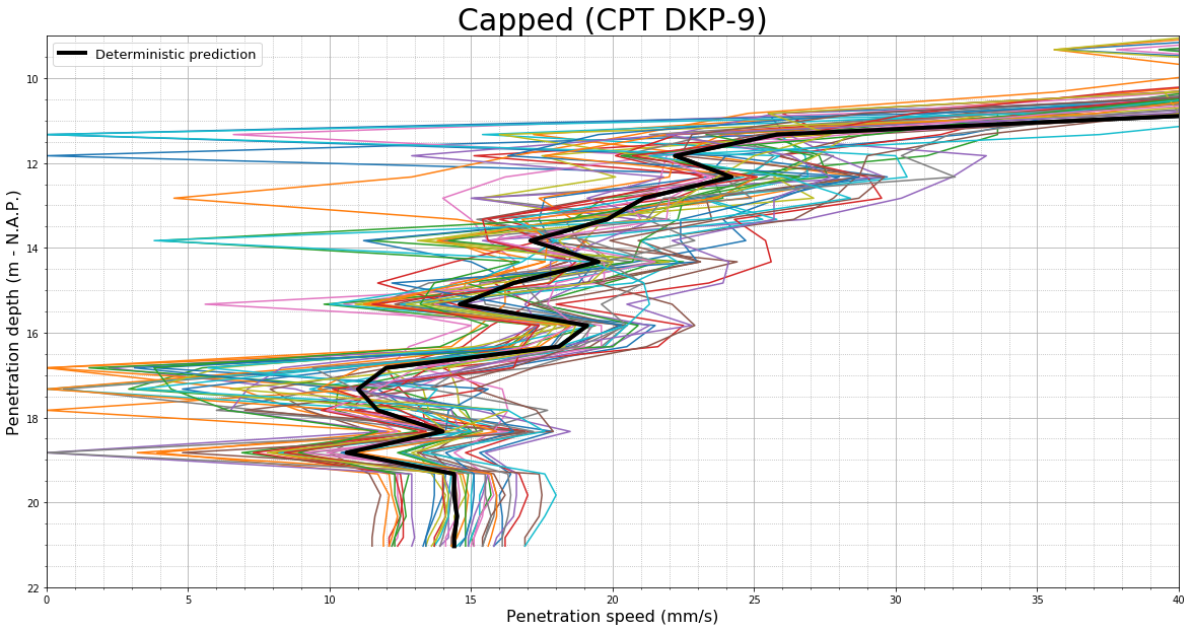


Figure 6.13: Probabilistic $v_p$-z-curve capped CPT Woudsend

## 6.3. Case study Rotterdam

### 6.3.1. Project

In project Maaskade, executed by contractor Hakkers and commissioned by Port of Rotterdam, 1,200 meter of sheet piles is driven in Rotterdam. 600 meter was part of the temporary cofferdam and another 600 meter part of the final quay wall. Various cross-sections and lengths of sheet piles are used during construction.

This project is used as a case study, because no significant problems were faced during driving of the sheet piles. The probabilistic prediction is made to check whether no false positives are found. This implies that is checked if the probabilistic method predicts a probability of refusal which is small enough to assume no cases of refusal in practice.

### 6.3.2. Conditions

As there are various CPTs provided to map the soil conditions and various sheet pile types are used throughout the project, a normative situation must be selected first. The sheet pile type AZ42-700 is the heaviest type used in this project. AZ42-700 sheet piles are used in the red-lined part of the quay wall shown in figure 6.20. Three CPTs are made in this area. The CPT with the hardest soil conditions is selected for the driveability prediction; CPTW11. This is not how a representative CPT is normally selected, as a representative CPT is normally a CPT with avereage properties. However, in this case study is investigated whether the prediction gives correct results in case of non-problematic driving projects. In the following sections further details are given on the three elements of the pile driving system.

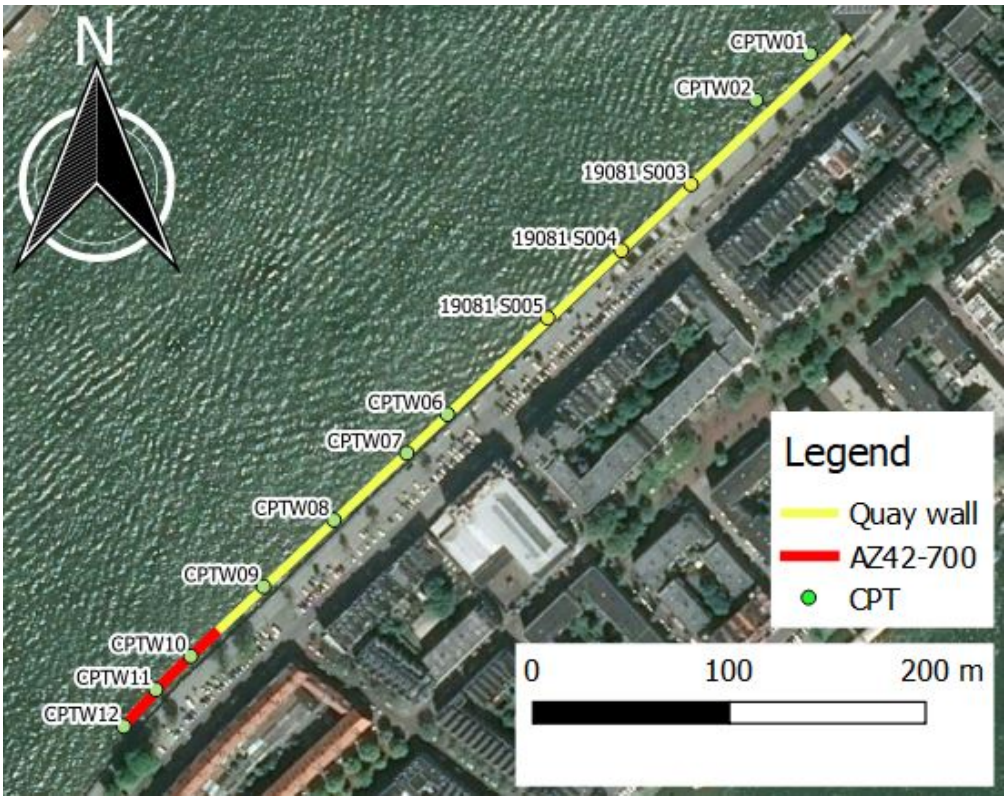


Figure 6.14: Project overview map

#### Pile

The normative part of the quay wall consists of 47 sheet pile of type AZ42-700N. The pile have a yield strength of 390 N/mm$^2$. In table 6.4 properties of this cross-section type are given and a cross section is shown in figure 6.15. The sheet piles have a length of 26.3 meter. The top of the sheet piles are placed at a final depth of +2.30 m N.A.P.. This implies a final driving depth at the toe of -24.00 m N.A.P.. The water bottom in CPTW11 is located at -5.50 m N.A.P..

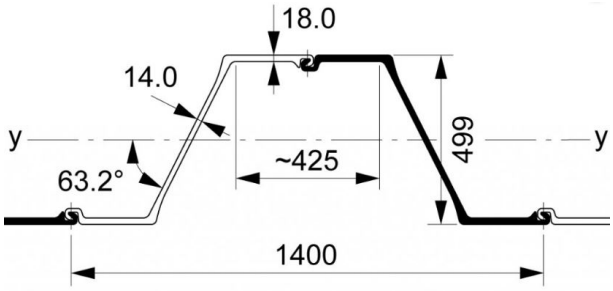


Figure 6.15: Cross sectional properties of AZ 42-700N (mm)

| AZ 42-700N (per double pile) | |
|---|---|
| Sectional area | 362.1 $cm^2$ |
| Mass per m | 284.3 kg/m |
| Moment of inertia | 146900 $cm^4$ |
| Coating area | 2.06 $m^2$/m |

Table 6.4: AZ 42-700N cross section properties

### Hammer

For driving the sheet piles a vibratory hammer PVE 2350VM is used. In table 6.8 specifications of this vibratory hammer are given. A clamp type DWK 350T is used. This clamp weighs 2,600 kg and connects the pile to the vibratory hammer.

| PVE 2350VM | |
|---|---|
| Ecc. moment | 0-50 kgm |
| Max. frequency | 2,300 rpm (38.3 Hz) |
| Centrifugal force | 0-2,900 kN |
| Amplitude | 0-14 mm |
| Total mass | 11,100 kg |
| Dynamic mass | 7,100 kg |

Table 6.5: PVE 2350VM specifications

### Soil

CPTW11 is the normative CPT when compared to CPTW10 and CPTW12. As mentioned before, the CPT with highest soil resistance is selected as a representative CPT. At CPTW11 the water bottom starts at -5.50 m N.A.P.. Between -5.50 and -19.0 m N.A.P. a clay layer is present and below -19.0 m N.A.P. a sand layer is present.

## 6.3.3. Representative CPT

The representative CPT is divided into three geological layers as there is a jump in cone resistance at -19 m N.A.P.. The third zone is not further investigated as the maximum penetration depth is only -24 m N.A.P.. Therefore, only two values per parameter are noted in table 6.9 for data scatter. In figure 6.17 the correlation length for the zones of the soil profile are given. The first zone, predominantly consisting of clay, has a scale of fluctuation of 0.5 meter. The other zones have a scale of fluctuation of 1.0 meter.

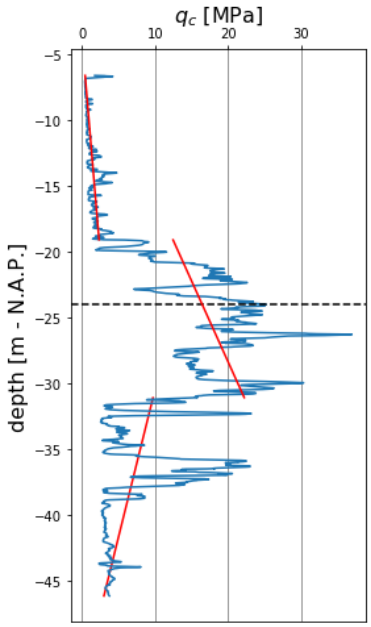


Figure 6.16: Cone resistance CPTW11 including trendlines

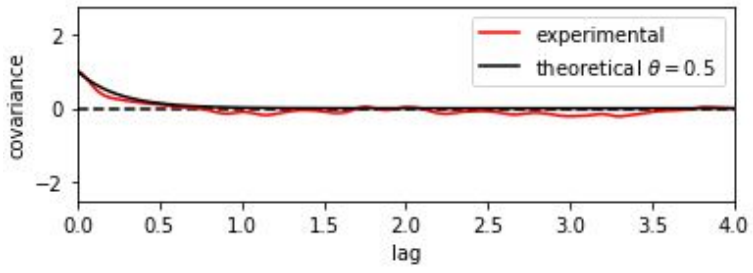


(a) Zone 1

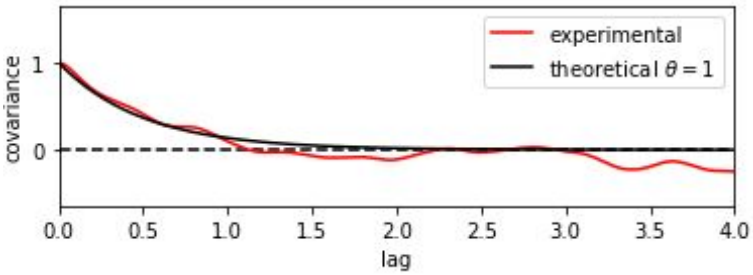


(b) Zone 2

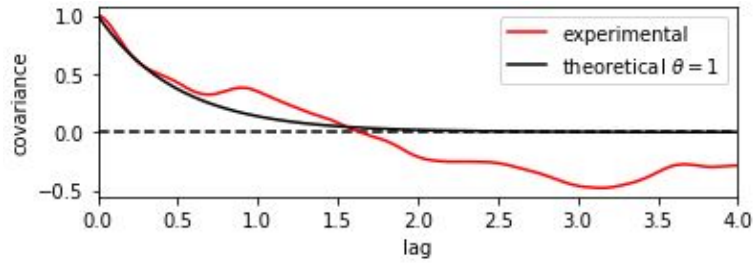


(c) Zone 3

Figure 6.17: Correlation length CPTW11 Maaskade

### 6.3.4. Probabilistic prediction

The probabilistic prediction is made with the parameters given in table 6.9. In figure 6.18 the results are shown for the default probabilistic prediction. This prediction corresponds with the situation in practice; no problems occurred during driving. The deterministic prediction is shown by the thick black line.

The correlation length of maximum 1.0 meter in this soil profile is relatively short compared to the penetration depth of 18.5 meter. It is hypothesized that the extreme values caused by spatial variability average out. This is tested by taking into account only the transformation uncertainty in the probabilistic soil model parameters. The result is shown in figure 6.19.

| | Soil heterogeneity | Transformation uncertainty |
|---|---|---|
| **Hammer** | | |
| Frequency | Deterministic (38.3 Hz) | |
| Excentric moment | Deterministic (50 kgm) | |
| Dynamic mass | Deterministic (7,100 kg) | |
| Static mass | Deterministic (4,000 kg) | |
| **Pile** | | |
| Geometry | Deterministic | |
| Material | Deterministic | |
| **Soil** | | |
| Shaft | | |
| Yield stress | Deterministic (see CPTW11) | |
| Loading quake | $\sigma$ = 0.2 [mm] | - |
| Unloading quake | $\sigma$ = 0.2 [mm] | - |
| Yield factor | Deterministic (Shaft: 1.0, Toe: 0.1) | |
| Damping constant | $\sigma$ = 2.8, 9.1 [kNs/m$^3$] | COV = 48.3 % |
| Power alpha | $\sigma$ = 0.34, 0.13 [-] | $\sigma$ = 0.038 |
| $\beta$-factor | COV = 0.32 - 0.64 | - |
| Toe | | |
| Yield stress | Deterministic (see CPTW11) | |
| Loading quake | $\sigma$ = 0.2 [mm] | - |
| Unloading quake | $\sigma$ = 0.2 [mm] | - |
| Yield factor | Deterministic (1.0/0.1) | |
| Damping constant | $\sigma$ = 37.9, 51.4 [kNs/m$^3$] | COV = 57.6 % |
| Power alpha | $\sigma$ = 0.00, 0.00 [-] | $\sigma$ = 0.038 |
| $\beta$-factor | COV = 0.32 - 0.73 | - |

Table 6.6: Allwave-PDP input parameters for probabilistic prediction

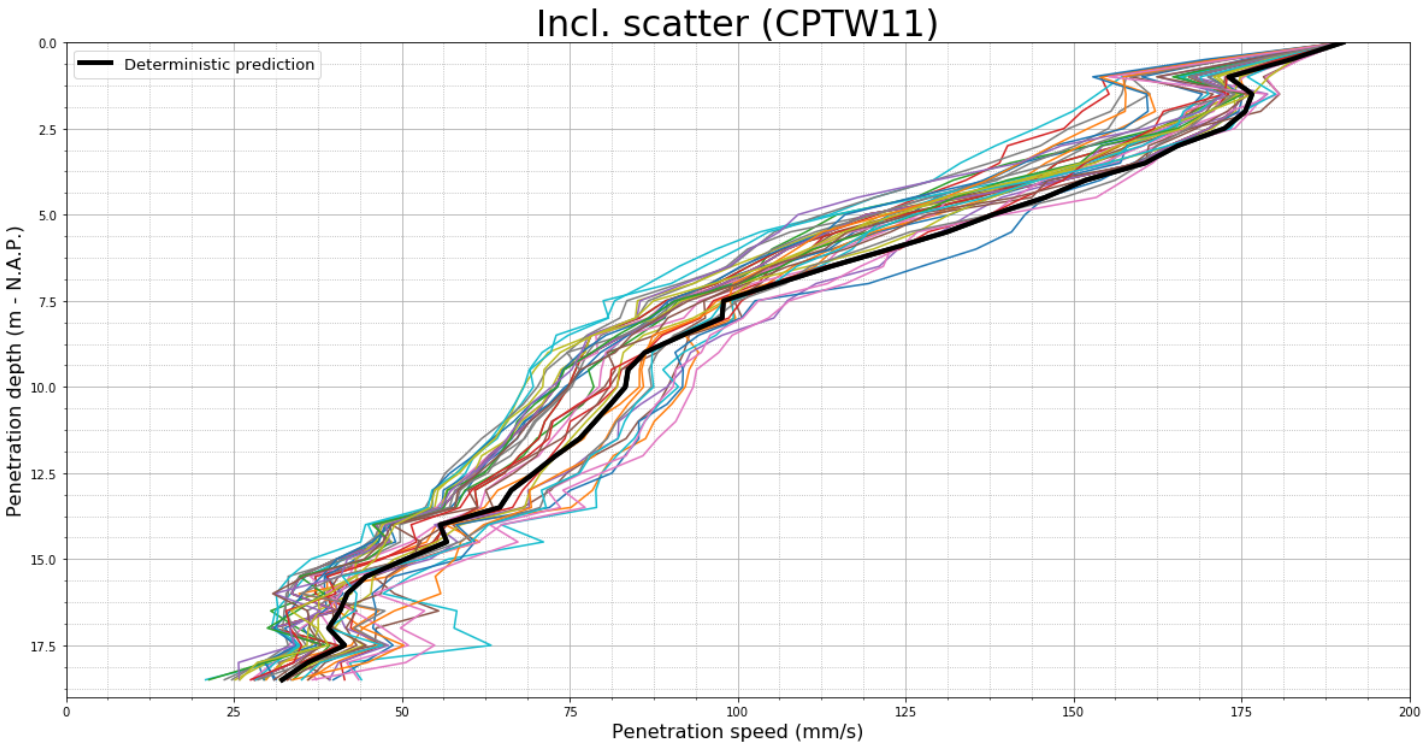


Figure 6.18: Probabilistic $v_p$-z-curve including data scatter Maaskade

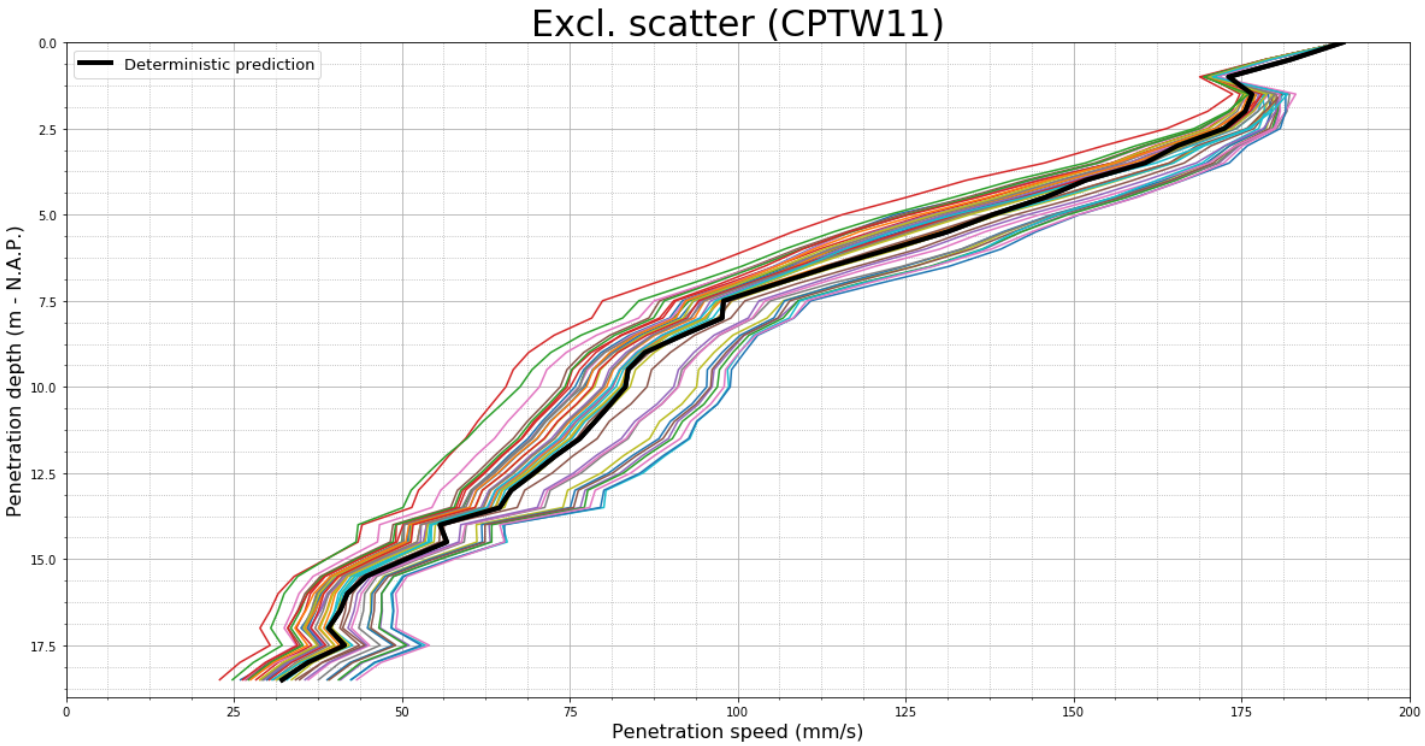


Figure 6.19: Probabilistic $v_p$-z-curve excluding data scatter Maaskade

# 6.4. Case study Den Oever

## 6.4.1. Project

As part of a renovation of a harbour in Den Oever, situated in the northwestern part of the Netherlands, new quay walls must be installed. This quay wall will consist of steel sheet piles and will be installed in front of the old wall. After installation of the new quay wall, the old quay wall will be removed. Sheet pile driving as part of the construction of the new quay wall started at February 20$^{th}$ 2.00 PM. On March 8th sheet pile driving of the new quay wall was completed. From the 38$^{th}$ element on fluidization was used to drive the sheet piles due to hard soil conditions. During fluidization water is injected in the soil under high pressure at the pile tip to loosen the soil.

## 6.4.2. Conditions

### Pile

The quay wall consists of sheet pile of type AZ44-700N. The pile have a yield strength of 355 N/mm$^2$. In table 6.7 properties of this cross-section type are given and a cross section is shown in figure 6.20. The sheet piles have a length of either 23 or 20 meters. From the starting point of installation 58 piles will have a length of 20 meters and the remainder of 34 piles has a length of 23 meters. In this case study only the pile with a length of 20 meters will be studied. The top of the sheet piles are placed at a final depth of +1.05 m N.A.P.. This implies a final depth at the toe of -19.00 m N.A.P.. Driving starts at the bottom level of the water at -5.00 m N.A.P..

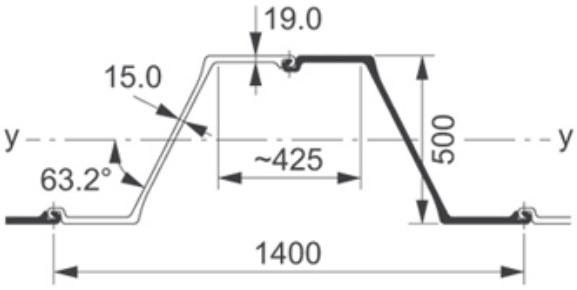


Figure 6.20: Cross sectional properties of AZ 44-700N (mm)

| AZ 44-700N (per double pile) | |
|---|---|
| Sectional area | 382.0 cm$^2$ |
| Mass per m | 299.8 kg/m |
| Moment of inertia | 154210 cm$^4$ |
| Coating area | 2.06 m$^2$/m |

Table 6.7: AZ 44-700N cross section properties

### Hammer

For driving the sheet piles PVE 2350VM is used. In table 6.8 specifications of this vibratory hammer are given. A clamp type DWK 350T is used. This clamp weighs 2,600 kg and connects the pile to the vibratory hammer.

| PVE 2350VM | |
|---|---|
| Ecc. moment | 0-50 kgm |
| Max. frequency | 2,300 rpm (38.3 Hz) |
| Centrifugal force | 0-2,900 kN |
| Amplitude | 0-14 mm |
| Total mass | 11,100 kg |
| Dynamic mass | 7,100 kg |

Table 6.8: PVE 2350VM specifications

### Soil

Near the quay wall 9 CPT's have been done, as shown in figure 6.21. However, none of the land-based tests, the BU series, do reach the installation depth of the sheet piles. The maximum depth reached by the land-based tests is -17.5 m N.A.P..


Figure 6.21: Map of CPT locations and quay wall

## 6.4.3. Representative CPT

CPT DKMP23 is selected as a representative CPT for case study Den Oever. This CPT is selected from CPT DKMP22 to DKMP26. Based on the visual judgment a DKMP25 and DKMP26 are determined not to be representative for the soil profile of the quay wall. Namely DKMP25 and DKMP26 contain an overconsolidated sand layer which is above and below average thickness respectively. As additional information a deterministic prediction is made for DKMP22, DKMP23 and DKMP24, see figure 6.22. No clear difference between those CPT's can be notified. DKMP23 is selected eventually, because it is positioned in between CPT DKMP22 and DKMP24.

The representative CPT is divided in three geological layers. The divisions are located at -9.5 m N.A.P. and -17 m N.A.P..

Due to lacking digital files of the CPT's, the correlation length of the soil profiles cannot be determined. Therefore, a vertical correlation length of 1.0 m is assumed. This length is often found in CPT's.

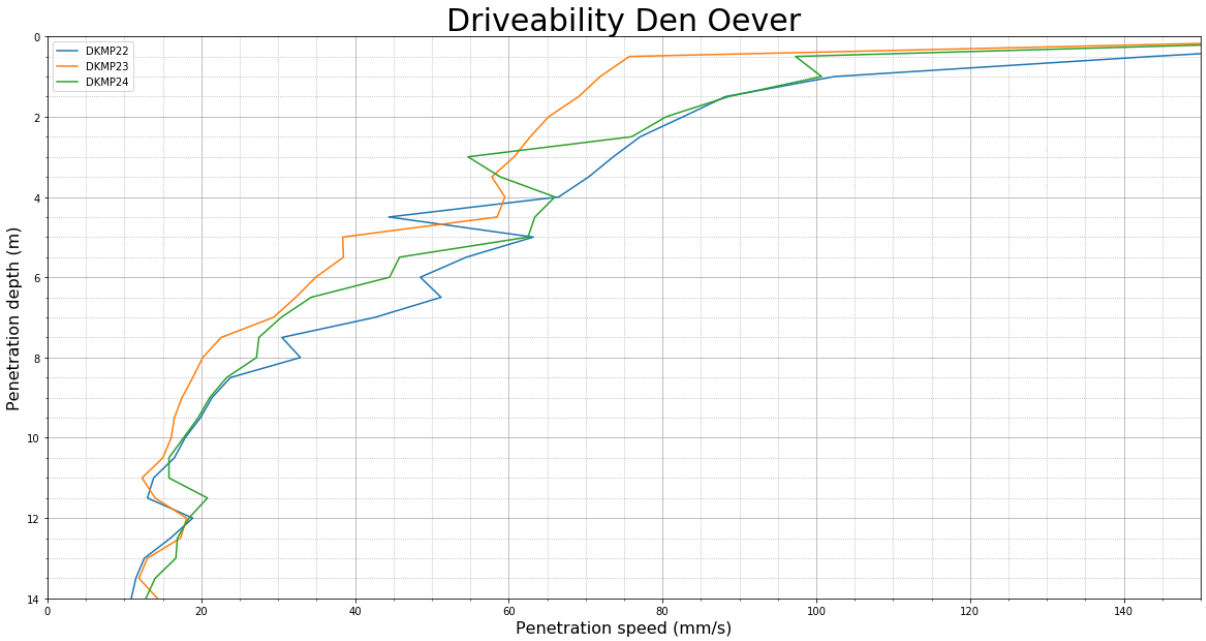


Figure 6.22: Depth-penetration speed-graph of prediction for DKMP22, DKMP23 and DKMP24

### 6.4.4. Probabilistic prediction

The probabilistic prediction input is given in table 6.9. Also a deterministic prediction is made as a comparison.

| | Soil heterogeneity | Transformation uncertainty |
|---|---|---|
| **Hammer** | | |
| Frequency | Deterministic (36 Hz) | |
| Excentric moment | Deterministic (50 kgm) | |
| Dynamic mass | Deterministic (7,100 kg) | |
| Static mass | Deterministic (4,000 kg) | |
| **Pile** | | |
| Geometry | Deterministic | |
| Material | Deterministic | |
| **Soil** | | |
| Shaft | | |
| Yield stress | Deterministic (see CPT DKMP23) | |
| Loading quake | $\sigma$ = 0.2 [mm] | - |
| Unloading quake | $\sigma$ = 0.2 [mm] | - |
| Yield factor | Deterministic (Shaft: 1.0, Toe: 0.1) | |
| Damping constant | $\sigma$ = 56.9, 32.6, 33.0 [kNs/m$^3$] | COV = 5.6 % |
| Power alpha | $\sigma$ = 0.21, 0.20, 0.14 [-] | $\sigma$ = 0.038 |
| $\beta$-factor | COV = 0.32 - 0.64 | - |
| Toe | | |
| Yield stress | Deterministic (see CPT DKMP23) | |
| Loading quake | $\sigma$ = 0.2 [mm] | - |
| Unloading quake | $\sigma$ = 0.2 [mm] | - |
| Yield factor | Deterministic (1.0/0.1) | |
| Damping constant | $\sigma$ = 36.2, 82.2, 151.7 [kNs/m$^3$] | COV = 5.6 % |
| Power alpha | $\sigma$ = 0.00, 0.00, 0.00 [-] | $\sigma$ = 0.038 |
| $\beta$-factor | COV = 0.32 - 0.73 | - |

Table 6.9: Allwave-PDP input parameters for probabilistic prediction

### 6.4.5. Results

13 out of 40 sheet piles refuse in the Monte Carlo simulation. This is 33% of the total amount. It can be seen in figure 6.23 that refusal occurs as a result of sudden jumps in penetration speed.

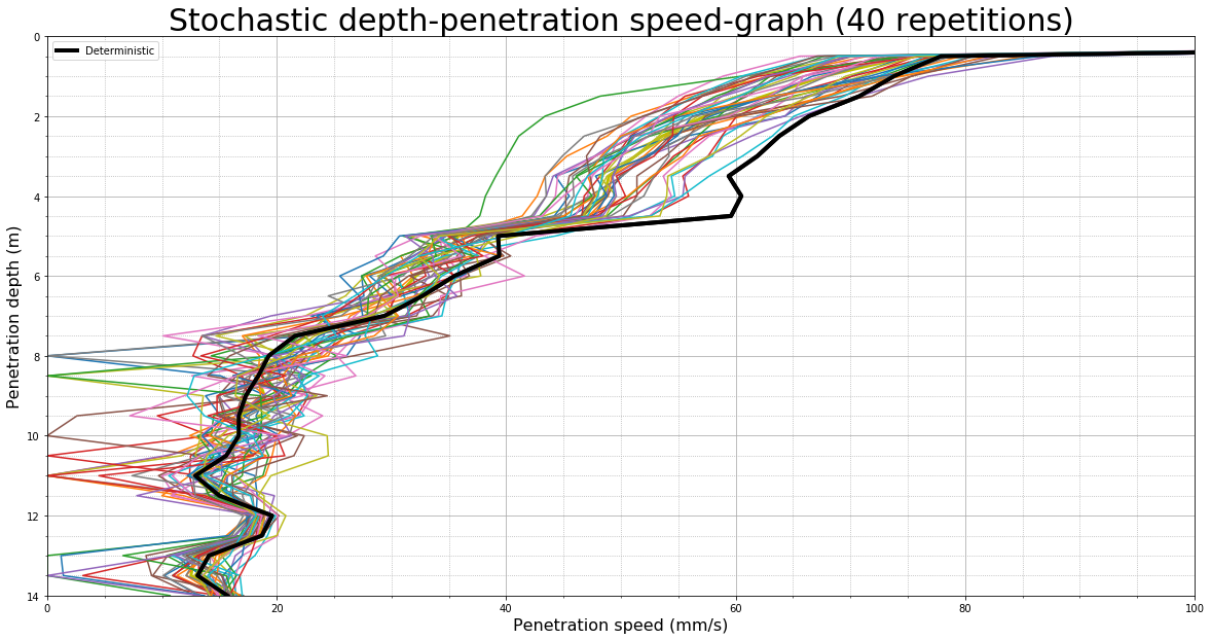


Figure 6.23: Stochastic depth-penetration speed-graph (40 repetitions)

## 6.5. Conclusion

The case studies validate the probabilistic method and prove that the order of magnitude of prediction and measurement agree.

In project Woudsend a refusal percentage of 18% is predicted, whilst a percentage of 25% is measured. The additional value of a probabilistic method is shown in project Woudsend. The capped deterministic prediction in project Woudsend predicts succesful installation for every usable CPT. Thus no risk of refusal would have been predicted by a deterministic method. However, in practice refusal occurred and was also predicted by the probabilistic method.

In case study Den Oever the probabilistic method predicts a significant probability of refusal, namely 33%. This is confirmed by observations in practice to be a good prediction. Halfway during the driving project refusal occurred. From that point on fluidization was used. Due to fluidization predicted and measured refusal percentage cannot be fairly compared. The probablistic method predicts problematic driving in contrast to the deterministic method which do not predict refusal.

In case study Rotterdam no false positives are found. A false positive is a case where a significant risk of refusal is predicted, whilst this is not the case in practice. It was hypothesized that the variability of soil model parameters could lead to sudden variation of the predicted driving speed. This appears not to be the case.

The deterministic prediction is made with default parameter values provided by Allwave-PDP. The Allwave-PDP parameter values are assumed to be the best estimate. This means that the deterministic $v_p$-z-curve is located in the middle of all generated $v_p$-z-curves. It is reasoned that in Allwave-PDP parameter values are used that result in the best estimated prediction.

It is promising to further investigate the role of spatial variability on the predicted refusal percentage. Incorporating spatial variability is labour-intensive and thus neglecting this would simplify tasks. In case study Rotterdam a probabilistic prediction with and without spatial variability considered show roughly the same spread of $v_p$-z-curves.

Application of the probabilistic method in practice leads to some conclusions on the method itself. In the case studies in this research the geological layer division is obvious. For other soil profiles the division might be less distinct. This introduces subjectivity into the probabilistic method. Division into three geological layers seems to be sufficient for the majority of soil profiles in the Netherlands. The selection of a representative CPT introduces ambiguity. A representative CPT must have average properties compared to other CPT's. A balance must be found

between multiple properties; layer division, variability and trend lines. In these case studies also the deterministic $v_p$-z-curve is taken into account when a representative CPT is selected. When the soil investigation does not give homogeneous CPT results, it must be considered to use multiple representative CPT's in the Monte Carlo simulation.

# 7

# Discussion

The objective of this research is to incorporate probability theory in the pile driveability prediction method. An existing, deterministic prediction method (Allwave-PDP) is extended to get a probabilistic method. In the deterministic method input parameters must be defined for the pile driving system (pile, hammer and soil). The deterministic soil model parameters are turned into as stochastic parameters in the probabilistic method. The variability is caused by transformation uncertainty and soil heterogeneity. The spatial variability of soil model parameters, caused by soil heterogeneity, is modelled by random fields. The transformation uncertainty is considered by a model error constant for each geological layer. The probabilistic method is applied to three case studies for validation. These case studies show agreement in the order of magnitude of predicted and measured probability of refusal.

The probabilistic method as designed in this research is a proof of concept that shows the potential of application of probability theory to driveability prediction methods. Probability theory has not been applied to driveability prediction methods before. Prior to this research there was concern that spread of results in the form of $v_p$-z-curves would be unrealistically large. This concern was caused by the fact that a large numbers of input parameters is used and that the variability of input parameter values can be large. This research is in line with path of development of geotechnics as described by Christian, 2004. It states that the geotechnical community long ago learned practical ways to deal with uncertainty. However, it has been reluctant to embrace the more formal and rational approach of probability theory, while other fields of civil engineering have made major commitments to probabilistic approaches. Nevertheless, over the last decades several researchers have made major advances in applying probabilistic methods to geotechnical problems (Christian, 2004).

A probabilistic prediction method should be considered as complementary to the deterministic prediction methods. The probabilistic method especially provides added value in high-risk projects. Uncertainty in a deterministic method is taken into account by safety factors. A probabilistic method provides a logical framework for choosing a safety factor appropriate for the degree of uncertainty. The relationship between safety factor and degree of uncertainty serves to distinguish conditions where lower-than-normal factors of safety are appropriate or where higher-than-normal factors of safety are needed (Duncan, M.J., 2000). See also the recommendations section where is advised to revise the safety factor.

Due to the low accuracy of the prediction use of nominal categories would provide satisfactory precision to classify driving projects. The use of specific refusal percentages would result in a false look of precision. It would be more appropriate to use nominal categories. E.g. a low-risk-category (0-33%), an intermediate-risk-category (34-66%) and a high-risk-category (67-100%), where the adequate refusal percentage is shown in brackets. The probabilistic prediction result is useful information in a risk assessment of a driving project. The risk assessment helps to deal in a proper way with uncertainty. Decision-making on hammer selection and remedial measures, e.g. fluidization or pre-drilling, is improved. Also experimental tests, e.g. test driving of piles, could be done when a high risk of refusal is predicted.

The probabilistic extension on Allwave-PDP is easily applicable to different pile types or impact hammer driving systems. The extensions to incorporate probability theory into the soil model parameters are written in Python. This programming language is accesible for most civil engineers.

## 7.1. Limitations

### 7.1.1. Horizontal correlation

In the probabilistic method there is assumed that horizontal correlation is absent in the soil. In practice, there will always be horizontal correlation as neighbouring vertical soil profiles will not be completely different. In a typical driving project the CPT's are approximately 25-50 m apart in the horizontal direction. This distance makes it impossible to accurately estimate the horizontal correlation Lloret-Cabot et al. (2014). In this research is sought for a horizontal correlation coefficient ($r$) somewhere between 0 and 1 as this is most realistic. This is done by assuming no horizontal correlation in the generation of the random field ($r = 0$). The geological layer division is taken as deterministic. Thus there is no variation in layer division between randomly generated soil profiles ($r = 1$). These fully uncorrelated and fully correlated functions are assumed to result in horizontal correlation somewhere between 0 and 1. This qualitative reasoning is assumed to be the best approximation of practice.

### 7.1.2. Transformation uncertainty

The inquiry to quantify transformation variability introduces a lot of uncertainty. The coefficient of variation of each soil model parameter to consider the transformation uncertainty is derived from literature. Originally, this literature was not intended for investigation of the statistics of soil model parameters. The research often has a limited amount of experiment repetitions under equal conditions. This makes it hard to define statistical parameters. Also the experiment set-up is varying throughout research. This adds further uncertainty to the soil model parameters. A few examples are given on the uncertainty of transformation variability. Two different experiment set-ups were used in research papers to determine damping constants. One set-up releases a weight on a specimen, whilst the other penetrates a soil specimen with a pile. Also the results of both experiments are expressed by the Smith damping constant, whilst in Allwave-PDP the TNOWAVE damping constant is used to express damping. Also the damping constant for the shaft of sand is assumed to be identical to that of clay as there are no experimental results on sand. For quake no experimental values for vibro driving were found. Only results for impact driving were found.

### 7.1.3. $v_p$-z-curve

The $v_p$-z-curve is more an indication of driveability than of the actual penetration speed against the depth according to experts of Allnamics. The prediction algorithm is not accurate enough to predict the driving time of an individual pile. This introduces uncertainty to the failure level. In this research failure is defined as when the driving speed becomes lower than 1 mm/s. When the driving speed is only an indication of driveability, the failure level cannot be defined accurately. For example, it is not clear if pile refusal occurs in a soil profile with a thin, hard layer. A $v_p$-z-curve hypothetically shows a peak with a minimum of 0 mm/s at the depth of the thin hard layer. According to the strict failure level definition, pile refusal would occur when the pile hit this thin, hard layer. In practice, when this thin, hard layer is hit by the pile and the driving speed is 0 mm/s, the crane operator would re-lift the pile to regain momentum and driving force. In case the re-lifting leads to penetration of the 'impenetrable' layer, it might be concluded that defining failure level only by driving speed is unsatisfactory. Also a minimum distance over which the non-exceedance of the driving speed occurs might then be required to define pile refusal. Namely, re-lifting the pile can only be applied to a certain extent, namely repeating this process a large number of times could lead to damage and delays.

### 7.1.4. Interlock friction

In the Allwave-PDP software the interlock friction is not taken into account correctly. Therefore, interlock friction is neglected in this research. However, in interviews with construction workers of Hakkers B.V. it is mentioned that in some projects the interlock friction is higher than the soil resistance itself. Logically, this has a large impact on driveability. Data in literature on interlock friction is scarce. This makes it hard to incorporate interlock friction in the probabilistic prediction method in the future. Also the variability of interlock friction is expected to be large. Unpredictable parameters, like placement angle, crane operator's competence and the quality of the interlocks influence the magnitude of the interlock friction. A small placement angle (relative to the vertical line) is of great importance in reducing interlock friction. A larger placement angle causes higher interlock friction as it requires more force to slide the locks of both the installed and neighbouring element along each other. Strong winds cause more variation in the placement angle.

### 7.1.5. Slenderness
Slenderness of the pile results in a loss of driving force. Namely, during start of driving when a large part of the pile is above the ground, bending prevents vertical movement. The horizontal movement can absorb as much as 30% of the energy of the vibro hammer (Viking, 2002). This loss of energy as a function of the slenderness is not considered in Allwave-PDP and this research. This limitation is becoming increasingly important as manufacturers constantly strive for a higher section modulus/mass ratio. This results in a more economic cross-section type, but also in a higher slenderness.

## 7.2. Recommendations
### 7.2.1. Validation
It is recommended to validate the probabilistic method with more diverse case studies. In this research the probabilistic method is only applied to case studies where the soil profile consists predominantly of overconsolidated sandy soil. Case studies with clayey soil profiles would give insight in how the probabilistic method would behave under different conditions. For validation driving projects on different soil types must be monitored and documented. Next to that, more repetitions per Monte Carlo simulation must be made to obtain a more accurate outcome of the probabilistic prediction. In the Monte Carlo simulation 40 repetitions are made due to limited computation power and a labour-intensive simulation. Currently the accuracy of the results of the probabilistic method is low. The relative error of the Monte Carlo simulation is 0.47.

### 7.2.2. Safety factor
It is recommended to revise the safety factor of 1.25 which is often used driveability predictions to consider local variability (Jonker, 1987). In two case studies where pile refusal occurs (Den Oever and Woudsend) is tested whether this safety factor predicts refusal. This is not the case; a prediction with a safety factor predicts succesfull installation. In these case studies it appears that the safety factor is too low. For Woudsend, refusal was predicted for a safety factor of 1.7 or higher.

### 7.2.3. Application of full soil investigation
In future research all information offered by the CPT's in the soil investigation must be utilized. In the developed method, only one representative CPT is used to extract soil statistics to generate stochastic soil profiles. These soil statistics are trend lines, geological layer divisions and correlation length. The representative CPT must have average properties compared to the other CPT's provided in the soil investigation. Namely, the trend lines and layer division are intended to function as an 'average' base on which the randomly generated characteristics are added to create a random soil profile. In practice, the variation in trend layers and layer division adds extra uncertainty. This is not taken into account in the current probabilistic method. In figure 7.1 confidence intervals for layer divisions and trend lines are shown in respectively yellow and red. The statistical properties can be obtained by analyzing all CPT's of the soil investigation.

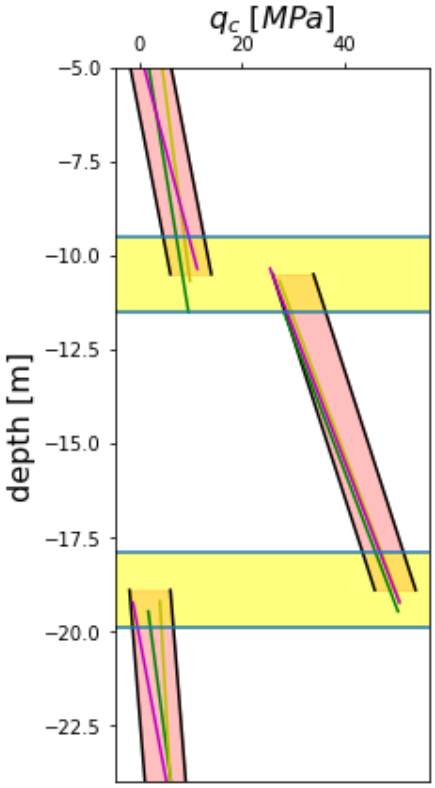


Figure 7.1: Statistics of layer division and trends

### 7.2.4. Hammer-soil resistance relation

In this research a strong, negative correlation between hammer frequency and soil resistance is found. Also the static mass of the hammer is observed to vary with driving speed. It is advised to the developers of Allwave-PDP to establish a relation between frequency and soil resistance in their software. It is advised to interpolate the hammer frequency between the maximum frequency (38.3 Hz) and the lowest observed frequency (32 Hz) depending on the soil resistance. When soil resistance is absent, maximum frequency is used. Minimum frequency is used when driving force and soil resistance are equal. The static mass applied to the pile driving system is varying throughout the pile installation. As the driving speed decreases, the static mass is more likely to be fully present. To resemble practice better static mass could be made a function of penetration speed. When the driving speed is below a certain value, the static mass is fully present. It is recommended to make static mass a function of driving speed with full application below 10 mm/s.

### 7.2.5. Effect of spatial variability

Not having to consider the spatial variability in the stochastic soil profile would save a significant amount of work. In future research the variation introduced by spatial variability should be compared to variation by transformation variability. Due to a relatively short correlation length (0.5-1.0 m) compared to penetration depth (approximately 15 m), the mean of the deviations caused by spatial variability tends to go to zero. When it appears that data scatter has no significant effect on the probabilistic prediction, the spatial variability uncertainty can be left out of the prediction. For sandy soil types, where the sheer part of resistance is tip resistance, spatial variability is expected to have a significant effect on driveability. In clayey soils, where most resistance is caused by shaft resistance, the total shaft resistance middles out. This results in only a small effect of the peaks in soil resistance.

In case of pile refusal due to excessive shaft resistance, the average shaft resistance is of importance. Namely,

# 8

# Conclusions

In this thesis an answer is sought to the following research question:

> **How can the probability of failure of a driving process of sheet piles installed by a vibro hammer be predicted by means of a $v_p$-z-curve?**

The answer to this question is formulated after answering four subquestions. The answers to the subquestions are formulated below. Consequently, the relevance of this research is elaborated on. Also future research recommendations are given.

## 8.1. Answers to subquestions

**What is the transformation uncertainty of soil parameters of the pile driveability prediction?** The transformation uncertainty is introduced when Cone Penetration Test (CPT) results are transformed to Allwave-PDP soil parameters ($\beta$-factor, quake, damping constant and damping exponent). The transformation uncertainty has been found by using experimental data. The scatter of experimental data is determined and results of different experiments vary. This two-fold variation leads to uncertainty of the transformation relation.

The transformation relation is assumed not to vary in a geological layer. A geological layer is defined as a layer with homogeneous soil properties. Soil properties like roundness of grains and overconsolidation, which are not measured by a CPT, influence soil parameters. These are assumed not to vary significantly throughout the layer and therefore the transformation variability can be modelled by a systematic deviation of parameters of the geological layer. The soil parameters are multipied by a randomly generated constant value for each geological layer, see step 3 in figure 8.1.

**What method incorporates the spatial variability of soil parameters in the pile driveability prediction?** The spatial variability is caused by soil heterogeneity. CPT's are only made at 25-50 m horizontal distance in a typical sheet pile driving project. This causes uncertainty in the values of the soil parameters of the installation location at a horizontal distance from the CPT location. The vertical autocorrelation is established by CPT data and quantifies the variation in the vertical direction around the trend line of a CPT. A one-dimensional, vertical random field is generated by the autocorrelation.

The horizontal spatial variability cannot be quantified, because horizontal distance between CPT's in a typical pile driving project is too large. It is assumed that in the generation of a one-dimensional random field there is no horizontal correlation. This implies that one-dimensional soil profiles can be completely different whilst right next to each other in the horizontal plane ($r = 0$). In practice, there will always be a certain amount of horizontal correlation in the soil. Therefore, the geological layer division is taken as deterministic. Thus there is no variation in layer division, which implies full horizontal correlation ($r = 1$). It is reasoned that using two extremes imitates a situation where the Pearson's correlation coefficient is an intermediate value between 0 and 1.

The stochastic soil parameter profile is composed in various steps. Firstly a trend line is established for the representative soil parameter values, which are derived from a representative CPT. To these trend lines a soil parameter-specific random field is added, see step 1 in figure 8.1. This specific random field is obtained by

multiplying a standard random field by the residual standard deviation ($\sigma_{res}$), see step 2 in figure 8.1. $\sigma_{res}$ expresses the variation around the trend line of a soil parameter.

To generate the soil parameter-specific random fields an identical standardized random field is used. This implies that the depth-dependent variation of the soil parameters is equal. All soil parameters are directly or indirectly related to the CPT, Therefore, the use of an identical random field is a reasonable model choice.

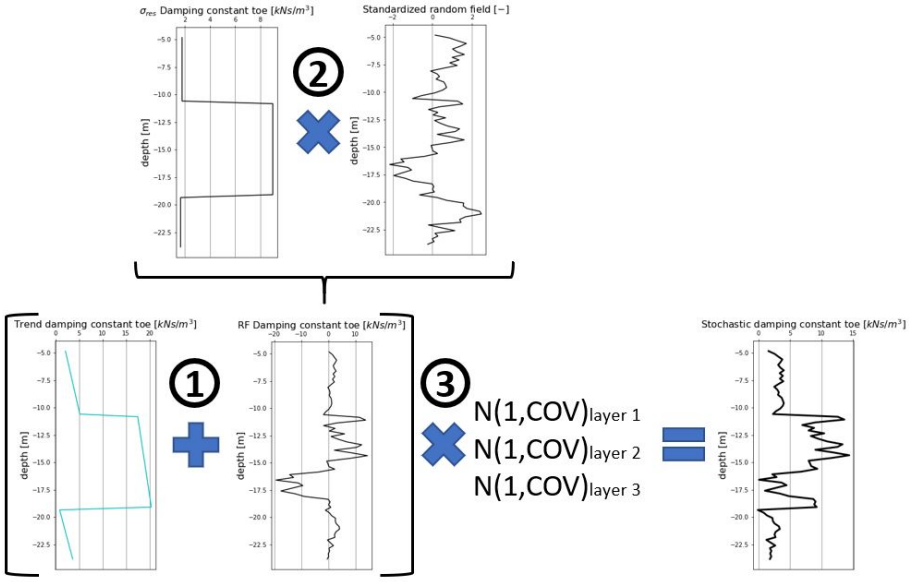


Figure 8.1: Composition of stochastic soil profile (Damping constant)

**What is the variability of hammer and pile properties?** The hammer and pile properties are considered to be deterministic properties in the probabilistic prediction method. Manufactured materials can be controlled within a narrow range, thus it is a reasonable assumption to neglect this variability (Phoon et al., 2016). Especially when compared to the magnitude of variability of soil properties. This assumption results in deterministic values for pile properties and static properties of the hammer (e.g. geometry and weight). The dynamic properties of the hammer, which are influenced by the driving process (e.g. soil resistance and pile weight), are the frequency and static mass. The frequency of the hammer decreases when resistance of the driving system increases. In field measurements a strong, negative correlation between soil resistance and frequency is found. However, in Allwave-PDP only a point statistic is allowed as an input parameter for the frequency. Therefore, based on field measurements a frequency of 36 Hz is chosen as deterministic value. The hammer used during these field measurements has a default frequency of 38.3 Hz. This implies that the frequency used in the probabilistic method is reduced by 6%. The static mass used in the probabilistic method is the full static mass of the hammer. As the penetration speed is low at failure or near-failure conditions, it is reasonable to assume that the crane operator can apply the full static mass to the driving system.

**What is the validity of the probabilistic pile driveability prediction method?** The predicted results of the probabilistic prediction method show agreement with the measured results; the order of magnitude of probability of failure agrees. The validity of the probabilistic method is tested by three case studies of sheet pile driving projects; Den Oever, Woudsend and Maaskade. In case study Maaskade no cases of refusal occurred during the project. This case study was done to check whether the probabilistic method would not give false positives, implying that refusal would be predicted whilst no driving problems occurred in practice. The conditions of the case studies were well-reported and also driveability problems were quantified (percentage of sheet piles that refuses). The probabilistic method predicts an expected percentage of refusal piles, which also indicates the probability of refusal of an individual pile.

## 8.2. Answer to research question

The information provided by the answers to the subquestions provides sufficient information to answer the research question.

The probability of failure of a driving process is predicted by incorporating probability theory into a practice-proven prediction method, Allwave-PDP. Allwave-PDP predicts driveability by a driving speed-depth-curve ($v_p$-z-curve) and requires properties of the driving system (pile, hammer and soil) as input. A Monte Carlo simulation is made to find the probability of failure of a driving process. In this simulation a unique $v_p$-z-curve is found for every repetition. When the penetration speed ($v_p$) falls below 1 mm/s refusal occurs.

Probability theory is incorporated by using stochastic values for the soil parameters (yield stress, $\beta$-factor, quake, damping constant and damping exponent). In the stochastic soil parameters uncertainty due to transformation and spatial variability is considered. The input parameters of hammer and pile remain deterministic. The default hammer frequency is decreased by 6% before being used as an input parameter in the probabilistic method.

## 8.3. Relevance

This probabilistic model is a proof of concept that shows the potential of applying probability theory to driveability prediction method. Probability theory had not been applied to driveability prediction methods before. Broadly, the proof of concept can be divided in a modelling and a methods part. The former part gives proof of concept of the modelling of uncertainty in the driveability prediction method. The latter proves that implementing stochastic input parameters to the well-established Allwave-PDP software is convenient. Instead of creating a new method, the probabilistic method is an extended version of Allwave-PDP. By using Allwave-PDP a lot of expertise on driveability predictions is indirectly incorporated in the probabilistic method. In this research modelling choices

Currently this method has a low accuracy and limited validity due to respectively a small number of repetitions and a small amount of case studies. Despite these limitations, the tool can help decision-makers on selection of hammer type or on taking remedial measures, like fluidization or pre-drilling. Unexpected refusal of piles can result in large costs due to delays or the need for additional equipment. The application is especially relevant to fields where consequences of failure are large, e.g. offshore engineering.

A probabilistic model should be considered as complementary to the deterministic methods. A probabilistic method provides a logical framework for choosing a safety factor appropriate for the degree of uncertainty. The safety factor is used in the deterministic method to take into account the local variability.

This probabilistic method can simply be extended to use for other pile types or impact hammers. When different pile types are used, only parameter change is required. When the model is extended to use for impact hammer a model modification is required. The probabilistic extensions on Allwave-PDP are written in Python and can easily be modified for use by other pile types or impact hammers.

## 8.4. Future research

Probabilistic methods provide a logical framework to choose a safety factor appropriate for the degree of uncertainty. The relationship between safety factor and degree of uncertainty serves to distinguish conditions where lower-than-normal factors of safety are appropriate or where higher-than-normal factors of safety are needed. In future research the safety factors, which take into account local variability in deterministic predictions, must be revised for different conditions. Currently, a safety factor of 1.25 is used in all conditions. This factor is empirically determined and not calibrated by any probabilistic model (Alm and Hamre, 2001) However, in a case study of Woudsend, where refusal repeatedly occured in practice, no refusal was predicted by the deterministic method until a safety factor of 1.7 was applied to the soil resistance.

In future research all available CPT's in the soil investigation of a driving project must be utilized. Typically, in a soil investigation horizontal distance a CPT is made at every 25-50 m. By considering the variation between CPT's (trend line, geological layer divisions and correlation length), a better image of the horizontal variation of the soil can be obtained.

# Bibliography


Allnamics. *Allwave-PDP User's Reference Manual (Draft) Revision 28-8-2017*. 2017.

T. Alm and L. Hamre. Soil model for pile driveability predictions based on CPT interpretations. *The 15th Int. Conf. on Soil Mech. and Geotech Vol(3) pp 1297-1302*, 2001.

J. Authier and B.H. Fellenius. Quake values determined from dynamic measurements). *Proceedings 1st International Conference on the Application of Stress-Wave Theory on Piles, Stockholm, 1980. A.A. Balkema, pp. 197-216*, 1980.

S. Azzouzi. *Intrillen van stalen damwanden in niet-cohesieve gronden*. TU Delft, 2003.

D.D. Barkan. Foundation an Drilling by the Vibration Method. *Proc. of the 4th Int. Conf. on Soil Mechanics and Foundation Engineering, London*, 1957.

M.P. Byfield and D.A. Nethercot. Material and geometric properties of structural steel for use in design. *Structural Engineer. 75. 363-367*, 1997.

J.T. Christian. Geotechnical engineering reliability: How well do we know what we are doing? *Journal of Geotechnical and Geoenvironmental Engineering 130(10):985*, 2004.

Cobouw. Conflict over meerwerk bij bouw aquaduct Woudsend. https://www.cobouw.nl/bouwbreed/nieuws/2007/07/conflict-over-meerwerk-bij-bouw-aquaduct-woudsend-10114507, 2007. Accessed: 8-10-2019.

H.M. Coyle and G.C. Gibson. Empirical damping constants for sands and clays. *Journal of the Soil Mechanics and Foundations Division, Proceedings of the American Society of Civil Engineers*, 1970.

CUR. *CUR 166 Damwandconstructies*. 2012.

S. de Cock. Comparison de modèles de vibrofoncage avec des résultats de labora-toire et de chantier. *Univ. Catholique de Louvain, Belgium, pp. 113*, 1998.

L. de Neef, P. Middendorp, and J. Bakker. Installation of Monopiles by Vibrohammers for the Riffgat Project. *Pfahlsymposium, Braunschweig*, 2013.

M. De Saint-Venant. Memoire sur le doc longitudinal de deux barrees elastiques. *Journal de Mathematique, 2, ser XII, pp 237-376*, 1867.

Deep Foundations Institute. *Comparison of impact versus vibratory driven piles*. 2015.

Deltares. Geobrain database. Accessed: 8-10-2019.

N. Denies, N. Huybrechts, M.P. Bourdouxhe, and A. Fagot. In-situ test campaign of vibrodriven sheet piles. *19th International Conference on Soil Mechanics and Geotechnical Engineering, Vol. 2017-September, pp. 1101-1112*, 2017.

Duncan, M.J. Factors of safety and reliability in Geotechnical Engineering. *Journal of Geotechnical and Geoenvironmental Engineering, 126(4), 307-316*, 2000.

D. Ferron. Eindringveralten von Spundwandenbohlen und Rammbarkeit von Böden bei der Vibrationsrammung. *Diplomarbeit Nr. 326653, Fachgeiet Bodenmechanik und Grundbau, Universität Kaiserslautern*, 2001.

Edward P. Heerema. Predicting Pile Driveability: Heather As An Illustration Of The Friction Fatigue Theory. *Ground Engineering. 13. 10.2118/8084-MS*, 1978.

E.P. Heerema. Relationships between wall friction, displacement velocity and horizontal stress in clay and in sand, for pile driveability analysis. *Ground Engineering*, 1979.

M.A Hicks. Application of the Random Finite Element Method. 2015.

T.J. Hirsch, L.L. Lowery, H.M. Coyle, and C.H. Samson. Pile-Driving analysis by One-Dimensional Wave Theory: State of the Art. *High Res. Rec.*, 1970.

M. Hussein, F. Rausche, and G.E. Likins. Wave Equation Analysis of Pile Driving: Methodology and Performance. *6th National Conference on Microcomputers in Civil Engineering*, 1988.

G. Jonker. Vibratory Pile Driving Hammers for Pile Installations and Soil Improvement Projects. *OTC 5422*, 1987.

S.N. Jonkman, R.D.J.M. Steenbergen, O. Morales-Nápoles, A.C.W.M. Vrouwenvelder, and J.K. Vrijling. *Probabilistic Design: Risk and Reliability Analysis in Civil Engineering*. TU Delft, 2017.

M. Korff and F. van Tol. Validating and Improving Models for Vibratory Installation of Steel Sheet Piles with Field Observations. *Geotechnical and Geological Engineering*, 2012.

S.L. Lee, Y.K. Chow, G.P. Karunaratne, and K.Y. Wong. Rational Wave Equation Model for Pile-Driving Equation Analysis. *Journal of Geotechnical Engineering*, 1988.

G. Likins, B. Fellenius, and R. Holtz. Pile Driving Formulas: Past and Present. *Geocongress 2012 737-753*, 2012.

S. Litkouhi and T.J. Poskitt. Damping constants for pile driveability calculations. *Géotechnique 30, No. 1, pg. 77-86*, 1980.

Hicks M.A.-Van den Eijnden A.P. Lloret, M. Investigation of the reduction in uncertainty due to soil variability when conditioning a random field using Kriging. *Géotechnique letters 2(3), 123-127*, 2012.

M. Lloret-Cabot, G.A. Fenton, and M.A. Hicks. On the estimation of scale of fluctuation in geostatistics. *Georisk, 2014, Vol. 8, No. 2, 129-140*, 2014.

M.C. McVay and C.L. Kuo. Estimate damping and quake by using traditional soil testings. *University of Florida, Department of Civil Engineering*, 1999.

A.V. Metrikine and A.W.C.M. Vrouwenvelder. Dynamics of Structures, Part 2 Wave Dynamics. *Lecture notes CT4140*, 2001.

P. Middendorp. Thirty years of experience with the wave equation solution based on the method of characteristics. *7th International Conference on the Application of Stress Wave Theory to Piles, Kuala Lumpur, Malaysia*, 2004.

P. Middendorp and P.J. van Brederode. Skin friction models for sand from static and dynamic laboratory load tests. *2nd International Conference on the Application of Stress Wave Theory on Piles, Stockholm, Sweden*, 1984.

P. Middendorp and A.F. van Weele. Application of characteristic stress wave method in offshore practice. *Proceedings of the 3rd International Conference on Numerical Methods in Offshore Piling*, 1986.

P. Middendorp and G.E.H. Verbeek. At the Cutting Edge of Pile Driving and Pile Testing. *The 9th International Conference on Testing and Design Methods for Deep Foundations (IS-Kanazawa 2012)*, 2012.

R. Moghaddam, F. Rausche, and S.D. Webster. Friction fatigue and drivability analysis of open ended pipe piles based on cone penetration testing results. 2018.

N. Moscoso. *Vibrodriveability analysis on sandy soils*. École polytechnique de Louvain, 2018.

NEN. NEN 9997-1 Geotechnical design. 2017.

S-H Ni and E-S Fan. Fines Content Effects on Liquefaction Potential Evaluation for Sites Liquefied during Chi-Chi Earthquake, 1999. *13th World Conference on Earthquake Engineering, Vancouver, Canada, Paper No. 2521*, 2004.

K.K Phoon. Reliability-based design in geotechnical engineering: Computations and Applications. *Taylor Francis Group*, 2008.

K.K. Phoon. Role of reliability calculations in geotechnical design. *Georisk: Assessment and Management of Risk for Engineered Systems and Geohazards. 11. 1-18*, 2016.

K.K. Phoon, J.V. Retief, J. Ching, M. Dithinde, T. Schweckendiek, Y. Wang, and L.M. Zhang. Some observations on ISO2394:2015 Annex D (Reliability of Geotechnical Structures). *Structural Safety 62, 24-33*, 2016.

PVE-Holland. PVE-Holland. https://www.pve-holland.com/content/217/309/Technology/Vibratory-Hammers/Principle-of-a-vibratory-hammer.html, 2019. [Online; accessed 23-July-2019].

P.M. Rao. Effect of pile geometry and soil saturation in the behavior of non-displacement piles installed by vibration. *MSc thesis presented to the Faculty of the Dep. of Civil and Environmental Engineering, University of Houston, Texas*, 1993.

F. Rausche. Modeling of vibratory pile driving. *Proceedings of TransVib2002 International Conference on Vibratory Driving, Louvain-la-Neuve, Belgium, September 9-10. 21-32*, 2002.

P.K. Robertson. Evaluation of Flow Liquefaction and Liquefied Strength Using the Cone Penetration Test. *Journal of Geotechnical and Geoenvironmental Engineering*, 2010.

P.K. Robertson, R.G. Campanella, D. Gillespie, and J. Greig. Use of Piezometer Cone Data. *IN-SITU '86 Use of In-Situ Testing in Geotechnical Engineering, ASCE Specialty Conference, June, 1986*, 1986.

M.P. Rooduijn and J.G. De Gijt. *Handboek Hei- en Trilbaarheid*. SBRCURnet, 2017.

J.A. Schneider and M. Senders. Foundation Design: A Comparison of Oil and Gas Platforms with Offshore Wind Turbines). *Journal of the Marine Technology Society, 44(1), 32-51*, 2010.

Seaway Heavy Lifting. Pile driveability and Installation. 2009.

A.W. Skempton. Residual strength of clays in landslides, folded strata and the laboratory. *Géotechnique 35, No. 1, 3-18*, 1985.

A.E.L. Smith. Pile Driving Analysis by Wave Equation. *Journal of SMFD ASCE 86(4) pp 35-61*, 1960.

D. Tara, P. Middendorp, and G. Verbeek. Modeling and observations of pile installation using Vibrohammers in Fraser River Delta Soils. 2014.

J-F. Van den Berghe. Sand Strength Degradation within the Framework of Vibratory Pile Driving. *PhD thesis presented to the Faculty of Applied Science, Université chatolique de Louvain, Belgium*, 2001.

R.F. van Dorp. PAO cursus heien en trillen. 2019.

K. Viking. *Vibro-driveability - a field study of vibratory driven sheet piles in non-cohesive soils*. PhD Thesis, Department of Civil and Architectural Engineering Royal Institute of Technology (KTH), Stockholm, Sweden, 2002.

G.E.J.S.L. Voitus van Hamme, J.W. Jansz, H. Bomer, and D. Arentsen. Hydroblok and improved piledriving analysis. *De Ingenieur, Jrg. 86, Nr. 18, 1974*, 1974.

Wisconsin Department of Transportation. WisDOT Structure inspection Manual Part 4 - Ancillary Structures, Chapter 4 - Retaining Walls. 2017.

K. Yasuhara, K. Hirao, and A.F.L. Hyde. Effects of Cyclic Loading on Undrained Strength and Compressibility of Clay. *Soils and Foundations, Vol. 32, No. 1, 100-116, Mar. 1992*, 1992.